The autoantigen TRIM21 assembles proinflammatory immune complexes following lytic cell death

Authors: Esther L. Jones Evans[1]†, Benjamin Demarco[1]‡, Han Cai[1], Madelon M.E. de Jong[1], Sarah Hill[1], Marcus A. Widdess[1], Joannah R. Fergusson[1], Ryan E. Glass[2], Gemma Harris[3], Gracie J. Mead[1], Yavuz F. Yazicioglu[1]‡, Saba Nayar[4], Benjamin A. Fisher[4,5], Mark S. Cragg[6], Alexander J. Clarke[1], Audrey Gérard[1], Jelena S. Bezbradica[1]*, Lynn B. Dustin[1]*

Affiliations:

[1]Kennedy Institute of Rheumatology, University of Oxford; Oxford, UK

[2]Quest Diagnostics; Chantilly, VA, USA

[3]Research Complex at Harwell; Didcot, UK

[4]School of Infection, Inflammation and Immunology, University of Birmingham; Birmingham, UK

[5]National Institute of Health Research (NIHR) Birmingham Biomedical Research Centre, University Hospitals Birmingham NHS Foundation Trust; Birmingham, UK

[6]Antibody and Vaccine Group, Centre for Cancer Immunology, School of Cancer Sciences, Faculty of Medicine, University of Southampton; Southampton, UK

*Corresponding author. Email: jelena.bezbradica@kennedy.ox.ac.uk (J.S.B.)

*Corresponding author. Email: lynn.dustin@kennedy.ox.ac.uk (L.B.D.)

†Current address: MRC Laboratory of Molecular Biology, Cambridge Biomedical Campus; Cambridge, UK

‡Current address: Department of Biomedicine, University of Basel; Basel, Switzerland

Abstract: Sjögren's disease (SjD) causes localized and systemic inflammation and autoantibody production against intracellular proteins such as TRIM21/Ro52 (tripartite motif-containing protein 21). TRIM21, an E3 ubiquitin ligase, binds antibody Fc domains on opsonized pathogens that have escaped extracellular immunity and entered the cytosol. TRIM21 then ubiquitinates these pathogens, driving their proteasomal degradation. How TRIM21 becomes an autoantigen remains unclear. We show that TRIM21 is released upon lytic cell death (pyroptosis/necroptosis) but not apoptosis. Although many cytosolic proteins are released by dead cells, liberated TRIM21 is distinct: its high antibody affinity enables binding to Fc domains of circulating immunoglobulins, forming large immune complexes (ICs). These ICs increase in SjD, where anti-TRIM21 autoantibodies interact with released TRIM21 via Fc and $F(ab')_2$. TRIM21 ICs are taken up by macrophages, which drive proinflammatory responses, antigen presentation, and metabolic changes in high interferon environments. Thus, TRIM21 may perpetuate inflammation and autoantigen presentation, resulting in high immunogenicity.

One-sentence Summary: TRIM21/Ro52 assembles proinflammatory immune complexes.

Main Text:

INTRODUCTION

Sjögren's disease (SjD) is the second most common autoimmune disease, affecting 2 to 4 million people in the United States *(1*, *2)*. Manifestations of SjD include lymphocytic infiltration of the lacrimal and salivary glands (SGs), which interferes with the ability of those tissues to produce tears and saliva, respectively, leading to keratoconjunctivitis sicca (dry eyes) and xerostomia (dry mouth) (*3*, *4*). Systemic clinical manifestations include fatigue, chronic joint pain, neurological, pulmonary, and renal sequelae, and increased risk of B cell and mucosal-associated lymphoid tissue lymphomas (*5*). There are few therapeutic options for SjD patients and no approved biological therapies (*6*), leaving an unmet clinical need for SjD-specific drugs.

SjD diagnosis includes labial (lip) SG biopsy plus serological testing for anti-Ro/SSA (Sjögren's-syndrome-related antigen A) autoantibodies [encompassing autoantibodies against TRIM21/Ro52 (anti-tripartite motif-containing protein 21) and TROVE2/Ro60 (telomerase, Ro, and vault domain 2)] and anti-La/SSB (*7–10*). Anti-TRIM21/Ro52 autoantibodies are common in several other autoimmune diseases. TRIM21 is an E3 ubiquitin ligase whose structure comprises N-terminal RING, inhibitory B-box, predicted central coiled-coil, and C-terminal pyrin, splA and ryanodine receptor (PRYSPRY) domains (*11*). Although PRYSPRY domains are found in other proteins, and multiple human TRIM proteins exist, the PRYSPRY domain of TRIM21 is unique due to its high-affinity binding to antibody Fc domains (*12*). TRIM21 acts as an intracellular Fc receptor (FcR), sensing antibody-opsonized pathogens that escape into the cytosol (*13*, *14*). TRIM21's capacity for high-affinity cytosolic Fc binding has been exploited for antibody-based targeted degradation of cytosolic proteins and therapeutic innovation (*15–17*). TRIM21 is ubiquitously expressed, with particularly high expression at mucosal and immune tissue sites (*18*). Why TRIM21 is such a common autoantigen is unknown.

Models for autoantibody production often cite impaired clearance of apoptotic cell debris (*19*, *20*) or uptake of antigen-containing apoptotic blebs by antigen-presenting cells (*21*). However, apoptotic blebs typically prevent inadvertent release of intracellular contents to limit autoimmunity (*22*). Instead, lytic cell death mechanisms (e.g., pyroptosis, necroptosis, and necrosis) promote immune activation through the uncontrolled release of intracellular contents that act as alarmins (*23*). Pyroptotic cell death may also contribute to SG damage and dysfunction in SjD (*24*). As TRIM21 is expressed in most cells, unscheduled proinflammatory death of any cell could expose this autoantigen. Combined with the proinflammatory signature demonstrated by elevated serum type I interferons (IFNs) in patients (*25*, *26*), we propose that lytic cell death may contribute to the loss of tolerance in SjD.

Here, we find that TRIM21 is released upon lytic, but not apoptotic, cell death. Liberated TRIM21 maintains its Fc-binding function and forms higher-order immune complexes (ICs) with circulating antibodies. ICs can be formed with both healthy plasma via Fc binding and with plasma from anti-TRIM21/Ro52–seropositive SjD patients, via both Fc and $F(ab')_2$ binding. Following uptake by IFN-primed macrophages, TRIM21 ICs stimulate antigen presentation, cytokine release, and metabolic changes. These findings increase our understanding of how TRIM21 perpetuates inflammation and self-antigen presentation in SjD.

RESULTS

Cytosolic TRIM21 is widely expressed in control and SjD tissues

To determine TRIM21 expression in SjD patient SGs, we examined biopsy slides from anti-TRIM21/Ro52–seropositive and/or anti-TROVE2/Ro60–seropositive SjD patients. Tissues from patients with sicca (SjD-seronegative with dry mouth symptoms) were used as controls. H&E-stained slides were assessed for total area of mononuclear cell infiltration, the number of foci (≥ 50 mononuclear cell infiltrates), and the focus score [number of foci per 4 mm^2 (*7*)] (table S1). Adjacent sections were subjected to immunofluorescent staining.

Sicca control SG biopsies were anatomically normal, with clear glandular acini and ducts, as indicated by H&E and cytokeratin (CK) epithelial staining (Fig. 1A). TRIM21 was expressed throughout the SG (Fig. 1A). By contrast, SjD biopsies (Fig. 1, B and C) exhibited areas of focal infiltration, demonstrated by higher focus scoring (≥ 1) (table S1) than sicca controls, consistent with SjD diagnostic criteria (*7*, *27*). One representative SjD biopsy had extensive adipose tissue replacement and glandular deformation, as commonly observed in SjD (*28*) (Fig. 1B and table S1), and was too atrophied to assess TRIM21 expression (Fig. 1B).

Another representative SjD biopsy showed fibrotic regions surrounding areas of acinar atrophy (Fig. 1, C and D), with ubiquitous TRIM21 immunostaining (Fig. 1C). Immune cell infiltrates included plasma cells (determined via H&E stain morphology, IgG, and IgA), T cells (CD3), macrophages (CD163, CD68, and MerTK), and granulocytes (CD66b), in regions with HLA-DR and immunoglobulin staining (Fig. 1, C and D). Although previous studies have provided evidence of epithelial cell death (*29*, *30*), we did not observe cell death in situ, likely due to rapid clearance of cell debris. Furthermore, cell death commonly occurs before tissue atrophy (*31*) and glandular deformation that characterize the late-stage SjD presented here.

To investigate TRIM21's subcellular localization, we overexpressed TRIM21-monomeric-GFP (WT TRIM21-GFP) in HeLa cells. We observed cytosolic TRIM21 expression (Fig. 1E and fig S2A), as previously reported (*32*, *33*). TRIM21 was also widely expressed throughout the human tonsil (Fig. 1F) and SG (Fig. 1C). Thus, TRIM21 expression is ubiquitous, cytosolic and similar in patients with and without evidence of SjD.

TRIM21 is up-regulated by inflammatory signals and released during lytic cell death

IFN signaling up-regulates TRIM21 expression (*32*, *34*). We found TRIM21 expressed in untreated (UT) mouse wild-type (WT) bone marrow–derived macrophages (BMDMs) and HeLa cells (of human epithelial origin) (Fig. 2, A to C). TRIM21 was further up-regulated by treatment with lipopolysaccharide (LPS) (Fig. 2A), poly I:C (Fig. 2A), or IFN (α, β, and γ) (Fig. 2B) in BMDMs and by IFN-γ in HeLa cells (Fig. 2C). TRIM21 antibody specificity was validated using gene overexpression and silencing (fig. S2, B and C). Thus, TRIM21 can be up-regulated by IFNs and pathogen-associated molecular patterns (PAMPs) (*13*).

We next asked how TRIM21 is released from cells. Proinflammatory forms of lytic cell death, such as pyroptosis, may induce autoimmunity by promoting the release of self-antigens and inflammatory alarmins (*35*, *36*), whereas membrane-bound apoptotic blebs containing nuclear and cytoplasmic material are normally cleared by neighboring phagocytes, preventing extracellular exposure of intracellular contents (*37*). We therefore sought to compare apoptosis with lytic cell death as possible mechanisms for intracellular TRIM21 release (Fig. 2, D to I). Different forms of cell death were induced (fig. S2D). Apoptotic bodies (blebs) containing TRIM21 were visualized in ABT-737/MCL1i–treated HeLa cells (Fig. 2, D and E). Live confocal microscopy time-lapse recording of the same field of view showed cytoplasmic condensation and blebbing 30 min after drug treatment (movie S1). Highly condensed WT TRIM21-GFP puncta were still visible 180 min after drug treatment, after many cells had undergone secondary necrosis (Fig. 2E).

Extracellular TRIM21 release was tested by immunoblotting cell lysates and supernatants after cell death, with GAPDH release used as a control. TRIM21 and GAPDH were high in supernatants of pyroptotic [LPS+nigericin treated, to activate the NLRP3 (NLR family pyrin domain containing 3) inflammasome], but not apoptotic BMDMs (Fig. 2F). Low levels of GAPDH in apoptotic cell supernatants were likely due to secondary necrosis during late apoptosis. Other forms of lytic death, namely necroptosis (using an LPS/QVD/SMAC mimetic) (Fig. 2G), pyroptosis [via spinfection of calf-thymus DNA (ctDNA) to activate the AIM2 (absent in melanoma 2) inflammasome] (Fig. 2H), and necrosis [using needle shear (mimicking mechanical lysis) or Triton X-100] (Fig. 2I), all led to the release of TRIM21 and GAPDH.

To define TRIM21 release mechanisms during pyroptosis/necroptosis, we used BMDMs from WT and gasdermin D–knockout (*Gsdmd*-KO) mice (fig. S2E). *Gsdmd*-KO BMDMs cannot form membrane GSDMD pores required for lytic death and release of mature interleukin 1 beta (IL-1β) (*38*, *39*). TRIM21 and GAPDH were absent from supernatants of LPS/nigericin–treated *Gsdmd*-KO BMDMs, indicating that TRIM21 release depended on cell lysis (Fig. 2G). To test whether TRIM21 passes through the GSDMD pore or is released during later pyroptotic cell rupture, we added osmoprotectant glycine, permitting GSDMD pore formation but inhibiting downstream membrane lysis (*40*). IL-1β, but not TRIM21, was detected in the supernatants of glycine-treated WT BMDMs after pyroptosis was induced (Fig. 2G), suggesting that TRIM21 release depends on cell lysis. Thus, cytosolic TRIM21 is released during proinflammatory lytic cell death following membrane rupture but remains trapped in membrane blebs during apoptosis.

Extracellular TRIM21 binds serum antibody Fc domains

Cytosolic TRIM21 binds immunoglobulin Fc domains via its PRYSPRY domain (*41*). We tested whether TRIM21 maintains antibody-binding activity after release through lytic cell death. We overexpressed three GFP-tagged TRIM21 constructs in HeLa cells (fig. S2F): full-length WT TRIM21_w_PRYSPRY, TRIM21_NO_PRYSPRY, which lacks the PRYSPRY domain, and TRIM21_FcMUT, the full-length form of the protein containing two PRYSPRY domain point mutations (W381A/W383A) that ablate Fc binding (*42*).

Free TRIM21_w_PRYSPRY-GFP bound to plate-immobilized normal human serum (NHS) antibodies (Fig. 3A). Consistent with our results showing TRIM21 trapped inside apoptotic blebs (Fig. 2F), minimal binding was observed between NHS antibodies and supernatant from UT or apoptotic HeLa_TRIM21_w_PRYSPRY cells. As HeLa cells lack NLRP3 inflammasomes, we induced death by noncanonical pyroptosis, using LPS spinfection after IFN priming. Noncanonical inflammasomes detect cytosolic LPS and trigger GSDMD-mediated cell lysis (*43*). TRIM21 released from pyroptotic HeLa TRIM21_w_PRYSPRY cells strongly bound plate-bound antibodies at levels similar to binding of TRIM21 released by mechanical/detergent lysis (“TRIM21 lysate”). Binding was PRYSPRY-dependent, as it was lost in HeLa TRIM21_NO_PRYSPRY (Fig. 3A) and HeLa TRIM21_FcMUT lysates (Fig. 3B).

To test whether extracellular TRIM21 also binds circulating (not plate-bound) antibodies, we performed GFP-trap coimmunoprecipitation (co-IP) experiments. Here, GFP-tagged TRIM21 was released by cell lysis, incubated with NHS, and then captured with an anti-GFP nanobody lacking an Fc domain. Only lysates containing TRIM21-GFP pulled down the serum antibodies, as detected by anti-IgG heavy-chain immunoblotting (Fig. 3C).

Finally, we tested whether TRIM21-Fc binding differs between healthy control (HC) versus SjD patient antibodies in plasma. TRIM21-Fc binding was similar for all samples (Fig. 3D),

thus confirming that PRYSPRY domain–mediated TRIM21-Fc binding is independent of autoreactivity and is maintained after lytic cell death.

SjD patient plasma generates higher-order TRIM21–IgG complexes

Clinical tests for SjD often do not distinguish between Ro antigens (i.e, TRIM21/Ro52 and TROVE2/Ro60). We therefore employed the luciferase immunoprecipitation system (LIPS) assay to distinguish patients with autoantibodies to Ro52/TRIM21_NO PRYSPRY, Ro60/TROVE2, and La (*44*) (Fig. 4A and fig. S3A). We selected three HC plasma samples (HC099, HC077, and HC087) without any SjD autoantigen reactivity (Fig. 4A) and three SjD patient plasma samples (SjD58, SjD59, and SjD61) with increasing anti-TRIM21/Ro52 autoantibody titers (Fig. 4A).

As TRIM21 bound Fc domains of both HC and SjD antibodies in a PRYSPRY-dependent manner (Fig. 3, B and D), we tested whether $F(ab')_2$–mediated TRIM21 binding in SjD patient plasma assembled larger TRIM21 ICs. For this, cell-free TRIM21_w_PRYSPRY-GFP was incubated with HC or SjD plasma and analyzed by nondenaturing blue native polyacrylamide gel electrophoresis (BN-PAGE) to detect higher-order complexes (*45*). In lysates alone, TRIM21-GFP was identified in both monomeric (~70 kDa) and oligomeric forms (Fig. 4, B to G), consistent with intrinsic PRYSPRY protein self-oligomerization. With HC plasma, TRIM21_w_PRYSPRY-GFP formed larger ICs (Fig. 4, B to D) that were not observed in plasma alone. With SjD plasma, these ICs were even larger than those formed with HC plasma, and complex size correlated with levels of anti-TRIM21/Ro52 antibodies (Fig. 4, A to D). TRIM21_SjD58 plasma complexes migrated with sizes > 480 kDa (Fig. 4B). Complexes with SjD59, with the highest anti-TRIM21-autoantibody levels, were too large for adequate BN-PAGE resolution and barely entered the gel (Fig. 4C). SjD61, with lower autoantibody levels, formed the smallest ICs with some TRIM21 remaining monomeric (Fig. 4D). Total IgG levels were similar in all plasma samples (Fig. 4, B to D). Thus, TRIM21 IC size correlates with SjD anti-TRIM21 autoantibody levels.

To determine whether PRYSPRY-mediated Fc binding was necessary and sufficient for generating large ICs, BN-PAGE analyses were repeated using TRIM21_FcMUT-GFP. Higher-order complex formation between TRIM21_FcMUT and HC plasma was impaired, with complex size matching TRIM21_FcMUT lysates alone (Fig. 4, E to G). This confirmed PRYSPRY-dependent binding of TRIM21 to the Fc of HC antibodies. However, higher-order complex formation was retained when TRIM21_FcMUT lysates were incubated with SjD plasma and even enhanced with SjD58 and SjD61 when Fc-binding was eliminated (Fig. 4, E to G). TRIM21_FcMUT complexes with SjD59 plasma again could not be adequately resolved by BN-PAGE methods (Fig. 4F and fig. S3, B and C). Thus, SjD plasma antibodies can form higher-order TRIM21 ICs even when PRYSPRY-Fc interactions are blocked, with binding likely mediated by TRIM21-reactive $F(ab')_2$.

To more accurately quantify complex sizes, we utilized flow-induced dispersion analysis (FIDA) technology. This enabled us to track the GFP-tag on TRIM21 using small sample volumes and measure Taylor dispersion to characterize complex sizes. Experiments were performed at 30, 10, 5, and 2.5 kPa. Species are outside Taylor conditions above certain kPa values (*46*), namely at 30 kPa when species are larger than ~17 nm, at 10 kPa when > ~53 nm, at 5 kPa when > ~106 nm, and at 2.5 kPa when > ~212 nm. Soluble aggregates outside of Taylor conditions can be seen in the Taylorgram as a baseline shift that occurs at ~1/2 the retention time of the main peak (~1/2tR). TRIM21-GFP alone did not exhibit a shift in baseline at ~1/2tR at any of the pressures tested. TRIM21-GFP complexed with HC plasma exhibited a

baseline shift at 30 kPa alone, suggesting a hydrodynamic radius of 17 to 53 nm. TRIM21-GFP complexed with SjD plasma exhibited a baseline shift at 30, 10, and 5 kPa, suggesting a hydrodynamic radius range of 17 to 212 nm. Some large complexes formed insoluble aggregates, presenting as "spikes" when graphically represented (Fig. 4H). Thus, SjD patient plasma generates higher-order TRIM21–IgG complexes.

Macrophages take up higher-order TRIM21–IgG complexes

Macrophages internalize IgG-opsonized materials via Fcγ receptors (FcγRs) (*47, 48*). To evaluate TRIM21 IC uptake, we incubated cell-free TRIM21-GFP with serum/plasma antibodies to prepare ICs. We primed macrophages with IFN-γ to up-regulate FcγR expression and mimic SjD inflammatory states, then compared uptake of TRIM21-GFP alone versus TRIM21-GFP_NHS ICs by immunoblot. BMDMs more readily took up TRIM21-GFP_NHS compared to TRIM21-GFP alone (Fig. 5A and fig. S4A). Increased uptake was PRYPSRY-dependent, as TRIM21_FcMUT_NHS uptake was less efficient than uptake of TRIM21-GFP_NHS (Fig. 5B and fig. S4B). Next, we found that larger TRIM21_SjD ICs had faster uptake kinetics compared to smaller TRIM21_HC ICs (Fig. 5C). These assays were repeated for three SjD patients with variable anti-TRIM21/Ro52 autoantibodies (SjD58, SjD59, and SjD61) (Fig. 5C, fig. S5A to C). Uptake was slightly increased and accelerated for patient SjD58 with medium autoantibody levels, compared to SjD61 with lower autoantibody levels (fig. S5, A and B). TRIM21 IC uptake was also recapitulated in IFN-primed human monocyte-derived macrophages (HMDMs), with accelerated and stronger uptake of TRIM21_SjD-ICs (Fig. 5D and fig. S6, A and B). TRIM21 IC uptake was mostly FcγR-dependent, as it was reduced back to the level of TRIM21 uptake alone in *Fcgr1-4*-KO BMDMs compared to WT (fig. S7A). Uptake of both TRIM21 alone or TRIM21 IC was also reduced by the actin polymerization inhibitor cytochalasin D (CytoD) (fig. S7B), suggesting that the TRIM21 uptake occurred via actin-dependent phagocytic or endocytic pathways (*49*).

Internalized TRIM21 escapes into the cytosol and is preferentially degraded by the proteasome

Reduced TRIM21 levels were consistently detected 60 min post-uptake in macrophages during our feeding experiments. We consequently explored whether this reduction was due to TRIM21 degradation and could be rescued with lysosomal (bafilomycin A1 (BafA1)) or proteasomal (MG132) inhibitors (Fig. 6A). After uptake, BafA1 protected TRIM21 in ICs, but not TRIM21 alone, from degradation. MG132 protected TRIM21 from degradation, either alone or complexed with HC/SjD plasma. MG132 provided greater protection of TRIM21 in ICs than did BafA1. Thus, both proteasomes and lysosomes can degrade TRIM21 within ICs, but the proteasome pathway dominates, suggesting internalized TRIM21 can escape endolysosomes and enter cytosols for proteasomal degradation.

To confirm that TRIM21 ICs escaped endolysosomes after uptake, TRIM21 IC–fed BMDMs were imaged 60 min post-feeding. Cells were fed TRIM21-GFP_NHS ICs, fixed, then stained with Alexa Fluor 488–conjugated anti-GFP. Cytosolic TRIM21-GFP was significantly increased following MG132 pretreatment (Fig. 6B). Endosomal escape was verified by scoring colocalization between TRIM21-GFP and EEA1 (early endosome antigen 1) (Fig. 6C). There was little colocalization between endosomes and TRIM21-GFP, consistent with TRIM21 cytosolic escape (Fig. 6C). Endosomes were perinuclear in UT BMDM cells, but colocalized with phagocytosed beads, confirming bead maintenance within endosomal compartments as a control (fig. S8, A and B). We also stained for galectin-3 (Gal-3), a marker of endolysosomal

rupture (*50, 51*) (Fig. 6D and fig. S8, C and D). No Gal-3 staining was observed with beads, which do not rupture endosomes (fig. S8C), whereas Gal-3 levels were highest after feeding with monosodium urate (MSU) crystals, which heavily damage endosomes (*52, 53*) (fig. S8D). Gal-3 levels were intermediate after TRIM21 IC uptake (Fig. 6D), indicating some endosomal rupture, but also implying additional escape routes for TRIM21.

Endogenous cytosolic TRIM21 undergoes autoubiquitination, leading to its degradation together with any pathogen–antibody cargo (*54, 55*). To confirm whether ingested exogenous TRIM21-GFP was ubiquitinated upon endolysosomal escape, we performed a pan-ubiquitin tandem ubiquitin-binding entity (Ub-TUBE) IP from BMDM lysates after TRIM21 IC uptake. From the eluted Ub-TUBE material, we detected TRIM21-GFP from UT and especially MG132-treated BMDMs (Fig. 6E, and fig S8E). Notably, TRIM21 feeding material was not ubiquitinated before uptake (fig. S8F). Ubiquitinated TRIM21-GFP captured by Ub-TUBE was heavier (~70 kDa) than endogenous WT TRIM21, allowing us to separate the two TRIM21 pools (fig. S8F). Thus, both free TRIM21 and TRIM21 IC can escape endolysosomal compartments into the cytosol and undergo ubiquitination after macrophage uptake. For TRIM21 ICs, both lysosomal and proteasomal degradation pathways become engaged, with proteasomal degradation dominating (fig. S8G).

TRIM21 enhances antigen cross-presentation in vitro

Since TRIM21 and TRIM21 ICs escaped endolysosomal compartments into the cytosol, we asked whether they facilitated antigen cross-presentation via MHC-I (*56*). As there are no TRIM21-reactive transgenic mice, CD8 T cells were purified from ovalbumin (OVA)–reactive OT-I transgenic mice. We then exploited TRIM21 Fc binding to generate ICs containing OVA, anti-OVA antiserum, and GFP trap–purified TRIM21 (OVA–α-OVA–TRIM21). IFN-γ–primed BMDMs were treated with ICs, and OVA-specific CD8 T cell activation (by $CD69^+$ expression) was evaluated by flow cytometry (fig. S9, A and B).

Relative to OVA alone, OVA–α-OVA ICs increased T cell activation at all concentrations tested (Fig. 7). At low OVA concentrations (10 ng/ml), OVA–α-OVA–TRIM21 significantly increased T cell activation compared to OVA–α-OVA ICs and to an OVA–normal rabbit serum–TRIM21 control (Fig. 7, A to C). Responses to ICs plateaued at higher OVA concentrations. CD3 and TCRVβ5.1 were down-regulated following T cell activation (figs. S8, C and D, and S9, A to F). Down-regulation was greater with OVA–α-OVA and OVA–α-OVA–TRIM21 compared to controls (fig. S10, A to F), indicating enhanced TCR activation. Thus, TRIM21 complexed with OVA ICs increases in vitro OVA uptake, antigen presentation, and OVA-specific T cell activation.

TRIM21 uptake induces proinflammatory and metabolic changes in macrophages

In IFN-γ–primed HMDMs, TRIM21_SjD plasma ICs, but not TRIM21_HC ICs, or SjD plasma alone, stimulated secretion of multiple proinflammatory cytokines, including IL-1β, IL-6, IL-8, IL-12, and IL-18 (Fig. 8A). Tumor necrosis factor (TNF) levels tended to correlate with IC size, with SjD59 plasma alone inducing some TNF secretion (fig. S11A).

We also performed bulk RNA-seq on IFN-γ–primed HMDM 6 hours post-feeding. Principal component analysis discriminated TRIM21-positive/negative conditions (Fig. 8B). IFN-γ–primed HMDMs already express many proinflammatory genes. Nevertheless, further gene expression changes were observed when comparing TRIM21 or TRIM21_SjD59 versus UT conditions (Fig. 8, C to E). TRIM21 feeding up-regulated genes in inflammatory, lysosomal response, TNF via NF-κB, and mTORC signaling pathways (Fig. 8, C and D). Similar

pathways were enriched following TRIM21_SjD59 feeding (versus UT), only with more genes up-regulated and down-regulated when compared to TRIM21 alone (Fig. 8E). Querying specific pathway gene sets, we observed enrichment in TNF via NF-κB, ribosomal, and MAPK pathways in the Hallmark (fig. S11, B and C), Kyoto Encyclopedia of Genes and Genomes (KEGG) (fig. S12, A and B), and Biocarta (fig. S13, A and B) databases. We also noted TRIM21-induced changes in the mTOR pathway, possibly NF-κB signaling, and metabolic solute carrier (SLC) transporter genes (Fig. 8, F and G, and fig. S14). Validating our RNA-seq findings, immunoblotting demonstrated that both TRIM21 and TRIM21 ICs activated metabolic and stress-response pathways, including AMPKα (AMP-activated protein kinase alpha) phosphorylation (regulator of global cellular energetic state) after treatment of IFN-γ–primed HMDMs (Fig. 8H). eIF2α (eukaryotic translation initiation factor 2 subunit α) phosphorylation and ATF4 (activating transcription factor 4) protein were slightly increased in all TRIM21-treated conditions (Fig. 8H). Therefore, TRIM21-alone, or complexed with SjD patient plasma, induced proinflammatory, metabolic and stress responses in IFN-γ–primed HMDMs.

Some SjD plasma-only effects on IFN-γ–primed HMDMs were observed. For example, SjD59 plasma alone promoted expression of some mTOR and NF-κB pathway genes (Fig. 8, F and G), and SjD61 plasma alone caused an increase in ATF4 protein levels (Fig. 8H). Thus, high autoantibody levels in SjD plasma may be sufficient to activate low-grade inflammatory and metabolic changes in IFN-γ–primed HMDMs.

DISCUSSION

We demonstrated that TRIM21 is released during lytic cell death and forms extracellular ICs by binding healthy plasma antibody Fc domains and binding both Fc and $F(ab')_2$ domains in SjD plasma. These extracellular ICs are detected, internalized, and processed by macrophages, at levels and kinetics of uptake commensurate with IC size. Large TRIM21 ICs drive proinflammatory cytokine secretion, antigen cross-presentation, and stress responses in macrophages. We speculate this contributes to IC deposition and local inflammation in SjD (*57, 58*).

TRIM21 up-regulation by IFNs, LPS, and poly(I:C) may be relevant for SjD, as proinflammatory and antiviral IFN signatures are notable in SjD patient tissues and peripheral blood (*59, 60*). SjD is associated with chronic viral infection, particularly Epstein–Barr virus (EBV) (*61*). Many viral infections, including EBV (*62*), gain entry through the mouth and may drive local TRIM21 up-regulation, lytic death, and TRIM21 IC deposition in SGs, perpetuating local inflammation.

Identifying true TRIM21-binding proteins remains challenging. False-positive interactions occur by TRIM21 binding to Fc domains of antibodies used for co-IP (*63*). To avoid this pitfall, we employed Fc-free, nanobody-based GFP-trap micropurification to isolate TRIM21-GFP. We also used TRIM21-GFP (~70 kDa) to distinguish it from endogenous TRIM21 (52 kDa), and track IC size using FIDA (*64*). Our studies were performed in Opti-MEM to avoid confounding results due to antibodies in FBS. Finally, FcγR-blocking reagents containing mAbs against CD16 and CD32 (*65*) cannot be used to block TRIM21 IC uptake as TRIM21 binds to the Fc of anti-FcγR antibodies. Instead, we utilized BMDMs differentiated from mice lacking all FcγRs (*Fcgr1-4*-KO) to demonstrate FcγR-dependent uptake of TRIM21 ICs.

Cross-presentation and activation of granzyme K (GZMK)–producing CD8 T cells are relevant in SjD, as they contribute to the epithelial destruction of SjD SGs (*30, 66, 67*). Using the OT-I system (*68, 69*), we showed that by forming large ICs, TRIM21 promoted cross-presentation

of anti-OVA–opsonized OVA protein in vitro. We propose this is via enhanced uptake and endosomal escape, but cannot exclude the possibility that endogenous TRIM21 also engages internalized α-OVA–OVA complexes to drive cross-presentation. As previously reported, Fc-specific modifications to increase TRIM21 binding can enhance cross-presentation of opsonized adenovirus (*70*). Together, a model emerges whereby TRIM21 may promote antigen presentation at multiple steps, including increased antigen uptake, endolysosomal escape, and cytosolic processing.

In addition to driving cross-presentation, TRIM21_SjD-ICs stimulated HMDMs to secrete multiple proinflammatory cytokines and undergo gene expression changes for inflammatory, lysosomal, mTOR, and TNF (via NF-κB) pathways. This was validated at the protein level, with increased AMPKα and eIF2α phosphorylation. AMPK and mTORC1 are reciprocally regulated. Thus, increased phospho-AMPKα immediately post-feeding with TRIM21 (alone or in IC) may indicate early stress and/or activation of autophagy (*71, 72*). AMPK senses energy deprivation, and eIF2α is phosphorylated as part of the integrated stress response (*73, 74*). This can increase translation of stress-induced genes such as ATF4 (*75*). We propose that ingestion of large amounts of extracellular TRIM21 may promote lysosomal stress responses, perhaps by endo/lysosomal damage. Fewer differences were observed at the gene and protein level when comparing TRIM21_SjD versus TRIM21_HC ICs. However, larger ICs (TRIM21_SjD61/TRIM21_SjD59) were ingested faster and promoted more cytokine secretion than TRIM21_HC ICs. The internalization rates and the kinetics or magnitude of the response may consequently be IC size-dependent. In SjD tissues, large ICs may synergize with other inflammatory signals—which are missing in our in vitro system—to drive qualitative differences in downstream responses.

This study was limited to small-scale methods for detecting uptake, endosomal escape, and antigen presentation. We propose that TRIM21-GFP escapes endosomes into the cytosol for ubiquitination, but escape mechanisms remain to be determined. The levels of cell-free TRIM21 in SjD plasma and tissue are not yet known, nor have we determined whether macrophages or DCs present TRIM21 peptides to autoimmune T cells after uptake. Another limitation of this study is that we were unable to define cell death mechanisms in situ in SjD SG biopsies. These patient biopsies represent a single time point, typically after significant tissue damage has already occurred. It remains unclear what happens during the early stages of SjD, before visible pathology. Few reagents are available to discriminate cell death mechanisms by immunofluorescence microscopy, making identification of apoptotic versus lytic cell death challenging in fixed tissues (*76, 77*). Finally, we investigated only one mechanism contributing to the immunogenicity of TRIM21. Additional factors, such as HLA type and the presence of pathogens such as EBV, were not explored. These are worth investigating to explore why lytic cell death in healthy individuals does not drive autoimmune responses despite the possibility that TRIM21 may bind circulating antibodies.

In conclusion, we propose that although many cytosolic proteins are released during lytic cell death, TRIM21 may be particularly immunogenic due to its inherent capacity to bind Fc domains of circulating antibodies to form large extracellular ICs. For SjD, tissue damage (e.g., in SGs) may release intracellular TRIM21, which binds circulating antibodies to form ICs. Together with elevated IFN levels in SjD patients, this may drive TRIM21 uptake, macrophage activation, metabolic changes, and antigen presentation, which together perpetuate additional inflammation and anti-TRIM21/Ro52 autoantibody production.

MATERIALS AND METHODS

Study design

This study was designed to assess mechanisms for how intracellular TRIM21 may become an autoantigen, using in vitro experiments. Anonymized human samples used in this study were obtained from the following sources. Tonsillar tissue was processed and provided by the Oxford Centre for Histopathology Research. Commercially supplied SjD patient plasma samples were obtained from NeoBiotech (custom order) and normal serum controls from Invitrogen. HC plasma was originally obtained as part of a study approved by the Institutional Review Board at Rockefeller University Hospital (RUH) under human subjects protocol LDU-0437. Healthy donors were recruited through the RUH outpatient clinic. Samples were coded and anonymized. Blood was collected into acid citrate dextrose–treated vacutainer tube. Plasma was isolated by centrifugation within 1 hour of collection, aliquoted, and stored at −80°C until used. Storage and use of these samples at the University of Oxford was approved by the Berkshire Research Ethics Committee, REC; 13/SC/0466 (*78*). SjD and sicca syndrome (dry mouth syndrome without SjD autoantibodies) patient biopsies were obtained from the Optimising Assessment of Sjögren's Syndrome (OASIS) cohort (*79*). All plasma donors, and subjects in the OASIS cohort, signed written informed consent according to the principles of Helsinki. The OASIS study was approved by the Wales Research Ethics Committee 7 (WREC 7), formerly Dyfed Powys REC; 13/WA/0392. FFPE slides from the OASIS cohort were used for H&E and Cell DIVE multiplex imaging. The images represented in this study were chosen to reflect the SG damage, cellular infiltration and possible immune mechanisms present in SjD patients. Patient information is shown in Table S1 for salivary gland biopsies, and in Table S2 for plasma samples.

Due to limited availability of SjD patient plasma, we developed small-scale purification and in vitro methods to form ICs and to assay uptake and antigen presentation. Where possible, experiments were performed and analyzed as independent triplicates. For experiments using SjD patient plasma, experiments were executed as independent biological replicates. We used the LIPS assay to select three SjD plasma samples with a range of autoantibody titers. Three HC plasmas (autoantibody negative) were also used. These same patient plasmas were used throughout the study. For BMDM and HMDM experiments, different donors (mouse/human) were used for each replicate.

Mice

C57BL/6J and *Gsdmd*-KO mice (The Jackson Laboratory) were used to derive BMDMs. OT-I mice (Charles River) were bred with B6.SJL-*Ptprc*^{a}*Pepc*^{b}*/BoyCrl* (Ly5.1) mice (Charles River) to generate congenically marked CD45.1^{+} OT-I cells. Mice were bred in-house and kept in specific pathogen–free conditions, according to ethical standards approved by the UK Home Office and University of Oxford. Male or female mice aged 9 to 14 weeks were used for all experiments. *Fcgr1-4*-KO mice were generated and reported as previously described (*80*). Age and sex-matched *Fcgr1-4*-KO and WT control C57BL/6J mice were housed in facilities at Southampton University. Bone marrow was isolated on-site by Dr. R. Oldham and transported to the Kennedy Institute for storage.

Cell lines

HeLa cells were kindly gifted by Dr. I. Lim-Manley (U. Gruneberg lab, Dunn School of Pathology, University of Oxford) (originally purchased from ATCC). HEK293c18 (clone CRL-10852) were obtained from ATCC. HEK293T cells were kindly gifted by Prof. M.L. Dustin (Kennedy Institute of Rheumatology, University of Oxford). Cell lines were cultured in complete DMEM (data file S1) at 37°C and 5% CO_2 in T75 vented tissue culture (TC)–treated

flasks. Cells were washed with DPBS, trypsinized with Gibco™ Trypsin-EDTA (0.05%) for cell detachment. Cells were seeded at the desired confluency as described in the relevant sections.

Media and supplements

For media and supplements used, please see data file S1.

Buffers and solutions

For buffers and solutions used, please see data file S1.

Cell Preparation

Generating day 6 primary mouse BMDMs

Total mouse bone marrow (C57BL/6J and *Gsdmd*-KO) was isolated, cultured in four non-TC–treated 100-mm Sterilin square dishes per mouse and differentiated for 6 days in complete DMEM using hM-CSF (50 ng/ml), which cross-reacts with mouse M-CSF receptor, at 37°C with 5% CO_2. On day 3, cultures were topped up with 7 ml of media supplemented with hM-CSF (50 ng/ml). On day 6, adherent cells were harvested using ice-cold PBS and cell lifters and cryopreserved at a concentration of 1×10^7 cells per vial in cryopreservative solution (90% FBS and 10% DMSO).

Culture and plating of day 6 BMDMs

Cryopreserved day 6 BMDMs were thawed, diluted in complete DMEM media, and centrifuged at 500*g* for 3 min at room temperature to remove DMSO. The pellet was resuspended in complete DMEM containing 50 ng/ml of hM-CSF. Cells were plated in 10-cm non-TC–treated petri dishes and incubated for 48 hours to recover at 37°C with 5% CO_2. After 48 hours, BMDMs (day 8) were harvested using ice-cold PBS and cell lifters, counted, and seeded at a 5×10^4 cells/ml density for all experiments unless otherwise specified, in 100 µl per well in a 96-well plate, in complete DMEM containing 50 ng/ml of hM-CSF. After plating, the cells were left undisturbed at room temperature for ~20 min to promote even attachment density. The plate was incubated at 37°C with 5% CO_2 for 16 hours before experimentation. For uptake experiments, cells were primed with 100 ng/ml of murine IFN-γ (mIFN-γ) for ~24 hours.

Generation of BMDMs from frozen murine bone marrow progenitors

Murine bone marrow (from *Fcgr1-4*-KO and WT C57BL/6J mice) had previously been isolated and cryopreserved in two vials per mouse of cryopreservative solution (90% FBS and 10% DMSO). Vials were thawed, diluted in complete DMEM and centrifuged at 500*g* for 3 min at room temperature to remove DMSO. The pellet was resuspended in 15 ml of complete DMEM containing 50 ng/ml of hM-CSF. Cells were plated in 100-mm non-TC–treated square Sterilin square dishes (one per vial) and incubated for 7 days with media topped up on days 2 and 5 using 5 ml of complete DMEM containing 50 ng/ml of hM-CSF. On day 7, adherent cells were lifted with 10 ml of cold PBS and cell lifters, counted, and seeded at a 5×10^4 cells/ml density for all experiments in 100 µl per well in a 96-well plate in complete DMEM containing 50 ng/ml of hM-CSF and 100 ng/ml of mIFN-γ for ~24 hours.

Isolation of $CD14^+$ human monocytes

Peripheral blood mononuclear cells (PBMCs) were isolated from anonymized, healthy donor blood cones (obtained from NHS Oxford blood bank). Blood volume was adjusted to 25 ml using HBSS supplemented with 0.3 mM EDTA. PBMCs were isolated by Ficoll gradient centrifugation (700*g,* 25 min, room temperature, without brake), transferred to a fresh tube, and washed twice in 50 ml supplemented HBSS (500*g*, 10 min at room temperature). From PBMCs, $CD14^+$ monocytes were positively selected using MagniSort™ Positive Selection Protocol according to the manufacturer's instructions, and then frozen in 90% FBS, 10% DMSO at a concentration of 3×10^7 cells per vial.

Generation of HMDMs from frozen $CD14^+$ monocytes

Frozen $CD14^+$ monocytes were thawed, diluted in complete RPMI and centrifuged at 500*g* for 3 min at room temperature to remove DMSO. The pellet was resuspended in complete RPMI supplemented with 100 ng/ml of hM-CSF. Cells were plated in 10 cm TC-treated dishes and differentiated into HMDMs for 7 days at 37°C with 5% CO_2, with media topped up on days 2 and 5 using 5 ml of complete RPMI containing 100 ng/ml of hM-CSF. On day 7, adherent cells were lifted with cold PBS (incubated in the fridge for 10 min to aid detachment) and cell lifters, counted and seeded at a 5×10^4 cells/ml density for all experiments, in 100 µl per well in a 96-well plate, in complete RPMI containing 100 ng/ml of hM-CSF. For uptake and activation assays, cells were also primed with 100 ng/ml of hIFN-γ for ~24-hours.

Murine OT-I T cell isolation

Spleens and lymph nodes were harvested from OT-I TCR transgenic mice and mechanically homogenized by dissociating tissue through a 70-µm cell strainer using a syringe plunger. CD8 T cells were then isolated using the MojoSort™ $CD8^+$ T-cell isolation kit and magnets, in accordance with the manufacturer's protocol. Isolated OT-I cells were resuspended in complete RPMI (data file S1) and used for antigen presentation assays.

Expression of TRIM21 in HeLa cells and its release by cell death

TRIM21 expression constructs

The following antigen sequences were purchased from ThermoFisher Scientific: TRIM21_w_PRYSPRY, TRIM21_NO_PRYSPRY, TRIM21_FcMut, HIV_NES. These cDNA sequences were subcloned N-terminally to the fluorescent-protein tag of the pHR-mEGFP expression vector (data file S2), kindly supplied by Dr. A. Mørch (Kennedy Institute of Rheumatology, University of Oxford). Sequences encoded the open reading frames of TRIM21/Ro52 protein (Gene ID: 6737, NCBI Reference Sequence: NM_003141.4). Sequences were modified to contain the following: suitable restriction sites, Kozak sequence upstream of the open reading frame, and, for GFP fusion proteins, a GGSSGG linker between the last codon of TRIM21 and the first codon of the mEGFP tag. WT TRIM21 (w_PRYSPRY) is a full-length construct (aa 476), whilst TRIM21_NO_PRYSPRY is a truncated protein construct with no PRYSPRY (aa 1 to 276). TRIM21_FcMUT (aa 476) contains two point mutations (W381A/W383A) within the PRYSPRY domain. HeLa cells expressing TRIM21 constructs were prepared by lentiviral transduction as detailed in Supplemental Materials and Methods.

Induction of cell death in HeLa expressing TRIM21-GFP

Unless otherwise stated, before treatments, HeLa_TRIM21_w_PRYSPRY-GFP, HeLa_TRIM21_NO_PRYSPRY-GFP, or HeLa_TRIM21_FcMUT-GFP were seeded in 96-well culture plates at a density of 20,000 cells per well in 100 µl supplemented DMEM and incubated overnight at 37°C.

Pyroptosis via noncanonical inflammasome

Cells were preprimed with 10 ng/ml of hIFN-γ during seeding. To induce pyroptosis, LPS transfection mixture was prepared (material for one well): 2 μg of LPS (from stock 1 mg/ml) or 2 μl of Opti-MEM (for mock transfection control) in 10 μl of prewarmed Opti-MEM, vigorously vortexed for 30 s and centrifuged briefly before adding 0.5 μl of Lipofectamine 2000. The mixture was flicked 10 to 15 times and incubated at room temperature for 20 min. During this incubation, the cells were washed and the media replaced with 100 μl of Opti-MEM. After 20 min, an additional 90 μl of Opti-MEM was added to the transfection mixture, and the final 100 μl of transfection mix was added to the cells. Cells were centrifuged for 5 min, 500*g* at 37°C and returned to the incubator for 24 hours.

Apoptosis

Media was replaced with 200 μl of fresh Opti-MEM and cells treated for 2 hours with ABT-737 (1 μM) and S63845 (10 μM). The uppermost 150 μl of SN was collected into low-protein-binding tubes without disturbing the cells and stored at 4°C for downstream analyses within 24 hours.

Detergent lysis

Cells were lifted with prewarmed trypsin/EDTA (50 μl per well), pooled, transferred to low-binding microfuge tubes, washed, and lysed in 50 μl per well cold Pierce IP lysis buffer for 30 min. The insoluble fraction was removed by centrifugation at 16,400*g* (5 min, 4°C), and SNs were transferred to fresh low-binding microfuge tubes on ice for downstream analyses within 24 hours.

Needle shear lysis

Medium was replaced with 200 μl of cold PBS, cells were lifted and passed forcibly, approximately 20 times, through a fine 30G needle with additional scraping at the base of the well to aid resuspension. The plate was centrifuged at 500*g* for 5 min, and the uppermost 150 μl of SN was collected in low-protein-binding microfuge tubes on ice for downstream analyses within 24 hours.

Preparation and analysis of TRIM21-ICs

Magnetic GFP-trap agarose co-IP of TRIM21 and antibodies

Thirty microliters of SN/lysate (UT cells, needle sheer lysate, or Opti-MEM only) was mixed with 10 μl of 4X Laemmli loading buffer containing 40 mM DTT, boiled for 5 min at 95°C, and stored at −20°C as an input control for IP.

One milliliter of each SN sample was mixed with 0.01 mg/ml of normal human serum (final concentration of total serum proteins), diluted to final of 500 μl of cold Pierce IP lysis buffer in low binding microfuge tube, and incubated at 4°C for 2 hours under rotation. Magnetic GFP-trap agarose beads were washed in Pierce IP lysis buffer, and 30 μl of beads were added to each sample for incubation at 4°C for 1 hour under rotation. Samples were washed four times with 500 μl cold Pierce IP lysis buffer, transferred to fresh low-binding tubes and washed once with cold 1X TBS pH 7.4 (150 mM Tris, 50 mM NaCl). Beads were resuspended in 15 μl of elution buffer (100 mM Glycine, pH 2.5) and incubated for 10 min on a room temperature rocker at high speed. Tubes were gently flicked every 2 to 3 min to mix the beads. Final collection tubes were prepared by adding 15 μl of neutralizing 1M Tris pH 8.0 into each tube. These tubes were then placed on ice. Sample tubes were magnetized and 15 μl of SN was transferred into the neutralizing tubes, discarding the beads. Ten microliters of 4X Laemmli loading buffer

containing 40 mM DTT was added. This final eluate sample was stored at −20°C in preparation for immunoblotting.

Micropurification of TRIM21-GFP and IC formation

A single T75 flask of ~80% confluent HeLa_TRIM21_w_PRYSPRY-GFP cells was lifted by trypsin-EDTA, washed in PBS and lysed at 4°C for 30 min with 2 ml of cold Pierce IP buffer. After removing insoluble debris by centrifuging at 16,400*g*, 5 min at 4°C. SN were transferred into fresh low-protein-binding tubes, TRIM21-GFP was captured and eluted as described in "Magnetic GFP-trap agarose co-IP of TRIM21 and antibodies". The 30-µl elution volume was brought to 200 µl with 170 µl Opti-MEM. To the relevant samples, the following antibodies were added: normal human serum (0.01 mg/ml final concentration) or patient/HC plasma (1:100 dilution). To generate TRIM21-OVA ICs, the following initial concentrations/dilutions were used: OVA (10 µg/ml), rabbit α-OVA antiserum (1:100), and normal rabbit serum (1:100). Samples were serially diluted to obtain 10X solutions, which gave final OVA concentrations in culture of 10 ng/ml, 100 ng/ml, and 1000 ng/ml. Samples were incubated at 4°C for 2 hours under rotation for IC formation.

LIPS assay

We used the LIPS assay (*81, 82*) to determine relative levels of anti-Ro52 autoantibodies in patient and control plasma samples. Plasmids encoding the autoantigen-Renilla luciferase fusion proteins [i.e,. pREN-2_Ro52_Luc (encoding a truncated TRIM21 lacking the PRYSPRY domain, fused to luciferase), pREN-2_Ro60_Luc, and pREN-2_La_Luc] were generously provided by Dr. P. Burbelo, National Institute of Dental and Craniofacial Research, NIH, USA. Luciferase activity was measured using a Berthold Luminometer with the following settings: 50 µl of 1X Renilla luciferase substrate was directly added into the wells, with a 2-s shake, followed by a 5-s luminescence read.

BN-PAGE

HeLa_TRIM21_w_PRYSPRY-GFP or HeLa_TRIM21_FcMUT-GFP were washed once with 200 µl of PBS and lysed in 50 µl prepared NativePAGE™ Sample Buffer containing 1% digitonin. Triplicate cell lysate wells were pooled (150 µl), transferred to low-protein-binding tubes, and centrifuged at 16,400*g* for 30 min at 4°C using a table-top microcentrifuge. SN were transferred to new low-protein-binding tubes on ice without disturbing the pellet. The following relevant materials were added to the 150-µl sample tubes: 0.01 mg/ml (final concentration) of normal human serum or 1:100 final dilutions of patient/HC plasma. Additional tubes were prepared containing 1:100 final dilutions of patient/HC plasma in 150 µl of lysis buffer alone. Sample tubes were incubated under rotation at 4°C for 2 hours.

After incubation, 19 µl of the sample was transferred to fresh microcentrifuge tubes and the remaining material was stored at −20°C. One microliter of 5% G-250 BN-PAGE additive was added to the samples just before loading the gel. One microliter of 5% G-250 sample additive was also added to 19 µl of Invitrogen™ NativeMark™ Unstained Protein Standard.

Samples were run on 4 to 16% native PAGE gels and transferred to methanol-activated PVDF membranes following the manufacturer's recommendation. Antibodies used for immunoblot are listed in data file S1, and proteins were visualized by ECL detection. Between TRIM21 and anti-human IgG detection, the membranes were stripped using Restore™ Western Blot Stripping Buffer.

IC formation and analysis by FIDA

A single T75 flask of ~80% confluent HeLa_TRIM21_w_PRYSPRY-GFP cells was lifted by trypsin-EDTA, washed in PBS and lysed at 4°C for 30 min with 1 ml of cold native PAGE

buffer containing 1% digitonin in low-protein-binding tubes. Insoluble debris was removed by centrifuging at 16,400*g*, 5 min at 4°C. 30 µl SN were transferred into fresh low-protein-binding tubes, and where relevant, plasma was added in a 1:10 ratio (3 µl per sample) and incubated under rotation for 2 hours at 4°C. Samples were analyzed fresh by FIDA as detailed in Supplementary Materials and Methods.

Analysis of TRIM21-IC uptake and processing by BMDM and HMDM

TRIM21-IC uptake assays

BMDM and HMDM were IFN-γ–primed for 24 hours, cells were washed, and media replaced with 100 µl of prewarmed Opti-MEM to remove serum. To block degradation, cells were treated 2 hours before feeding with 10 nM BafA1 or 10 µM MG132. To inhibit uptake, cells were treated 1 hour before feeding with 5 µM cytochalasin D (CytoD). The negative control 4°C plate was prechilled on ice for ~10 min before the experiment. TRIM21-GFP proteins were eluted from GFP-trap and complexed with normal human serum or patient plasma, as described in "Micropurification of TRIM21-GFP and IC formation" and 10 µl was added to cells. The following IC were used: TRIM21_w_PRYSPRY-GFP (± normal human serum), TRIM21_FcMUT-GFP (± normal human serum), TRIM21_w_PRYSPRY-GFP (± HC plasma), or TRIM21_w_PRYSPRY-GFP (± patient plasma). Plates were returned to 37°C incubator, control plate remained on ice. After 5, 15, 30, and 60 min, the media was aspirated, and cells were washed three times with excess cold PBS to remove unbound TRIM21 and antibodies. Cells were lysed in 30 µl of lysis buffer (66 mM Tris-HCl (pH 7.4), 2% SDS) and triplicate wells were pooled for analysis. Lysates were collected and stored at −20°C.

Imaging TRIM21-IC processing in macrophages

BMDMs were seeded in µ-Slide 8 Well High ibiTreat (ibidi.com) culture plates at a density of 50,000 cells per well in 300 µl complete DMEM with 50 ng/ml of rhM-CSF, primed with mIFN-γ and incubated overnight. Cells were washed and media replaced with 200 µl of prewarmed Opti-MEM before feeding with GFP-trap eluted TRIM21-GFP. Where relevant, cells were preincubated for 2 hours with 10 µM MG132 before feeding. For wells receiving TRIM21-GFP complexed with 0.01 mg/ml of normal human serum, 100 µl of Opti-MEM was gently removed from the top of the well and replaced with 100 µl of TRIM21-GFP (+ antibodies). Plates were incubated for 60 min at 37°C and 5% CO_2.

Bead or monosodium urate treatment

IFN-γ–primed BMDMs were seeded as described above. Bead-supported lipid bilayers (BSLBs) were prepared as previously described (83) and following washes with HBSS, 2 µg/ml of RH5-His was incubated with the beads before opsonization with an anti-RH5 hIgG1 antibody. The opsonized beads at a concentration of 1×10^6 beads/ml of BSLBs were fed to cells in 300 µl of Opti-MEM and incubated for 1 hour for uptake. MSU crystals were resuspended in ultrapure water according to the manufacturer's instructions. Cells were treated with 125 µg/ml of monosodium urate (MSU) diluted in prewarmed Opti-MEM and incubated for 3 hours for sufficient uptake.

Fixation

Media was aspirated from the µ-Slide 8 Well High ibiTreat culture plates and cells were gently washed twice with 300 µl of prewarmed PBS per well. Cells were fixed with 4% PFA (prepared in PBS) and incubated for 20 min at room temperature. Cells were washed twice with sterile-filtered HBSS wash buffer with 0.1% BSA (see data file S1).

Triton X-100 permeabilization

Two hundred microliters of 0.5% Triton® X-100 (v/v) prepared in HBSS wash buffer was added to each well. Plates were incubated for 5 min, covered, at room temperature. Wells were blocked with 5% BSA prepared in HBSS wash buffer for 1 hour at room temperature. Antibody staining solutions were prepared in HBSS wash buffer. The following antibodies were used: anti-GFP-AF488 (1 µl per well), anti-EEA1-AF594 (2 µl per well), Phalloidin-AF405 (1:100 dilution), sources described in data file S1. Staining was 2 hours, covered, at room temperature. Plates were washed three times with 300 µl per well HBSS wash buffer, then stored with 300 µl per well PBS at 4°C, covered, until image acquisition.

Saponin permeabilization

Two hundred microliters of sterile-filtered 0.1% saponin permeabilization solution (prepared in HBSS wash buffer) was added to each well. Plates were incubated for 20 min, covered, at room temperature. Wells were blocked for 1 hour at room temperature, with 5% BSA, prepared in HBSS wash buffer containing 0.02% saponin. Antibody staining and imaging were conducted as described for Triton X-100, except that staining and washing steps used HBSS wash buffer containing 0.02% saponin.

Image acquisition, visualization, scoring and statistical testing

Samples were imaged, within 72 hours of preparation, on a Zeiss LSM980 Airyscan 2 microscope using a C-Apochromat 40X/1.2 NA objective in confocal unidirectional line scanning mode (scan speed:5, pixel time: 3.26 µs). Sample acquisition was performed on Zeiss Zen Blue v3.3 software, using 405 nm (for phalloidin-405), 488 nm (for anti-GFP Alexa Fluor (AF) 488), 594 nm (for AF594), and 639 nm (for AF647) lasers to excite fluorophores. For EEA1 staining, simultaneous 488 nm and 594 nm laser excitation was used, followed by 405 nm laser excitation, with a pinhole of 38 µm (1 AU at 488 nm). For Galectin-3 staining, simultaneous 488 nm and 647 nm laser excitation was used, followed by 405 nm laser excitation, with a pinhole of 38 µm (1 AU at 488 nm). Detection used either a 32 channel GaAsP-PMT, with an emission band of 499-570 nm for 488 nm, or a 2 channel Multialkali-PMT detector, with emission bands of 396-495 nm, 602-759 nm, and 643-759 nm for AF405, AF594 and AF647 respectively. Confocal image analysis was performed in FIJI (ImageJ) v1.54p. Confocal images were converted to 8-bit files and then a threshold of 8-255 was set on the phalloidin staining segment cell area. Macrophage area was segmented on the phalloidin staining, followed by analysing TRIM21-GFP staining area and Galectin-3 staining area. Positive staining area was then summed and divided by the phalloidin positive area per image. For TRIM21-GFP – EEA1 co-localisation analysis, macrophage area, segmented by phalloidin staining, was used as a mask to perform co-localisation analysis using default settings on Coloc2 in FIJI (ImageJ) v1.54p, comparing TRIM21-GFP staining and EEA1 staining. Pearson correlation co-efficient (PCC) for TRIM21-GFP vs EEA1 was reported. At least five images were taken per treatment condition, obtaining adequate cell numbers for unbiased scoring. Image statistical testing was performed using GraphPad Prism (v10.0.3). The %GFPhi area per cell area (per image) comparisons between conditions were analyzed using ordinary one-way ANOVA, with Tukey's post-hoc testing. The % Gal-3^{hi} area per cell area (per image) comparisons were analyzed by a two-tailed unpaired *t* test between the preselected pair of UT MG132 and TRIM21 MG132.

BMDM Ub-TUBE assay

BMDMs were plated at 2×10^6 cells per well in TC-treated flat-bottom six-well plates and primed with 100 ng/ml of mIFN-γ. Two hours before feeding, BMDMs were washed and media replaced with 1 ml of OptiMEM ± 10 µM MG132. Cells were fed with 100 µl of GFP-trap–

eluted TRIM21 (± complexed with antibodies), for 60 min. Cells were gently washed three times with room temperature PBS to remove unbound TRIM21/antibodies, and then lysed in 500 µl of cold Pierce IP-lysis buffer in low protein-binding microfuge tubes at 4°C for 30 min. Insoluble debris was removed by centrifugation at 16,400*g*, 5 min at 4°C and SNs were transferred to fresh low-binding microfuge tubes. Thirty microliters of each SN sample was transferred to a fresh tube and combined with 10 µl of 4X Laemmli loading buffer containing 40 mM DTT, boiled at 95°C for 5 min and stored at −20°C as an input control. Magnetic Ub-TUBE pull-down and protein elution were done using the same methods as for "Magnetic GFP-Trap Agarose co-IP of TRIM21 and Antibodies". To the 30 µl elution volume, 10 µl of 4X Laemmli loading buffer containing 40 mM DTT, was added. This was the final eluate sample, which was boiled at 95°C for 5 min and stored at −20°C ready for immunoblotting.

Statistical analyses

Immunoblots were quantified using FIJI (ImageJ) v1.54p, according to a previously published protocol (*90*). Results were analyzed using GraphPad Prism v9 by ordinary one-way ANOVA, multiple mean comparisons between either: UT and treated conditions or preselected pairs. Post-hoc testing used either Fisher's least significant difference or Tukey's post-test, as indicated in figure legends. *$P \leq 0.05$, **$P \leq 0.01$, and ***$P \leq 0.001$.

Supplementary Materials

Supplementary Materials and Methods

Fig. S1. Single-channel greyscale images of multiplex CellDive data shown in Fig. 1.

Fig. S2. TRIM21 overexpression and antibody controls.

Fig. S3. LIPS assay and BN-PAGE.

Fig. S4. Semiquantification of 70 kDa TRIM21-GFP protein in BMDMs treated with TRIM21 or TRIM21-NHS ICs.

Fig. S5. BMDM uptake of TRIM21-GFP or TRIM21-GFP_ICs produced with HC or SjD plasma.

Fig. S6. HMDM uptake of TRIM21-GFP or TRIM21-GFP_ICs produced with HC or SjD plasma.

Fig. S7. Roles of Fcγ receptors and actin-dependent phagocytosis in TRIM21-IC uptake.

Fig. S8. Internalized TRIM21 escapes into cytosols and is preferentially degraded by the proteasome.

Fig. S9. TRIM21-OVA antigen presentation in vitro experimental set up and analysis.

Fig. S10. TRIM21-OVA antigen presentation in vitro, summary of TCR changes.

Fig. S11. Proinflammatory and transcriptional changes in HMDM following TRIM21 and TRIM21-IC feeding.

Fig. S12. KEGG gene set enrichment analysis of RNA sequencing results.

Fig. S13. Biocarta gene set enrichment analysis of RNA sequencing results.

Fig. S14. Differential expression of metabolic genes.

Table S1. Table S1. Sicca and SjD SG biopsy information.

Table S2. Table S2. Plasma samples used in this study.

Data file S1. List of all reagents, resources and commercial sources used in this manuscript. Antibody dilutions and applications are listed. Media and buffers, including their application are listed.

Data file S2. Sequences and maps of TRIM21-GFP expression constructs.

Data file S3. Raw tabulated data for all figures.

Data file S4. Full uncut images of all immunoblots.

Movie S1. Live microscopy of HeLa cells overexpressing TRIM21-GFP undergoing apoptosis.

MDAR Reproducibility Checklist

Acknowledgements: We thank members of the L.B.D, J.S.B., A.G., and A.J.C. laboratories for helpful discussions. We also thank everyone at the Kennedy Institute of Rheumatology Digital Pathology Omics Core and Cell Dynamics Core for their technical expertise and support in multicolor imaging and flow cytometry. Henrietta Lacks and the HeLa cell line established from her tumor cells without her knowledge or consent in 1951, have made significant contributions to scientific progress and advances in human health. We are grateful to Henrietta Lacks, now deceased, and her surviving family members for their contributions to biomedical research.

Funding: This research was supported by Kennedy Trust for Rheumatology Research Studentship KENN 192001 (E.L.J.E.), Henni Mester Fellowship, University College, University of Oxford (E.L.J.E.), Wellcome Trust Collaborative Award 224343/Z/21/Z (M.A.W.), Oxford-Bristol Myers Squibb Celgene Research Fellowship Programme Project 2302 (L.B.D.), Kennedy Trust for Rheumatology Research KENN212202 (J.S.B.) and KENN202112 (A.G.), Medical Research Council MR/W001217/1 (J.S.B.), and NIHR Birmingham Biomedical Research Centre NIHR 203326 (B.A.F.). The views expressed in this publication are those of the authors and not necessarily those of the NHS, the NIHR or the Department of Health.

Author contributions: Conceptualization: E.L.J.E., B.D., J.S.B., and L.B.D. Funding acquisition: A.G., J.S.B., and L.B.D. Investigation: E.L.J.E., B.D., M.M.E.d.J., H.C., G.H., Y.F.Y., and A.J.C. Methodology: E.L.J.E., B.D., M.M.E.d.J., H.C,. S.H., R.E.G., G.H., S.N., M.A.W., J.R.F., M.S.C., and G.J.M. Project administration: E.J.E., J.S.B., and L.B.D. Supervision: B.A.F., A.G., A.J.C., J.S.B., and L.B.D. Visualization: E.L.J.E., M.M.E.d.J., and J.R.F. Writing—original draft: E.L.J.E. Writing—review and editing: E.L.J.E., J.S.B., L.B.D., A.J.C., and A.G.

Competing interests: B.A.F. has undertaken consultancy or participated in advisory boards in the field of Sjogren's Disease for Novartis, BMS, Servier, Galapagos, Roche, Sanofi, Johnson & Johnson, AstraZeneca, Otsuka, Amgen, Kiniksa, Cullinan, OneFour Bio, Spero and Catalys Pacific. No financial support from any of the above parties was received for any part of the work reported in this manuscript. These organisations had no part in the design or reporting of this study. All other authors declare that they have no competing interests.

Data, code, and materials availability: RNA-seq data have been deposited in a GEO database with accession number GSE318852. TRIM21-GFP constructs were generated by the authors

and are available upon reasonable request. All other materials are commercially available [or were obtained via MTA from outside sources as described in Materials and Methods. A list of media, reagents, and mice is provided in data file S1. TRIM21-GFP construct sequences are provided in data file S2. Uncropped protein immunoblots are provided in data file S3. Tabulated data underlying the figures are provided in data file S4. All other data are available in the main text or the supplementary materials.

REFERENCES AND NOTES

1. P. Brito-Zeron, C. Baldini, H. Bootsma, S. J. Bowman, R. Jonsson, X. Mariette, K. Sivils, E. Theander, A. Tzioufas, M. Ramos-Casals, Sjogren syndrome. *Nat Rev Dis Primers* **2**, 16047 (2016).

2. P. C. Fox, Autoimmune diseases and Sjogren's syndrome: an autoimmune exocrinopathy. *Ann N Y Acad Sci* **1098**, 15–21 (2007).

3. S. Rani, M. K. Sunil, K. Jaskirat, K. Dilip, Sjogren′s Syndrome: A Review. *Journal of Indian Academy of Oral Medicine and Radiology* **23**, 61–64 (2011).

4. M. Ramos-Casals, P. Brito-Zeron, B. Kostov, A. Siso-Almirall, X. Bosch, D. Buss, A. Trilla, J. H. Stone, M. A. Khamashta, Y. Shoenfeld, Google-driven search for big data in autoimmune geoepidemiology: analysis of 394,827 patients with systemic autoimmune diseases. *Autoimmun Rev* **14**, 670–679 (2015).

5. K. Psianou, I. Panagoulias, A. D. Papanastasiou, A. L. de Lastic, M. Rodi, P. I. Spantidea, S. E. Degn, P. Georgiou, A. Mouzaki, Clinical and immunological parameters of Sjogren's syndrome. *Autoimmun Rev* **17**, 1053–1064 (2018).

6. F. Chowdhury, A. Tappuni, M. Bombardieri, Biological Therapy in Primary Sjogren's Syndrome: Effect on Salivary Gland Function and Inflammation. *Front Med (Lausanne)* **8**, 707104 (2021).

7. B. A. Fisher, R. Jonsson, T. Daniels, M. Bombardieri, R. M. Brown, P. Morgan, S. Bombardieri, W. F. Ng, A. G. Tzioufas, C. Vitali, P. Shirlaw, E. Haacke, S. Costa, H. Bootsma, V. Devauchelle-Pensec, T. R. Radstake, X. Mariette, A. Richards, R. Stack, S. J. Bowman, F. Barone, E. Sjogren's histopathology workshop group from, Standardisation of labial salivary gland histopathology in clinical trials in primary Sjogren's syndrome. *Ann Rheum Dis* **76**, 1161–1168 (2017).

8. F. Franceschini, I. Cavazzana, L. Andreoli, A. Tincani, The 2016 classification criteria for primary Sjogren's syndrome: what's new? *BMC Med* **15**, 69 (2017).

9. L. Shen, L. Suresh, M. Lindemann, J. Xuan, P. Kowal, K. Malyavantham, J. L. Ambrus, Jr., Novel autoantibodies in Sjogren's syndrome. *Clin Immunol* **145**, 251–255 (2012).

10. S. Veenbergen, A. Kozmar, P. L. A. van Daele, M. W. J. Schreurs, Autoantibodies in Sjogren's syndrome and its classification criteria. *J Transl Autoimmun* **5**, 100138 (2022).

11. E. L. Jones, S. M. Laidlaw, L. B. Dustin, TRIM21/Ro52 - Roles in Innate Immunity and Autoimmune Disease. *Front Immunol* **12**, 738473 (2021).

12. H. T. Wang, S. Hur, Substrate recognition by TRIM and TRIM-like proteins in innate immunity. *Semin Cell Dev Biol* **111**, 76–85 (2021).

13. M. Vaysburd, R. E. Watkinson, H. Cooper, M. Reed, K. O'Connell, J. Smith, J. Cruickshanks, L. C. James, Intracellular antibody receptor TRIM21 prevents fatal viral infection. *Proc Natl Acad Sci U S A* **110**, 12397–12401 (2013).

14. C. Dickson, A. J. Fletcher, M. Vaysburd, J. C. Yang, D. L. Mallery, J. Zeng, C. M. Johnson, S. H. McLaughlin, M. Skehel, S. Maslen, J. Cruickshank, N. Huguenin-Dezot, J. W. Chin, D. Neuhaus, L. C. James, Intracellular antibody signalling is regulated by phosphorylation of the Fc receptor TRIM21. *Elife* **7**, (2018).

15. A. Fletcher, D. Clift, E. de Vries, S. Martinez Cuesta, T. Malcolm, F. Meghini, R. Chaerkady, J. Wang, A. Chiang, S. H. S. Weng, J. Tart, E. Wong, G. Donohoe, P. Rawlins, E. Gordon, J. D. Taylor, L. James, J. Hunt, A TRIM21-based bioPROTAC highlights the therapeutic benefit of HuR degradation. *Nat Commun* **14**, 7093 (2023).

16. J. Benn, S. Cheng, S. Keeling, A. E. Smith, M. J. Vaysburd, D. Boken, L. V. C. Miller, T. Katsinelos, C. Franco, E. Dupre, C. Danis, I. Landrieu, L. Buee, D. Klenerman, L. C. James, W. A. McEwan, Aggregate-selective removal of pathological tau by clustering-activated degraders. *Science* **385**, 1009–1016 (2024).

17. J. Reusch, L. E. Franken, J. Then, P. Ringler, J. Butzer, T. Juroschek, C. Klein, T. Schlothauer, L. Lariviere, TRIM21 and Fc-engineered antibodies: decoding its complex antibody binding mode with implications for viral neutralization. *Front Immunol* **15**, 1401471 (2024).

18. M. Uhlen, L. Fagerberg, B. M. Hallstrom, C. Lindskog, P. Oksvold, A. Mardinoglu, A. Sivertsson, C. Kampf, E. Sjostedt, A. Asplund, I. Olsson, K. Edlund, E. Lundberg, S. Navani, C. A. Szigyarto, J. Odeberg, D. Djureinovic, J. O. Takanen, S. Hober, T. Alm, P. H. Edqvist, H. Berling, H. Tegel, J. Mulder, J. Rockberg, P. Nilsson, J. M. Schwenk, M. Hamsten, K. von Feilitzen, M. Forsberg, L. Persson, F. Johansson, M. Zwahlen, G. von Heijne, J. Nielsen, F. Ponten, Proteomics. Tissue-based map of the human proteome. *Science* **347**, 1260419 (2015).

19. S. Caruso, I. K. H. Poon, Apoptotic Cell-Derived Extracellular Vesicles: More Than Just Debris. *Front Immunol* **9**, 1486 (2018).

20. C. T. Mayer, J. P. Nieke, A. Gazumyan, M. Cipolla, Q. Wang, T. Y. Oliveira, V. Ramos, S. Monette, Q. Z. Li, M. E. Gershwin, H. Kashkar, M. C. Nussenzweig, An apoptosis-dependent checkpoint for autoimmunity in memory B and plasma cells. *Proc Natl Acad Sci U S A* **117**, 24957–24963 (2020).

21. U. E. Schaible, F. Winau, P. A. Sieling, K. Fischer, H. L. Collins, K. Hagens, R. L. Modlin, V. Brinkmann, S. H. Kaufmann, Apoptosis facilitates antigen presentation to T lymphocytes through MHC-I and CD1 in tuberculosis. *Nat Med* **9**, 1039–1046 (2003).

22. Z. Szondy, Z. Sarang, B. Kiss, E. Garabuczi, K. Koroskenyi, Anti-inflammatory Mechanisms Triggered by Apoptotic Cells during Their Clearance. *Front Immunol* **8**, 909 (2017).

23. D. Frank, J. E. Vince, Pyroptosis versus necroptosis: similarities, differences, and crosstalk. *Cell Death Differ* **26**, 99–114 (2019).

24. J. Zhou, J. L. Pathak, Q. Liu, S. Hu, T. Cao, N. Watanabe, Y. Huo, J. Li, Modes and Mechanisms of Salivary Gland Epithelial Cell Death in Sjogren's Syndrome. *Adv Biol (Weinh)* **7**, e2300173 (2023).

25. N. Del Papa, A. Minniti, M. Lorini, V. Carbonelli, W. Maglione, F. Pignataro, N. Montano, R. Caporali, C. Vitali, The Role of Interferons in the Pathogenesis of Sjogren's Syndrome and Future Therapeutic Perspectives. *Biomolecules* **11**, (2021).

26. H. Li, J. A. Ice, C. J. Lessard, K. L. Sivils, Interferons in Sjogren's Syndrome: Genes, Mechanisms, and Effects. *Front Immunol* **4**, 290 (2013).

27. C. Vitali, S. Bombardieri, R. Jonsson, H. M. Moutsopoulos, E. L. Alexander, S. E. Carsons, T. E. Daniels, P. C. Fox, R. I. Fox, S. S. Kassan, S. R. Pillemer, N. Talal, M. H. Weisman, S. European Study Group on Classification Criteria for Sjogren's, Classification criteria for Sjogren's syndrome: a revised version of the European criteria proposed by the American-European Consensus Group. *Ann Rheum Dis* **61**, 554–558 (2002).

28. M. Izumi, K. Eguchi, H. Nakamura, S. Nagataki, T. Nakamura, Premature fat deposition in the salivary glands associated with Sjogren syndrome: MR and CT evidence. *AJNR Am J Neuroradiol* **18**, 951–958 (1997).

29. M. Polihronis, N. I. Tapinos, S. E. Theocharis, A. Economou, C. Kittas, H. M. Moutsopoulos, Modes of epithelial cell death and repair in Sjogren's syndrome (SS). *Clin Exp Immunol* **114**, 485–490 (1998).

30. N. Kaneko, H. Chen, C. A. Perugino, T. Maehara, R. Munemura, S. Yokomizo, J. Sameshima, T. J. Diefenbach, K. R. Premo, A. Chinju, Y. Miyahara, M. Sakamoto, M. Moriyama, J. H. Stone, S. Nakamura, S. Pillai, Cytotoxic CD8(+) T cells may be drivers of tissue destruction in Sjogren's syndrome. *Sci Rep* **12**, 15427 (2022).

31. K. L. Rock, H. Kono, The inflammatory response to cell death. *Annu Rev Pathol* **3**, 99–126 (2008).

32. D. A. Rhodes, G. Ihrke, A. T. Reinicke, G. Malcherek, M. Towey, D. A. Isenberg, J. Trowsdale, The 52 000 MW Ro/SS-A autoantigen in Sjogren's syndrome/systemic lupus erythematosus (Ro52) is an interferon-gamma inducible tripartite motif protein associated with membrane proximal structures. *Immunology* **106**, 246–256 (2002).

33. W. A. McEwan, B. Falcon, M. Vaysburd, D. Clift, A. L. Oblak, B. Ghetti, M. Goedert, L. C. James, Cytosolic Fc receptor TRIM21 inhibits seeded tau aggregation. *Proc Natl Acad Sci U S A* **114**, 574–579 (2017).

34. S. Foss, M. Bottermann, A. Jonsson, I. Sandlie, L. C. James, J. T. Andersen, TRIM21-From Intracellular Immunity to Therapy. *Front Immunol* **10**, 2049 (2019).

35. F. Yang, Y. He, Z. Zhai, E. Sun, Programmed Cell Death Pathways in the Pathogenesis of Systemic Lupus Erythematosus. *J Immunol Res* **2019**, 3638562 (2019).

36. C. L. Holley, M. Monteleone, D. Fisch, A. E. S. Libert, R. J. Ju, J. H. Choi, N. D. Condon, S. Emming, J. Crawford, G. Lawrence, J. R. Coombs, J. G. Lefevre, R. Bajracharya, M. H. Lahoud, A. S. Yap, N. Hamilton, S. J. Stehbens, J. C. Kagan, N. Ariotti, S. S. Burgener, K. Schroder, Pyroptotic cell corpses are crowned with F-actin-rich filopodia that engage CLEC9A signaling in incoming dendritic cells. *Nat Immunol* **26**, 42–52 (2025).

37. S. Gupta, A. Agrawal, S. Agrawal, H. Su, S. Gollapudi, A paradox of immunodeficiency and inflammation in human aging: lessons learned from apoptosis. *Immun Ageing* **3**, 5 (2006).

38. C. L. Evavold, J. Ruan, Y. Tan, S. Xia, H. Wu, J. C. Kagan, The Pore-Forming Protein Gasdermin D Regulates Interleukin-1 Secretion from Living Macrophages. *Immunity* **48**, 35–44 e36 (2018).

39. R. Heilig, M. S. Dick, L. Sborgi, E. Meunier, S. Hiller, P. Broz, The Gasdermin-D pore acts as a conduit for IL-1beta secretion in mice. *Eur J Immunol* **48**, 584–592 (2018).

40. J. P. Borges, R. S. R. Saetra, A. Volchuk, M. Bugge, P. Devant, B. Sporsheim, B. R. Kilburn, C. L. Evavold, J. C. Kagan, N. M. Goldenberg, T. H. Flo, B. E. Steinberg, Glycine inhibits NINJ1 membrane clustering to suppress plasma membrane rupture in cell death. *Elife* **11**, (2022).

41. L. C. James, A. H. Keeble, Z. Khan, D. A. Rhodes, J. Trowsdale, Structural basis for PRYSPRY-mediated tripartite motif (TRIM) protein function. *Proc Natl Acad Sci U S A* **104**, 6200–6205 (2007).

42. A. H. Keeble, Z. Khan, A. Forster, L. C. James, TRIM21 is an IgG receptor that is structurally, thermodynamically, and kinetically conserved. *Proc Natl Acad Sci U S A* **105**, 6045–6050 (2008).

43. J. C. Santos, D. Boucher, L. K. Schneider, B. Demarco, M. Dilucca, K. Shkarina, R. Heilig, K. W. Chen, R. Y. H. Lim, P. Broz, Human GBP1 binds LPS to initiate assembly of a caspase-4 activating platform on cytosolic bacteria. *Nat Commun* **11**, 3276 (2020).

44. P. D. Burbelo, L. Y. Teos, J. L. Herche, M. J. Iadarola, I. Alevizos, Autoantibodies against the Immunoglobulin-Binding Region of Ro52 Link its Autoantigenicity with Pathogen Neutralization. *Sci Rep* **8**, 3345 (2018).

45. I. Wittig, H. P. Braun, H. Schagger, Blue native PAGE. *Nat Protoc* **1**, 418–428 (2006).

46. N. N. Poulsen, N. Z. Andersen, J. Østergaard, G. Zhuang, N. J. Petersen, H. Jensen, Flow induced dispersion analysis rapidly quantifies proteins in human plasma samples. *Analyst* **140**, 4365–4369 (2015).

47. B. Mantovani, M. Rabinovitch, V. Nussenzweig, Phagocytosis of immune complexes by macrophages. Different roles of the macrophage receptor sites for complement (C3) and for immunoglobulin (IgG). *J Exp Med* **135**, 780–792 (1972).

48. E. Uribe-Querol, C. Rosales, Phagocytosis: Our Current Understanding of a Universal Biological Process. *Front Immunol* **11**, 1066 (2020).

49. D. W. Goddette, C. Frieden, Actin polymerization. The mechanism of action of cytochalasin D. *J Biol Chem* **261**, 15974–15980 (1986).

50. J. Jia, A. Claude-Taupin, Y. Gu, S. W. Choi, R. Peters, B. Bissa, M. H. Mudd, L. Allers, S. Pallikkuth, K. A. Lidke, M. Salemi, B. Phinney, M. Mari, F. Reggiori, V. Deretic, Galectin-3 Coordinates a Cellular System for Lysosomal Repair and Removal. *Dev Cell* **52**, 69–87 e68 (2020).

51. S. Aits, Methods to Detect Loss of Lysosomal Membrane Integrity. *Methods Mol Biol* **1880**, 315–329 (2019).

52. I. Maejima, A. Takahashi, H. Omori, T. Kimura, Y. Takabatake, T. Saitoh, A. Yamamoto, M. Hamasaki, T. Noda, Y. Isaka, T. Yoshimori, Autophagy sequesters damaged lysosomes to control lysosomal biogenesis and kidney injury. *EMBO J* **32**, 2336–2347 (2013).

53. T. Shirahama, A. S. Cohen, Ultrastructural evidence for leakage of lysosomal contents after phagocytosis of monosodium urate crystals. A mechanism of gouty inflammation. *Am J Pathol* **76**, 501–520 (1974).

54. J. Zeng, A. F. Santos, A. S. Mukadam, M. Osswald, D. A. Jacques, C. F. Dickson, S. H. McLaughlin, C. M. Johnson, L. Kiss, J. Luptak, N. Renner, M. Vaysburd, W. A. McEwan, E. Morais-de-Sa, D. Clift, L. C. James, Target-induced clustering activates Trim-Away of pathogens and proteins. *Nat Struct Mol Biol* **28**, 278–289 (2021).

55. M. Anandapadamanaban, N. C. Kyriakidis, V. Csizmok, A. Wallenhammar, A. C. Espinosa, A. Ahlner, A. R. Round, J. Trewhella, M. Moche, M. Wahren-Herlenius, M. Sunnerhagen, E3 ubiquitin-protein ligase TRIM21-mediated lysine capture by UBE2E1 reveals substrate-targeting mode of a ubiquitin-conjugating E2. *J Biol Chem* **294**, 11404–11419 (2019).

56. J. D. Colbert, F. M. Cruz, K. L. Rock, Cross-presentation of exogenous antigens on MHC I molecules. *Curr Opin Immunol* **64**, 1–8 (2020).

57. K. Yamane, H. Nakamura, M. Hamasaki, Y. Minei, N. Aibara, T. Shimizu, A. Kawakami, M. Nakashima, N. Kuroda, K. Ohyama, Immune complexome analysis reveals the presence of immune complexes and identifies disease-specific immune complex antigens in saliva samples from patients with Sjogren's syndrome. *Clin Exp Immunol* **204**, 212–220 (2021).

58. A. C. Horsfall, L. M. Rose, R. N. Maini, Autoantibody synthesis in salivary glands of Sjogren's syndrome patients. *J Autoimmun* **2**, 559–568 (1989).

59. T. O. Hjelmervik, K. Petersen, I. Jonassen, R. Jonsson, A. I. Bolstad, Gene expression profiling of minor salivary glands clearly distinguishes primary Sjogren's syndrome patients from healthy control subjects. *Arthritis Rheum* **52**, 1534–1544 (2005).

60. O. Kimoto, J. Sawada, K. Shimoyama, D. Suzuki, S. Nakamura, H. Hayashi, N. Ogawa, Activation of the interferon pathway in peripheral blood of patients with Sjogren's syndrome. *J Rheumatol* **38**, 310–316 (2011).

61. F. Barcelos, C. Martins, R. Monteiro, J. Cardigos, T. Prussiani, M. Sitima, N. Alves, J. Vaz-Patto, J. Cunha-Branco, L. M. Borrego, Association between EBV serological patterns and lymphocytic profile of SjS patients support a virally triggered autoimmune epithelitis. *Sci Rep* **11**, 4082 (2021).

62. Y. Torii, J. I. Kawada, T. Murata, H. Yoshiyama, H. Kimura, Y. Ito, Epstein-Barr virus infection-induced inflammasome activation in human monocytes. *PLoS One* **12**, e0175053 (2017).

63. L. C. James, Intracellular antibody immunity and the cytosolic Fc receptor TRIM21. *Curr Top Microbiol Immunol* **382**, 51–66 (2014).

64. D. E. Otzen, A. K. Buell, H. Jensen, Microfluidics and the quantification of biomolecular interactions. *Curr Opin Struct Biol* **70**, 8–15 (2021).

65. M. N. Andersen, S. N. Al-Karradi, T. W. Kragstrup, M. Hokland, Elimination of erroneous results in flow cytometry caused by antibody binding to Fc receptors on human monocytes and macrophages. *Cytometry A* **89**, 1001–1009 (2016).

66. T. J. F. Pranzatelli, P. Perez, A. Ku, B. Matuck, K. Huynh, S. Sakai, M. Abed, S. I. Jang, E. Yamada, K. Dominick, Z. Ahmed, A. J. Oliver, R. Bogle, Q. T. Easter, A. N. Baer, E. Pelayo, Z. Khavandgar, D. E. Kleiner, M. T. Magone, S. Gupta, C. Lessard, A. D. Farris, P. D. Burbelo, D. Martin, R. J. Morell, C. Zheng, N. Rachmaninoff, J. Maldonado-Ortiz, K. M. Tyc, X. Qu, M. Aure, M. H. Dezfulian, R. Lake, S. A. Teichmann, D. L. Barber, L. C. Tsoi, A. G. Sowalsky, J. Liu, J. Gudjonsson, K. M. Byrd, P. L. F. Johnson, J. A. Chiorini, B. M. Warner, GZMK(+)CD8(+) T cells target a specific acinar cell type in Sjogren's disease. *Ann Rheum Dis*, (2025).

67. T. Xu, H. X. Zhu, X. You, J. F. Ma, X. Li, P. Y. Luo, Y. Li, Z. X. Lian, C. Y. Gao, Single-cell profiling reveals pathogenic role and differentiation trajectory of granzyme K+CD8+ T cells in primary Sjogren's syndrome. *JCI Insight* **8**, (2023).

68. K. A. Hogquist, S. C. Jameson, W. R. Heath, J. L. Howard, M. J. Bevan, F. R. Carbone, T cell receptor antagonist peptides induce positive selection. *Cell* **76**, 17–27 (1994).

69. S. R. Clarke, M. Barnden, C. Kurts, F. R. Carbone, J. F. Miller, W. R. Heath, Characterization of the ovalbumin-specific TCR transgenic line OT-I: MHC elements for positive and negative selection. *Immunol Cell Biol* **78**, 110–117 (2000).

70. P. M. L. Ng, N. Kaliaperumal, C. Y. Lee, W. J. Chin, H. C. Tan, V. B. Au, A. X. Goh, Q. W. Tan, D. S. G. Yeo, J. E. Connolly, C. I. Wang, Enhancing Antigen Cross-Presentation in Human Monocyte-Derived Dendritic Cells by Recruiting the Intracellular Fc Receptor TRIM21. *J Immunol* **202**, 2307–2319 (2019).

71. A. Gonzalez, M. N. Hall, S. C. Lin, D. G. Hardie, AMPK and TOR: The Yin and Yang of Cellular Nutrient Sensing and Growth Control. *Cell Metab* **31**, 472–492 (2020).

72. J. Kim, M. Kundu, B. Viollet, K. L. Guan, AMPK and mTOR regulate autophagy through direct phosphorylation of Ulk1. *Nat Cell Biol* **13**, 132–141 (2011).

73. S. Horman, G. Browne, U. Krause, J. Patel, D. Vertommen, L. Bertrand, A. Lavoinne, L. Hue, C. Proud, M. Rider, Activation of AMP-activated protein kinase leads to the phosphorylation of elongation factor 2 and an inhibition of protein synthesis. *Curr Biol* **12**, 1419–1423 (2002).

74. M. Costa-Mattioli, P. Walter, The integrated stress response: From mechanism to disease. *Science* **368**, (2020).

75. J. Humeau, M. Leduc, G. Cerrato, F. Loos, O. Kepp, G. Kroemer, Phosphorylation of eukaryotic initiation factor-2alpha (eIF2alpha) in autophagy. *Cell Death Dis* **11**, 433 (2020).

76. D. Nandi, N. S. S. Farid, H. A. R. Karuppiah, A. Kulkarni, Imaging Approaches to Monitor Inflammasome Activation. *J Mol Biol* **434**, 167251 (2022).

77. L. J. Janke, J. M. Ward, P. Vogel, Classification, Scoring, and Quantification of Cell Death in Tissue Sections. *Vet Pathol* **56**, 33–38 (2019).

78. E. D. Charles, M. I. Orloff, E. Nishiuchi, S. Marukian, C. M. Rice, L. B. Dustin, Somatic hypermutations confer rheumatoid factor activity in hepatitis C virus-associated mixed cryoglobulinemia. *Arthritis Rheum* **65**, 2430–2440 (2013).

79. A. Machowicz, I. Hall, P. de Pablo, S. Rauz, A. Richards, J. Higham, A. Poveda-Gallego, F. Imamura, S. J. Bowman, F. Barone, B. A. Fisher, Mediterranean diet and risk of Sjogren's syndrome. *Clin Exp Rheumatol* **38 Suppl 126**, 216–221 (2020).

80. M. F. Fransen, H. Benonisson, W. W. van Maren, H. S. Sow, C. Breukel, M. M. Linssen, J. W. C. Claassens, C. Brouwers, J. van der Kaa, M. Camps, J. W. Kleinovink, K. K. Vonk, S. van Heiningen, N. Klar, L. van Beek, V. van Harmelen, L. Daxinger, K. S. Nandakumar, R. Holmdahl, C. Coward, Q. Lin, S. Hirose, D. Salvatori, T. van Hall, C. van Kooten, P. Mastroeni, F. Ossendorp, J. S. Verbeek, A Restricted Role for FcgammaR in the Regulation of Adaptive Immunity. *J Immunol* **200**, 2615–2626 (2018).

81. P. D. Burbelo, K. H. Ching, C. M. Klimavicz, M. J. Iadarola, Antibody profiling by Luciferase Immunoprecipitation Systems (LIPS). *J Vis Exp*, (2009).

82. P. D. Burbelo, R. Goldman, T. L. Mattson, A simplified immunoprecipitation method for quantitatively measuring antibody responses in clinical sera samples by using mammalian-produced Renilla luciferase-antigen fusion proteins. *BMC Biotechnol* **5**, 22 (2005).

83. P. Bankhead, M. B. Loughrey, J. A. Fernández, Y. Dombrowski, D. G. McArt, P. D. Dunne, S. McQuaid, R. T. Gray, L. J. Murray, H. G. Coleman, J. A. James, M. Salto-Tellez, P. W. Hamilton, QuPath: Open source software for digital pathology image analysis. *Sci Rep* **7**, 16878 (2017).

84. E. Jones Evans, Created in BioRender, https://BioRender.com/fx497at, (2026).

85. E. Jones Evans, Created in BioRender, https://BioRender.com/t9t063j, (2026).

86. E. Jones Evans, Created in BioRender, https://BioRender.com/in55r5f, (2026).

87. E. Jones Evans, Created in BioRender, https://BioRender.com/ib4rqg6, (2026).

88. I. Korsunsky, K. Wei, M. Pohin, E. Y. Kim, F. Barone, T. Major, E. Taylor, R. Ravindran, S. Kemble, G. F. M. Watts, A. H. Jonsson, Y. Jeong, H. Athar, D. Windell, J. B. Kang, M. Friedrich, J. Turner, S. Nayar, B. A. Fisher, K. Raza, J. L. Marshall, A. P. Croft, T. Tamura, L. M. Sholl, M. Vivero, I. O. Rosas, S. J. Bowman, M. Coles, A. P. Frei, K. Lassen, A. Filer, F. Powrie, C. D. Buckley, M. B. Brenner, S. Raychaudhuri, Cross-tissue, single-cell stromal atlas identifies shared pathological fibroblast phenotypes in four chronic inflammatory diseases. *Med* **3**, 481–518 e414 (2022).

Acknowledgements: We thank members of the L.B.D, J.S.B., A.G., and A.J.C. laboratories for helpful discussions. We also thank everyone at the Kennedy Institute of Rheumatology Digital Pathology Omics Core and Cell Dynamics Core for their technical expertise and support in multicolor imaging and flow cytometry. Henrietta Lacks and the HeLa cell line established from her tumor cells without her knowledge or consent in 1951, have made significant contributions to scientific progress and advances in human health. We are grateful to Henrietta Lacks, now deceased, and her surviving family members for their contributions to biomedical research.

Funding: This research was supported by Kennedy Trust for Rheumatology Research Studentship KENN 192001 (E.L.J.E.), Henni Mester Fellowship, University College, University of Oxford (E.L.J.E.), Wellcome Trust Collaborative Award 224343/Z/21/Z (M.A.W.), Oxford-Bristol Myers Squibb Celgene Research Fellowship Programme Project 2302 (L.B.D.), Kennedy Trust for Rheumatology Research KENN212202 (J.S.B.) and KENN202112 (A.G.), Medical Research Council MR/W001217/1 (J.S.B.), and NIHR Birmingham Biomedical Research Centre NIHR 203326 (B.A.F.). The views expressed in this publication are those of the authors and not necessarily those of the NHS, the NIHR or the Department of Health.

Author contributions: Conceptualization: E.L.J.E., B.D., J.S.B., and L.B.D. Funding acquisition: A.G., J.S.B., and L.B.D. Investigation: E.L.J.E., B.D., M.M.E.d.J., H.C., G.H., Y.F.Y., and A.J.C. Methodology: E.L.J.E., B.D., M.M.E.d.J., H.C,. S.H., R.E.G., G.H., S.N., M.A.W., J.R.F., M.S.C., and G.J.M. Project administration: E.J.E., J.S.B., and L.B.D. Supervision: B.A.F., A.G., A.J.C., J.S.B., and L.B.D. Visualization: E.L.J.E., M.M.E.d.J., and J.R.F. Writing—original draft: E.L.J.E. Writing—review and editing: E.L.J.E., J.S.B., L.B.D., A.J.C., and A.G.

Competing interests: B.A.F. has undertaken consultancy or participated in advisory boards in the field of Sjogren's Disease for Novartis, BMS, Servier, Galapagos, Roche, Sanofi, Johnson & Johnson, AstraZeneca, Otsuka, Amgen, Kiniksa, Cullinan, OneFour Bio, Spero and Catalys Pacific. No financial support from any of the above parties was received for any part of the work reported in this manuscript. These organisations had no part in the design or reporting of this study. All other authors declare that they have no competing interests.

Data, code, and materials availability: RNA-seq data have been deposited in a GEO database with accession number GSE318852. TRIM21_w_PRYSPRY-GFP, TRIM21_NO_PRYSPRY-GFP, and TRIM21_Fc_MUT-GFP expression constructs were generated by the authors and are available upon reasonable request. All other materials are commercially available [or were obtained via MTA from outside sources as described in Materials and Methods. A list of media, reagents, and mice is provided in data file S2. TRIM21-GFP construct sequences are provided in data file S3. Uncropped protein immunoblots are provided in data file S4. Tabulated data underlying the figures are provided in data file S5. All other data are available in the main text or the supplementary materials.

FIGURE LEGENDS

Fig. 1. **Cytosolic TRIM21 is widely expressed in control and SjD tissues.** (**A** to **D**) Serially sectioned FFPE fixed SG and sicca control biopsy slides were H&E-stained or imaged by multiplex fluorescence imaging. Representative SG scans from (A) sicca controls and [(B) to (D)] SjD patients were imaged by Zeiss Axioscan 7 at 20X magnification. Black and blue boxes highlight areas of interest at higher magnification. Black-framed arrows indicate collagen deposition (fibrosis). Red-framed arrows highlight plasma cells. (A) to (D) Sequential antibody stains and bleach rounds were performed using CellDIVE^{TM} protocols (*88*). In Cell Analyzer 2500HS (GE system) was used for image acquisition. Images were merged and visualized using QuPath. Scale bars: (A) 1 mm (H&E), 400 μm (CK13 and DAPI panels); (B) 250 μm (H&E), 200 μm (bottom left), 100 μm (Pan-cadherin panel); (C) 1 mm (upper left H&E), 100 μm (all others); (D) 1 mm (upper left H&E), 50 μm (all others). DAPI/antibody markers are indicated in the figure. Small squares in the top right corner of each image show the parental image, highlighting the area for zoom selection. Please see Fig. S1 for single-channel images of multicolor staining in (C) and (D). (**E**) Representative images of lentivirally transduced HeLa overexpressing TRIM21_w_PRYSPRY-GFP, imaged by live confocal microscopy. Scale bars, 50 μm. (**F**) Representative images of tonsil slide stained with DAPI and anti-TRIM21/SSA1 antibody, imaged using In Cell Analyzer 2500HS. Full tonsil section image scan. Scale bars, 1 mm (full tonsil, main image), 100 μm (follicle, top right), and 50 μm (follicle, bottom right).

Fig. 2. TRIM21 is up-regulated by inflammatory signals and released during lytic cell death. (**A** to **C**) Stimulation of [(A) and (B)] BMDMs and (C) HeLa cells was performed as indicated. Representative immunoblots are shown. Semi-quantification of TRIM21 relative to loading control was calculated and compared to UT 24 hours control. *$P \leq 0.05$, **$P \leq 0.01$, and ***$P \leq 0.001$. (**D** and **E**) HeLa overexpressing TRIM21_w_PRYSPRY-GFP were treated to induce apoptosis (ABT737, MCL1i) and imaged by live microscopy. White arrows highlight apoptotic blebs. Representative of three independent experiments. Scale bars, 15 μm (D, top), 20 μm (D, bottom), and 50 μm (E). (**F**) WT BMDMs were treated to induce apoptosis (ABT737, MCL1i) or NLRP3 pyroptosis (LPS + Nigericin). Osmoprotectant glycine inhibited lytic death. Pro-IL-1β induction was the LPS priming control. (**G**) WT and *Gsdmd*-KO BMDMs were treated to induce NLRP3 pyroptosis (LPS + Nigericin) or necroptosis (LPS primed, then Q-VD-Oph + AZD 5582 ± Nec1 necroptosis inhibitor as a control). (**H**) WT BMDMs were treated to induce AIM2 pyroptosis (transfected ctDNA). (**I**) WT BMDMs were treated to induce necrosis (Triton X-100 or needle shear). [(F) to (I)] Lys and SN were analyzed by immunoblot. Cell death was measured by LDH release. [(A) to (C) and (F) to (I)] Immunoblots show pooled lysates from three wells; plots show results of three independent experiments.

Fig. 3. Extracellular TRIM21 binds serum antibody Fc domains. (**A**) GFP ELISA to detect TRIM21-GFP binding to plate-bound NHS antibodies or PBS control. TRIM21-GFP was released from HeLa after apoptosis (ABT-737, MCL1i) or lytic death (noncanonical pyroptosis, hIFN-γ + spinfected LPS/Lipofectamine-2000). Binding was detected by anti-GFP-HRP antibody. Data shown as triplicates for a single experiment, representative of three independent experiments. (**B**) GFP ELISA to detect binding of different TRIM21 constructs, TRIM21_w_PRYSPRY-GFP or TRIM21_FcMUT-GFP, to NHS antibodies. Data shown as triplicates for a single experiment, representative of three independent experiments. (**C**) HeLa overexpressing TRIM21_w_PRYSPRY-GFP were lysed, and binding to magnetic GFP-trap beads was used to IP TRIM21. GFP-trap inputs and elutions were analyzed by immunoblot.

Results from one experiment shown and are representative of three independent experiments. (**D**) GFP ELISA to detect binding of TRIM21_w_PRYSPRY-GFP to antibodies from NHS, HC077, or SjD58 patient plasma. Plasma samples were diluted 1:100 and 1:1000, as indicated. Data are shown as triplicate points for a single experiment, representative of three independent experiments.

Fig. 4. SjD patient plasma generates higher-order TRIM21–IgG complexes due to Fc and Ag-specific Fab domain contributions. (**A**) LIPS assay to measure relative autoantibody levels in SjD and HC plasma samples. Plasmas were diluted 1:10 for analysis. Positive control antibodies were diluted to final concentration of 0.01 mg/ml. Samples were incubated with HeLa cell lysates containing autoantigen-luciferase fusion proteins as indicated. Antibody-captured luciferase activity was measured, subtracting background Luc_antigen-only activity. Representative data shown as mean with SD of triplicates, from one of three independent experiments. (**B** to **G**) Nondenaturing BN-PAGE separation of [(B) to (D)] TRIM21_w_PRYSPRY-GFP lysates or [(E) to (G)] TRIM21_Fc_MUT-GFP lysates from HeLa, TRIM21 lysates complexed with plasmas (HC/SjD). [(C) and (E)] Regular denaturing immunoblotting of samples identified TRIM21-GFP proteins at expected molecular weights. All biological replicate data are shown, representing the range of complex sizes formed, according to different autoantibody amounts in plasma samples. (**H**) TRIM21_w_PRYSPRY-GFP lysates alone or complexed with patient plasma (HC077 or SjD58) were analyzed by FIDA. All unsmoothed fluorescence intensity data obtained at 5 kPa are represented for a single experiment with technical triplicates.

Fig. 5. Macrophages take up higher TRIM21–IgG complexes. (**A** to **D**) IFN-γ–primed BMDMs/HMDMs were fed for indicated times with the following GFP-trap eluted proteins: (A) TRIM21_w_PRYSPRY-GFP alone, TRIM21_w_PRYSPRY-GFP complexed with NHS (0.01 mg/ml), (B) TRIM21_w_PRYSPRY-GFP and TRIM21_FcMUT-GFP, both complexed with NHS (0.01 mg/ml), and [(C) and (D)] TRIM21_w_PRYSPRY complexed with plasma (HC/SjD) (1:100 dilution). TRIM21 was detected in lysates by immunoblot. One representative immunoblot of three is shown. (C) Immunoblots using the following patient pairs: HC077 versus SjD58, HC099 versus SjD59, and HC087 versus SjD61. [(A) to (C)] Kinetic graph shows combined TRIM21-GFP uptake data from three experiments. (D) HMDM uptake immunoblot is representative of three independent biological replicates, using the following subject pairs: HC077 versus SjD58, HC099 versus SjD59, and HC087 versus SjD61. Kinetic graph shows combined relative immunoblot TRIM21-GFP uptake data (n = 3 HC and 3 SjD).

Fig. 6. Internalized TRIM21 escapes into the cytosol and is preferentially degraded by the proteasome. (**A**) mIFN-γ–primed BMDMs were pretreated with BafA1 or MG132 before feeding TRIM21_w_PRYSPRY-GFP or TRIM21_w_PRYSPRY-GFP complexed with plasma (HC/SjD). TRIM21-uptake was measured by immunoblot. Representative of three replicates. (**B** to **D**) mIFN-γ–primed BMDMs were pretreated with MG132 or control media, as indicated, and fed TRIM21_w_PRYSPRY-GFP complexed with NHS. TRIM21 uptake was determined by confocal microscopy. Phalloidin staining is shown in blue. Quantification used at least five images from two independent experiments. (**B**) Effects of MG132 pretreatment on TRIM21-GFP accumulation; quantification of % GFP^{hi} per cell area. **(C)** TRIM21-GFP colocalization with EEA1 in MG132-pretreated BMDMs. The white arrow highlights TRIM21-GFP in endosomes (colocalized with EEA1), whereas the aqua arrow highlights cytosolic TRIM21-GFP outside endosomes. Pearson correlation coefficient (EEA1 / TRIM21-GFP) was analyzed and graphed. (**D**) Gal3 staining in MG132-pretreated BMDMs fed with TRIM21-GFP ICs. White arrows highlight Gal-3 puncta (indicating lysosomal rupture).

Quantification of % Gal-3^{hi} signal per cell area. (**E**) IFN-γ–stimulated BMDMs were fed with TRIM21-GFP IC ± MG132. Ub-TUBE IP pulled down ubiquitinated cytosolic TRIM21-GFP. Representative of three replicates.

Fig. 7. TRIM21 enhances antigen cross-presentation in vitro. (**A** to **C**) mIFN-γ–primed BMDMs were cultured with stimuli as shown, then cocultured overnight with OT-I CD45.1 T cells. Cocultures were analyzed for CD45.1, CD8α, and CD69 surface expression. Frequency of $CD69^+$ expression as a percentage of $CD8^+$ OT-I cells was determined for a range of OVA concentrations: (A) 10 ng/ml, (B) 100 ng/ml, and (C) 1000 ng/ml. Results from two biologically independent experiments were pooled, normalized to UT, and analyzed by one-way ANOVA and Tukey's post-hoc test. Duplicate experiments are distinguished by filled or empty symbols. Data represented as means + SD for each condition. $*P \leq 0.05$, $**P \leq 0.01$, and $***P \leq 0.001$.

Fig. 8. Macrophage TRIM21 uptake induces proinflammatory and metabolic changes. (**A**) Cytokine release by IFN-γ–primed HMDMs fed with TRIM21-GFP ICs as indicated. (**B-G**) Results of bulk RNA sequencing from HMDMs (n = 3 donors [D8, D10, and D11]) incubated with GFP-trap eluted TRIM21 (± complexed with patient plasma). Significance was calculated using the Wald test (two-tailed) followed by the Bonferroni correction. (**B**) PCA plot for each donor and feeding condition. (**C**) Normalized enrichment scores for TRIM21 and TRIM21_SjD59 versus UT conditions for designated gene sets. **(D** and **E)** Volcano plots show log_2-fold changes in differentially expressed genes for (D) TRIM21 alone versus UT and (E) TRIM21_SjD59 complex versus UT feeding. Colors indicate genes assigned in Hallmark and KEGG gene set pathways. **(F** and **G)** Heatmaps highlighting changes in (F) mTOR and (G) NF-κB signaling gene expression. (**H**) Immunoblots showing changes in metabolism-related proteins in HMDMs fed with TRIM21-GFP and/or SjD plasma) at 0 hours (immediately post-feed), 3 hours, and 6 hours. Results are representative of three independent experiments.

Supplementary Materials for

The autoantigen TRIM21 assembles proinflammatory immune complexes following lytic cell death

Esther L. Jones Evans, Benjamin Demarco, Han Cai, Madelon M.E. de Jong, Sarah Hill, Marcus A. Widdess, Joannah R. Fergusson, Ryan E. Glass, Gemma Harris, Gracie J. Mead, Yavuz F. Yazicioglu, Saba Nayar, Benjamin A. Fisher, Mark S. Cragg, Alexander J. Clarke, Audrey Gérard, Jelena S. Bezbradica, Lynn B. Dustin

Corresponding authors: jelena.bezbradica@kennedy.ox.ac.uk (J.S.B.); lynn.dustin@kennedy.ox.ac.uk (L.B.D.)

The PDF file includes:

Other Supplementary Materials for this manuscript include the following:

SUPPLEMENTARY MATERIALS AND METHODS

Analysis of TRIM21 expression in cells and tissues

H&E and Cell DIVE slide preparation and imaging

Five micron–thick formalin-fixed paraffin-embedded (FFPE) tonsillar tissue mounted on TOMO slides was purchased from the Oxford Centre for Histopathology Research. Five-micron SG biopsy slides were obtained from the OASIS cohort (Birmingham). One SG slide for each patient was H&E-stained and imaged using a Zeiss Axioscan 7 at 20X magnification. SG biopsy histology was analyzed using QuPath (*83*) v0.5.0 to measure glandular area, count lymphocytic foci comprising ≥50 cells, and calculate focus score according to ACR-EULAR criteria (focus score = 4 × (number of lymphocytic foci) / (glandular area (mm^2)).

Antigen retrieval was performed according to the GE Cell DIVE system protocol. Slides were blocked overnight 4°C in blocking solution (PBS, 3% BSA, 10% donkey serum), washed for 5 min in PBS with orbital shaking and blocked for 1 hour at room temperature with human FcγR block, diluted 1:200 in antibody diluent (PBS, 3% BSA). Slides were washed three times in PBS for 5 min each, then stained with DAPI solution for 15 min with orbital shaking, before an additional wash in PBS for 5 min. Finally, slides were coverslipped in mounting media (90% glycerol, 4% propyl gallate).

Background imaging was performed according to the GE Cell DIVE system manufacturer's instructions on the IN Cell 2500HS. Briefly, an overall scan plan was acquired at 10X magnification. Entire tissue sections were selected for imaging and the background, and subsequent imaging rounds were imaged at 20X magnification. Background imaging enabled the removal of autofluorescence from subsequent imaging rounds.

For staining, slides were decoverslipped and washed three times in PBS, each for 5 min with orbital shaking. Primary antibodies source and dilutions used are listed in data file S1. Slides were stained with primary and directly conjugated antibodies overnight at 4°C before 3 washes in PBS, each for 5 min with orbital shaking. Alexa Fluor® 555–conjugated donkey anti-rabbit secondary antibody was diluted 1:500 and slides were incubated at room temperature for 1 hour in the secondary antibody.

Iterative rounds of staining and bleaching were performed according to the manufacturer's instructions. To inactivate the dyes, slides were decoverslipped and bleached twice in bleaching solution (0.1 M $NaHCO_3$ pH 11.2, 3% H_2O_2), which was freshly prepared every time, before a 1-min PBS wash. Slides were placed in DAPI solution for a further 2 min at room temperature, with orbital shaking. Slides were then washed in PBS and recoverslipped in mounting media. Images were acquired using the 20X objective, aligned to previous scan rounds and merged. Autofluorescence was subtracted from the background scan. Images were imported to the QuPath software (*89*) for visualization and selecting areas of interest.

BMDM and HeLa stimulation experiments for TRIM21 up-regulation

Day 8 BMDMs were plated in 100 µl per well in a 96-well plate in complete DMEM with 50 ng/ml of hM-CSF and incubated for 16 hours. HeLa cells were plated at a density of 15,000 cells per well in a 96-well plate, in complete DMEM and incubated for 16 hours. On the day of experimentation, media was aspirated and replaced with 200 µl of complete DMEM ± priming substances as indicated in figures: ultra-pure LPS (100 ng/ml), mTNF-α (100 ng/ml), poly I:C (2.5 µg/ml), mIFN-α (100 ng/ml), mIFN-β (100 ng/ml), mIFN-γ (10, 100 or 1000 ng/ml). After 4, 8, and 24 hours, media was aspirated, and the cells were lysed in 30 µl of lysis

buffer [66 mM Tris-HCl (pH 7.4), 2% SDS] for 2 min at room temperature. Triplicate lysate wells were pooled and stored at −20°C.

Lentiviral transduction of HeLa cells

To prepare lentiviruses, HEK293T cells were transfected at 80% confluency in 2 ml of complete DMEM in six-well TC-treated culture plates. The following transfection mixtures were prepared (volumes for one well): 100 µl serum-free DMEM with 4 µl of GeneJuice transfection reagent, incubated for 5 min at room temperature, then each of the following plasmids was added: TRIM21-GFP fusion protein vectors (see above) (0.50 µg), pMD.G (VSV-G envelope expressing plasmid) packaging vector (0.50 µg), and P8.91 (plasmid expressing gag and pol) packaging vector (0.50 µg). The total mixture was incubated at room temperature for 15 min, added to the wells and incubated for 72 hours. SNs were harvested, clarified by centrifugation, and passed through a 0.45-µm filter to be used for transduction.

One day before transduction, HeLa cells were seeded at a density of 5×10^4 cells per well in 2 ml of complete DMEM in six-well TC-treated culture plates. After overnight culture, cells were transduced by adding 1.5 ml of freshly-harvested filtered lentiviral suspension to the cells (3.5 ml final volume), and incubated for up to 72 hours for optimal transduction efficiency. Cells were checked for GFP expression.

Apoptosis live confocal microscopy

HeLa_TRIM21_w_PRYSPRY-GFP were seeded in µ-Slide 8 Well high ibiTreat culture plates at a density of 15,000 cells per well in 300 µl of complete DMEM and incubated overnight. On the day of experimentation, media was aspirated and replaced with 300 µl of serum-free media complete DMEM. The heating chamber at the microscope was set at 37°C, with 5% CO2, and allowed to equilibrate for 30 min before loading live samples. No additional buffering method was used. Thirty minutes before imaging, a 1 µM SiR-DNA stain was added. Apoptosis-inducing drugs 1 µM ABT and 10 µM MCL1i were added during live time-lapse microscopy. Live imaging performed on Zeiss LSM980 Airyscan 2 confocal microscope, using a water immersion C-Apochromat 40x/1.2 NA objective at opticoal zoom 1 (projected pixel size of 100 × 100 nm) in confocal unidirectional line scanning mode, and hardware autofocus (Definite Focus 2). Sample acquisition was performed using Zeiss Zen Blue (v3.3), with simultaneous 488 nm (for GFP) and 639nm lasers (for Alexa Fluor 647) laser excitationwith a pinhole size of 38 µm (1AU at 488 nm) and detection on GaAsP point detectors with emission bands centered on 509 nm (GFP) and 668 nm (Alexa Flour 647). Images were acquired every 60 seconds, for total of 240 images (4 hours).

Custom sandwich GFP ELISA

Corning® 96-well High Bind Microplates were coated overnight at 4°C with 100 µl of the following antibodies diluted in PBS in triplicate: normal human serum (5 µg/ml), patient/HC plasma (diluted 1:100, 1:1000, as indicated), or PBS-only coating blank control. Coated plates were washed in PBS-T and then blocked with 300 µl of blocking buffer for 1 hour at room temperature. The following cell lysate samples in IP-lysis buffer were diluted in blocking buffer: HeLa_TRIM21_w_PRYSPRY (1:10, 1:100, 1:1000, 1:10,000) and HeLa_TRIM21_NO_PRYSPRY (1:10, 1:100, 1:1000, 1:10,000). The following SN/control samples were added neat: Opti-MEM only, UT cell SN, apoptosis, and pyroptosis SN. One hundred microliters of the sample was added to the designated wells. Plates were incubated for

2 hours at room temperature with gentle shaking (~500 RPM). After three washes in PBS-T, 100 µl of anti-GFP-HRP detection antibody (diluted to 200 ng/ml in blocking buffer) was added for 1 hour at room temperature with shaking. After washing, 100 µl of TMB substrate solution was added for 30 min in the dark at room temperature before stopping with 100 µl of stop solution (2M sulphuric acid). Absorbance was measured at 450 and 570 nm. The specific OD was calculated as the A450 minus A570 values. PBS-only blanks were subtracted to calculate final OD values.

Cell death and release of TRIM21 from macrophages

Induction of cell death in BMDMs

For all experiments, unless otherwise specified, complete media was replaced with 200 µl of Opti-MEM on the day of stimulation. Cell death–inducing chemicals used and dilutions are listed in data file S1.

To induce intrinsic apoptosis, BMDMs were stimulated with apoptosis-inducing drugs ABT-737 (250 nM) and S63845 (250 nM) for 3 hours. To induce both necroptosis and pyroptosis, cells were first primed with ultra-pure LPS (100 ng/ml) for 4 hours. For NLRP3 pyroptosis, cells were then treated with nigericin (10 µM) for an additional 2 hours. For glycine-inhibited pyroptosis treatment, sterile-filtered glycine (20 mM final concentration) was added 3 min before nigericin treatment. For necroptosis, in the last 30 min of LPS priming, cells were treated with Q-VD-Oph (10 µM), before final stimulation using SM AZD 5582 (1 µM) for 5 hours. To inhibit necroptosis, the inhibitor Nec1 (10 µM) was added at the Q-VD-Oph time point. To induce AIM2 pyroptosis, the media was not replaced with Opti-MEM. Cells were treated per well with either 0.25% Lipofectamine 2000 alone as a vehicle control, 200 ng of ctDNA (2 µg/ml) alone, or combined ctDNA plus Lipofectamine 2000 (0.25%). Ten microliters of media was removed from the top of each well undergoing transfection, and 10 µl of the appropriate treatment/transfection mixture was added to the cells. To synchronize transfection, the plate was centrifuged for 10 min, 1000*g* at room temperature, before 4 hours of incubation.

To induce necrosis, BMDMs were treated with 0.1% Triton X-100 in 200 µl of Opti-MEM. For needle shearing, the media was replaced with 200 µl of cold PBS to aid cell resuspension. Using a 30G needle, cells were forcibly sheared multiple times in PBS. The plate was centrifuged at 500*g* for 5 min to separate the cells and SN.

At the end points, SNs were collected in fresh 96-well plates and stored at −20°C and cells were lysed in 30 µl of lysis buffer [66 mM Tris-HCl (pH 7.4), 2% SDS] for 2 min at room temperature. Triplicate lysate wells were pooled and stored at −20°C.

LDH and cell viability assays

LDH release was measured using the CytoTox 96® Non-Radioactive Cytotoxicity Assay kit, and cell viability was measured using the CellTiter-Glo Luminescent Cell Viability Assay, according to the manufacturer's instructions, except that all volumes in both assays were scaled down to 20 µl rather than 50 µl. The % LDH release and % cell viability values were normalized to 100% lysis treatments (Triton X-100 treated) and UT controls, respectively.

Supernatant precipitation before immunoblotting

For all supernatant (SN) precipitation experiments, complete media was replaced with 200 µl of Opti-MEM on the day of stimulation. The SN of stimulated cells stored in a 96-well plate at −20°C were retrieved and thawed at room temperature. The plate was centrifuged at 500*g* for 5 min at room temperature, and SN was then transferred to microcentrifuge tubes. Samples

were mixed with one volume of methanol and 0.33 volumes of chloroform, vortexed for 5 s and centrifuged at 4°C for 10 min at 17,000*g*. The upper phase (of three visible phases) was aspirated, and a 1.33-fold SN volume of methanol was added. Samples were vortexed and centrifuged as above. The SN was removed, leaving a final pellet which was dried at room temperature. Samples were dissolved in 40 µl of 1X Laemmli loading buffer containing 10 mM DTT before immunoblotting.

Immunoblotting

Cell lysates were thawed at room temperature and mixed with 0.33 volumes of 4X Laemmli loading buffer containing 40 mM DTT. Samples (Lys/SN) were boiled at 95°C for 5 min and centrifuged at 17,000*g* for 2 min before loading the gel. Proteins were separated on 4 to 20% precast polyacrylamide gels and transferred onto nitrocellulose membranes using a Trans-blot Turbo (Bio-Rad). Antibodies for immunoblot and dilutions used are listed in the data file S2. Proteins were visualized by ECL detection.

Trim21 siRNA knockdown

BMDMs were plated in 96-well plates in complete DMEM with 50 ng/ml hM-CSF. The next day media was replaced with Opti-MEM, and siRNA knockdown was performed according to the manufacturer's recommendations. Per well, cells were transfected with 4 pmol of the following siRNA: siGENOME nontargeting siRNA control pools, or ON-TARGETplus mouse *Trim21* siRNA, SMART pool, combined with 0.75 µl of Lipofectamine RNAiMax in Opti-MEM. After 6 hours, Opti-MEM was replaced with complete DMEM with 50 ng/ml hM-CSF. Lysates were collected 72 hours after transfection for immunoblotting.

Flow-induced dispersion analysis (FIDA) of TRIM21-ICs

FIDA experiments were performed using a Fida 1 instrument (Fida Biosystems ApS) employing light-emitting-diode induced fluorescence detection with an excitation wavelength of 480 nm and emission wavelength of > 515 nm. Standard silica capillaries with an inner diameter of 75 µm, an outer diameter of 375 µm, a total length of 100 cm, and length to detection window of 84 cm (Fida Biosystems) were used for all experiments. The capillaries were coated with high-sensitivity (HS) coating reagent before use. The following stepwise procedure was applied for the FIDA experiments. First, ultrapure water was used for flushing the HS-coated capillary at 350 kPa for 60 s. The analyte sample (assay buffer or assay buffer with antibody plasma) was then filled into the capillary at 350 kPa for 40 s followed by injection of the indicator (TRIM21-GFP alone or premixed with antibody plasma) at 5 kPa for 10 s. Finally, the indicator was mobilized to the fluorescence detector with analyte sample (assay buffer or assay buffer with antibody plasma) at either 30, 10, 5, or 2.5 kPa. For comparison, 1 atm (standard atmospheric pressure at sea level) equals 101.325 kPa. The equilibrium dispersion profile (Taylorgram) was recorded in the latter step. The Taylorgrams were analyzed using FIDA software (V 2.37, Fida Biosystems). The samples and buffer vials were kept in a temperature-controlled environment at 4°C inside the instrument. The capillary was kept at 25°C. The viscosity of the assay buffer at 25°C was measured using a Lovis 2000 ME microviscometer. Viscosity compensation was included in the data analyses to correct for any changes in viscosity caused by the addition of the antibody plasma. All samples were analyzed in at least triplicate.

Analysis of HMDM and BMDM functional responses to TRIM21-ICs

HMDM activation for cytokine and metabolism protein analysis

IFN-γ–primed HMDMs plated in 96-well plates as described for uptake and activation assays, were fed with 10 μl of GFP-trap–eluted TRIM21 (± complexed with antibodies), SN collected at 0 (immediately collected post-feed), 3, 6, and 18 hours and analyzed using the BioLegend LEGENDplex™ Human Inflammation Panel 1 (13-plex) with V-bottom Plate, according to the manufacturer's instructions. Data were collected on a Cytek Aurora spectral cytometer and analyzed by LEGENDplex™ Data Analysis Software Suite. For visualization, values above the limits of quantification were set to the corresponding limit values and at zero for values below the detection limit. The data were then *z*-score–scaled, and a heatmap was generated using the ComplexHeatmap package in RStudio (Version 2024.12.1+663).

Additionally, 6-hour SNs were analyzed using the TNFα Human ELISA Kit, according to the manufacturer's instructions. At 0-, 3-, and 6-hour timepoints, cells were also lysed in 30 μl of lysis buffer [66 mM Tris-HCl (pH 7.4), 2% SDS]. Triplicate samples were then pooled and stored for downstream metabolism protein immunoblot analyses.

RNA-seq of HMDMs

IFN-γ–primed HMDMs plated in 96-well plates as described for uptake and activation assays, were fed with 20 μl (1:5 ratio) of GFP-trap eluted TRIM21 (± complexed with antibodies) and incubated for 6 hours. Cells were washed and lysed in 100 μl of RLT buffer (with β-mercaptoethanol). Individual donor triplicates were pooled and RNA extracted using the RNeasy micro kit, according to the manufacturer's instructions. Library preparation and RNA-seq was performed by Novogene Inc. using the HiSeq 4000 (Illumina, paired-end mode, read length 150bp). Raw reads were aligned on the GRCh37 reference genome (release 103) using STAR mapper (v 2.7.11) (84). Read counts were estimated with RSEM (v 1.1.17) (85). Count normalization and differential gene expression analysis were performed using DESeq2 (v 1.44.0) (86). Gene set enrichment analysis was performed with the GSEA software (v 3.0, Broad Institute) using predefined gene sets from the Molecular Signatures Database (MSigDB 6.2). Classical enrichment statistics with 1000 permutations were used to determine significant enrichment within gene sets. Heat maps were generated using the pheatmap package (v 1.0.12) (87) and volcano plots were generated using the EnhancedVolcano package (v 1.16.0) (88).

OVA antigen presentation by BMDMs

IFN-γ–primed BMDMs were plated at 5×10^4 cells per well in TC-treated U-bottom 96-well plates, and treated with 10 μl of OVA, anti-OVA, OVA–anti-OVA complex, GFP-trap–eluted TRIM21, TRIM21 and OVA, TRIM21–anti-OVA–OVA complex, or TRIM21–normal rabbit serum and OVA (see "Micropurification of TRIM21-GFP and IC formation" for details). Plates were incubated for 5.5 hours at 37°C. SIINFEKL peptide (50 ng/ml) was then added to relevant positive control wells. Plates were incubated for an additional 30 min. Media was aspirated, cells were washed, and media was replaced with 100 μl of prewarmed RPMI (T cell formulation described in data file S1). Isolated OT-I cells, resuspended in complete RPMI, were added at 1×10^5 cells per well to achieve a 2:1 coculture ratio with the seeded BMDMs. The cells were incubated overnight at 37 °C in 5% CO_2 before staining and flow cytometry.

Flow cytometry to monitor OT-I responses to OVA-presenting BMDMs

Cell suspensions collected from OT-I/macrophage cocultures were stained in 96-well V-bottom plates. Live/dead staining and blocking were performed using Zombie NIR Fixable Viability Kit (1:1000) and TruStain FcXTM (1:200) diluted in 1X PBS. For extracellular staining, cells were incubated with fluorochrome-conjugated antibodies diluted (all 1:400) in flow cytometry buffer (see Media and supplements) for 30 min on ice. Antibodies used and dilutions are listed in data file S1. Cells were fixed in 4% paraformaldehyde for 15 min on ice

and analyzed on a BD LSRII using BD FACSDiva and FlowJo™ software (v10.9.0). Graphs and statistical tests were completed on GraphPad Prism (v10.0.3).

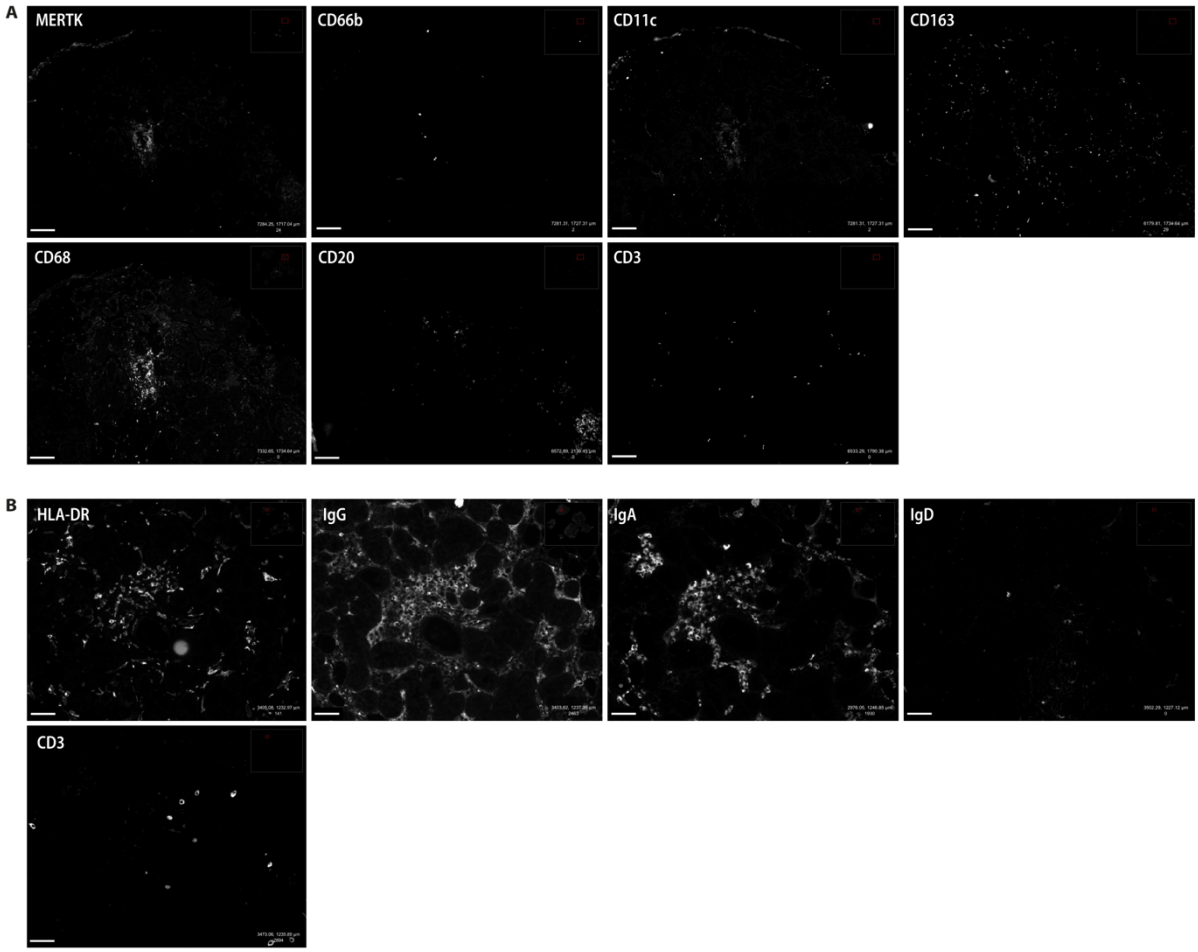

Fig. S1. Single-channel greyscale images of multiplex CellDive data shown in Fig. 1. (A) Greyscale images of individual channels for multiplex image shown at bottom right in Fig. 1C. (B) Greyscale images of individual channels for multicolor image shown at right in Fig. 1D. Scale bars, 50 µm.

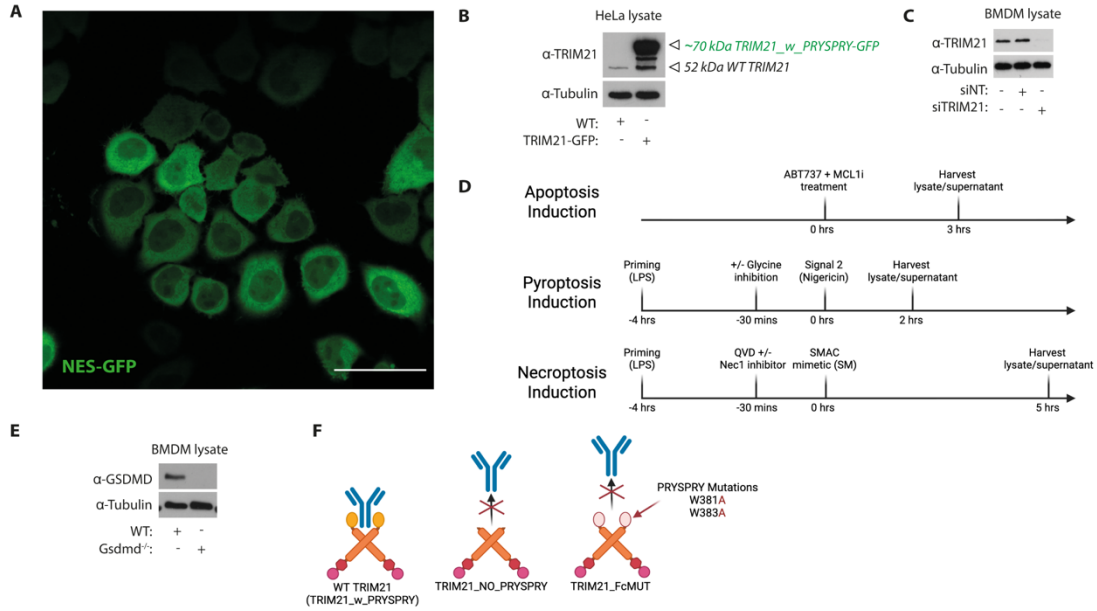

Fig. S2. TRIM21 overexpression and antibody controls. (**A**) HeLa overexpressing HIV_NES-GFP imaged by live confocal microscopy. Scale bar, 50 μm. (**B**) WT and TRIM21_w_PRYSPRY-GFP HeLa lysates were collected. (**C**) For siRNA knockdown, BMDMs were transfected with 4 pmol of either siGENOME non-targeting (NT) siRNA control pools, or ON-TARGETplus mouse Trim21 siRNA. Lysates were collected after 72 hours. [(B) and (C)] Lysates were analyzed by immunoblot using the Abcam anti-TRIM21/SSA rabbit monoclonal antibody (ab207728), 1:2000 dilution. (**D**) Schematic of induction of apoptosis, pyroptosis, and necrosis (*84*). (**E**) WT and *Gsdmd*$^{-/-}$ mouse lysates were collected and analyzed by immunoblot for GSDMD protein expression. (**F**) Schematic showing architectures and Fc-binding abilities of TRIM21 overexpression constructs used in this study (*85*).

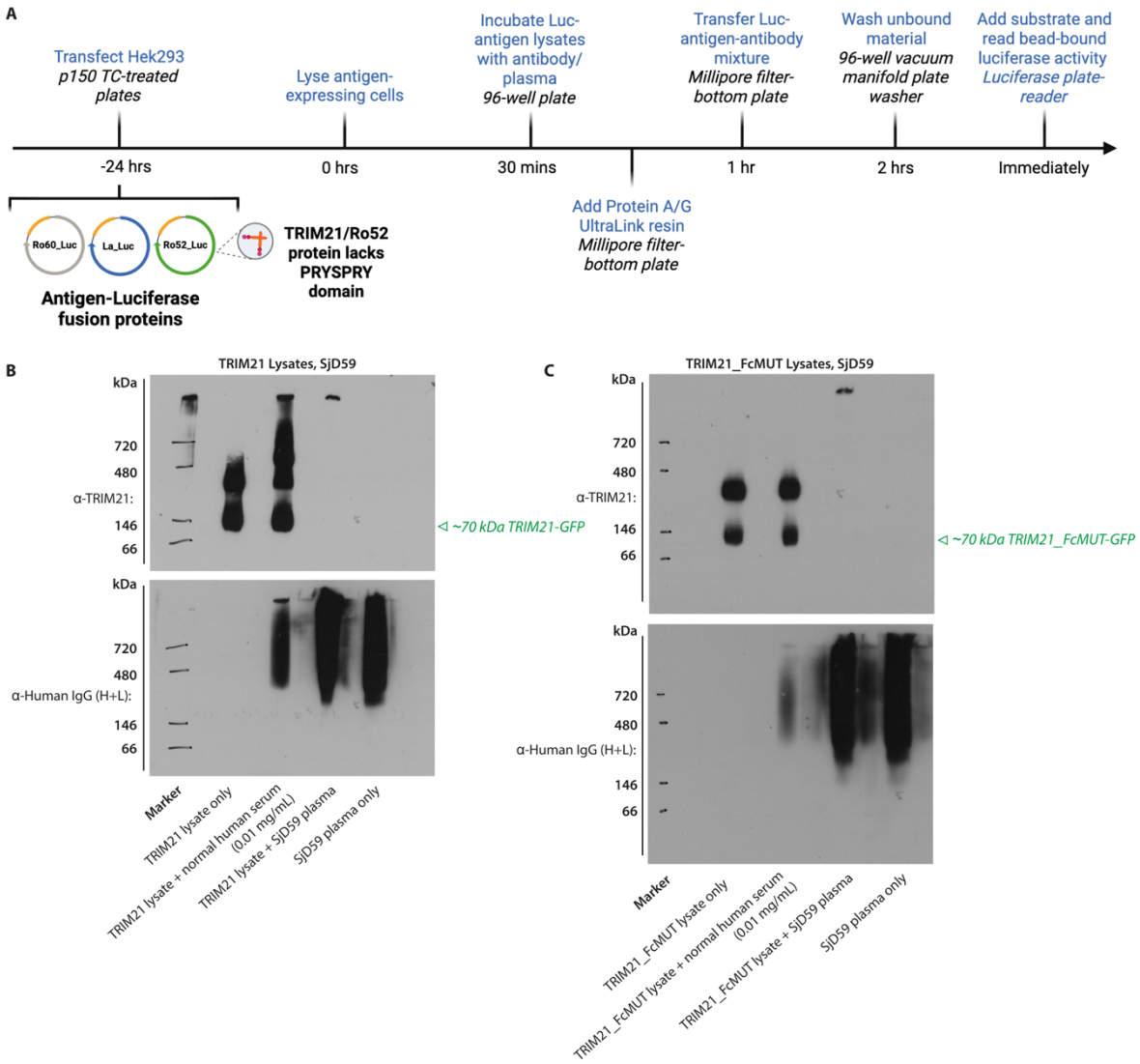

Fig. S3. LIPS assay and BN-PAGE. (**A**) Schematic illustrating the LIPS assay to quantify antigen-specific antibodies from plasma (*82*). Created in BioRender. Jones Evans, E. (2026) https://BioRender.com/wQpg3c. (**B** and **C**) SjD59 BN-Page gels. Non-denaturing BN-PAGE separation of (B) TRIM21_w_PRYSPRY-GFP lysates or (C) TRIM21_FcMUT-GFP lysates from HeLa, complexed with normal human serum (0.01 mg/ml), SjD59 patient plasma, or plasma alone as indicated. Molecular weight markers are indicated.

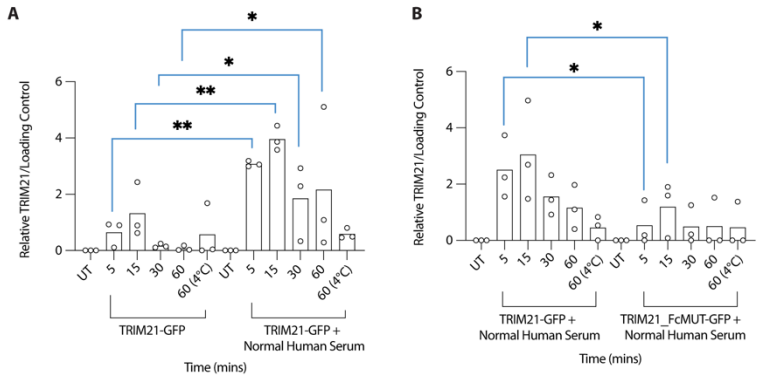

Fig. S4. Semiquantification of 70 kDa TRIM21-GFP protein in BMDMs treated with TRIM21 or TRIM21-NHS ICs. Representative immunoblots are shown in Fig. 5, A and B. Each graph shows the mean (bars) and individual results (symbols) of three independent experiments. (A) TRIM21-GFP levels relative to loading control in BMDM treated with medium only, TRIM21_w_PRYSPRY-GFP, or TRIM21_w_PRYSPRY-GFP complexed with NHS antibodies. (B) TRIM21-GFP levels relative to loading control in BMDM treated with medium, TRIM21_w_PRYSPRY-GFP complexed with NHS antibodies, or TRIM21_FcMUT-GFP complexed with NHS antibodies. Data were compared by one-way ANOVA and Fisher's least significant difference post-hoc test. * $P \leq 0.05$, ** $P \leq 0.01$, *** $P \leq 0.001$.

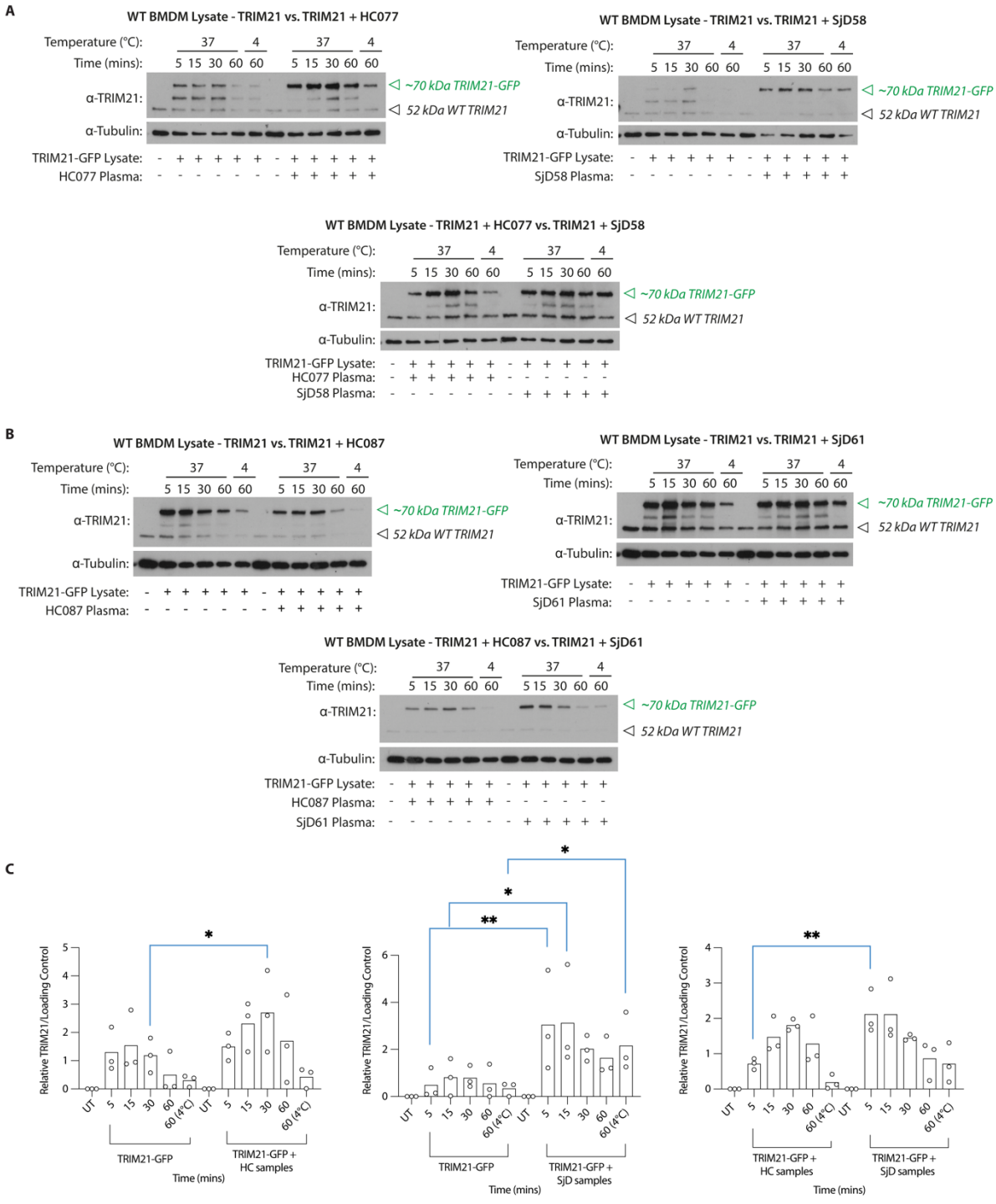

Fig. S5. BMDM uptake of TRIM21-GFP or TRIM21-GFP_ICs produced with HC or SjD plasma. (A, B) IFN-γ–primed BMDMs were fed for indicated times with the following GFP-trap eluted proteins: TRIM21_w_PRYSPRY-GFP alone or TRIM21_w_PRYSPRY-GFP complexed with plasma using the following patient pairs: (A, HC077 versus SjD58 B, HC087 vs SjD61). Following incubation for the indicated times at either 37°C or 4°C, cells were lysed for immunoblotting. Images show immunoblots of TRIM21 and α-tubulin loading control. ICs were prepared as detailed in Materials and Methods. Images show immunoblots of TRIM21 and loading controls in BMDMs treated with TRIM21-GFP alone, or TRIM21-GFP ICs prepared with HC or SjD patient plasma as indicated following culture for 5 to 60 min, as shown. (C) Semiquantitation of BMDM TRIM21-GFP levels relative to loading control for

all patient pairs (HC077 versus SjD58, HC099 versus SjD59, and HC087 versus. SjD61) for immunoblots shown in (A, B) and Fig. 5C. TRIM21-GFP protein level for each paired timepoint was compared by one-way ANOVA and Fisher's least significant difference post-hoc test. * $P \leq 0.05$, ** $P \leq 0.01$, *** $P \leq 0.001$.

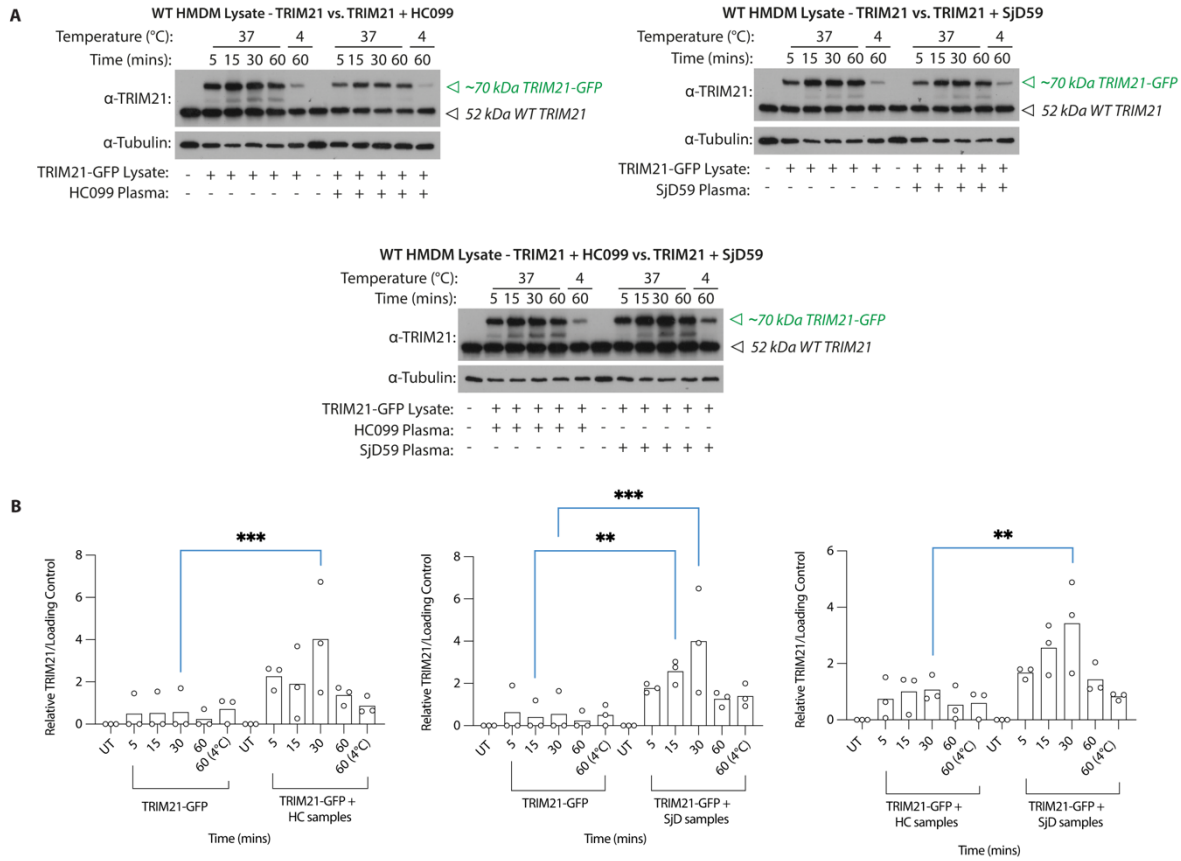

Fig. S6. HMDM uptake of TRIM21-GFP or TRIM21-GFP_ICs produced with HC or SjD plasma. (A) IFN-γ–stimulated HMDMs were fed with TRIM21_w_PRYSPRY-GFP alone or TRIM21_w_PRYSPRY-GFP complexed with either HC099 or SjD59 plasma antibodies, as indicated. Following incubation for the indicated times at either 37°C or 4°C, cells were lysed for immunoblotting. Images show immunoblots of TRIM21 and α-tubulin loading control. (B) Semiquantitation of HMDM TRIM21-GFP levels relative to loading control for all patient pairs (HC077 versus SjD58, HC099 versus SjD59, HC087 versus SjD61). TRIM21-GFP protein level for each paired timepoint was compared by one-way ANOVA and Fisher's least significant difference post-hoc test. $*P \leq 0.05$, $**P \leq 0.01$, $***P \leq 0.001$.

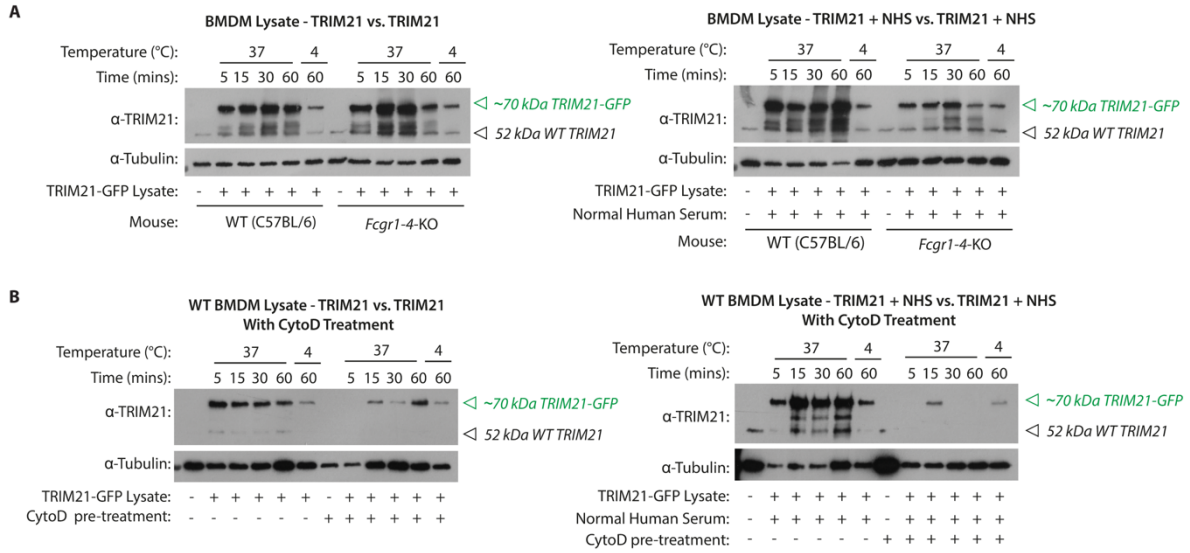

Fig. S7. Roles of Fcγ receptors and actin-dependent phagocytosis in TRIM21-IC uptake. TRIM21_w_PRYSPRY-GFP ± normal human serum uptake was compared for (A) BMDMs generated from WT versus *Fcgr1-4*-KO mice, and (B) WT BMDMs ± pre-treatment for 1 hour with 5 μM CytoD. (A, B) Immunoblots are representative of three independent experiments.

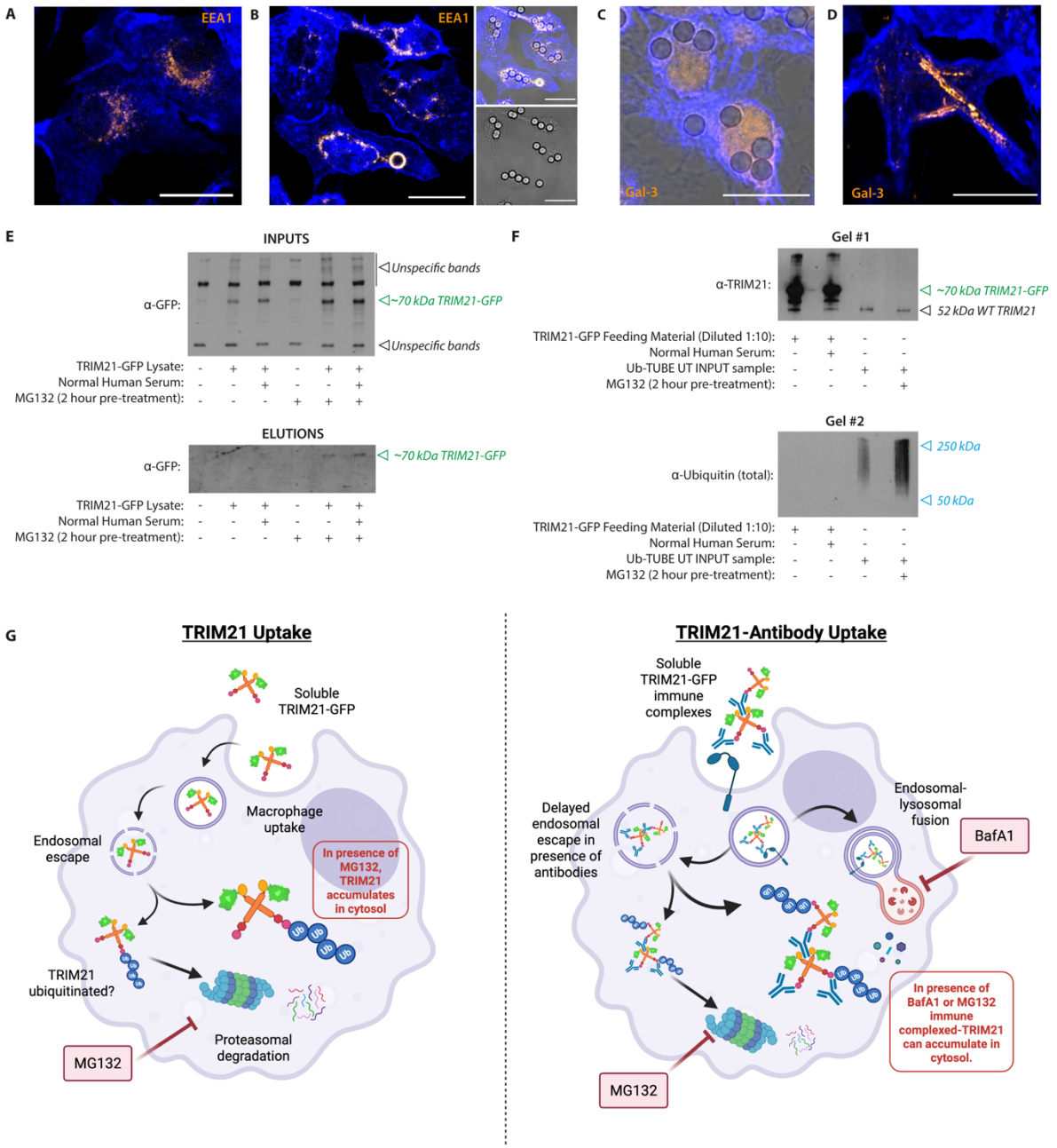

Fig. S8. Internalized TRIM21 escapes into cytosols and is preferentially degraded by the proteasome. (A, B) Localization of EEA1 in untreated BMDM (A) or BMDM treated with opsonized beads (B). (C, D) Gal3 staining in untreated BMDM (C) or BMDM treated with MSU positive control (D). (E, F) Ub-TUBE controls. (E) Ub-TUBE inputs and elutions were analyzed by immunoblot, detecting the GFP tag of TRIM21_w_PRYSPRY-GFP. (F) GFP-Trap eluted TRIM21 (± complexed with normal human serum) feeding material, and Ub-TUBE IP inputs (± 10 μM MG132) were analyzed by immunoblot. TRIM21 and total ubiquitin levels were detected using replicate membranes. (G) Proposed model for intracellular degradation of TRIM21 or TRIM21-IC following internalization (*86*).

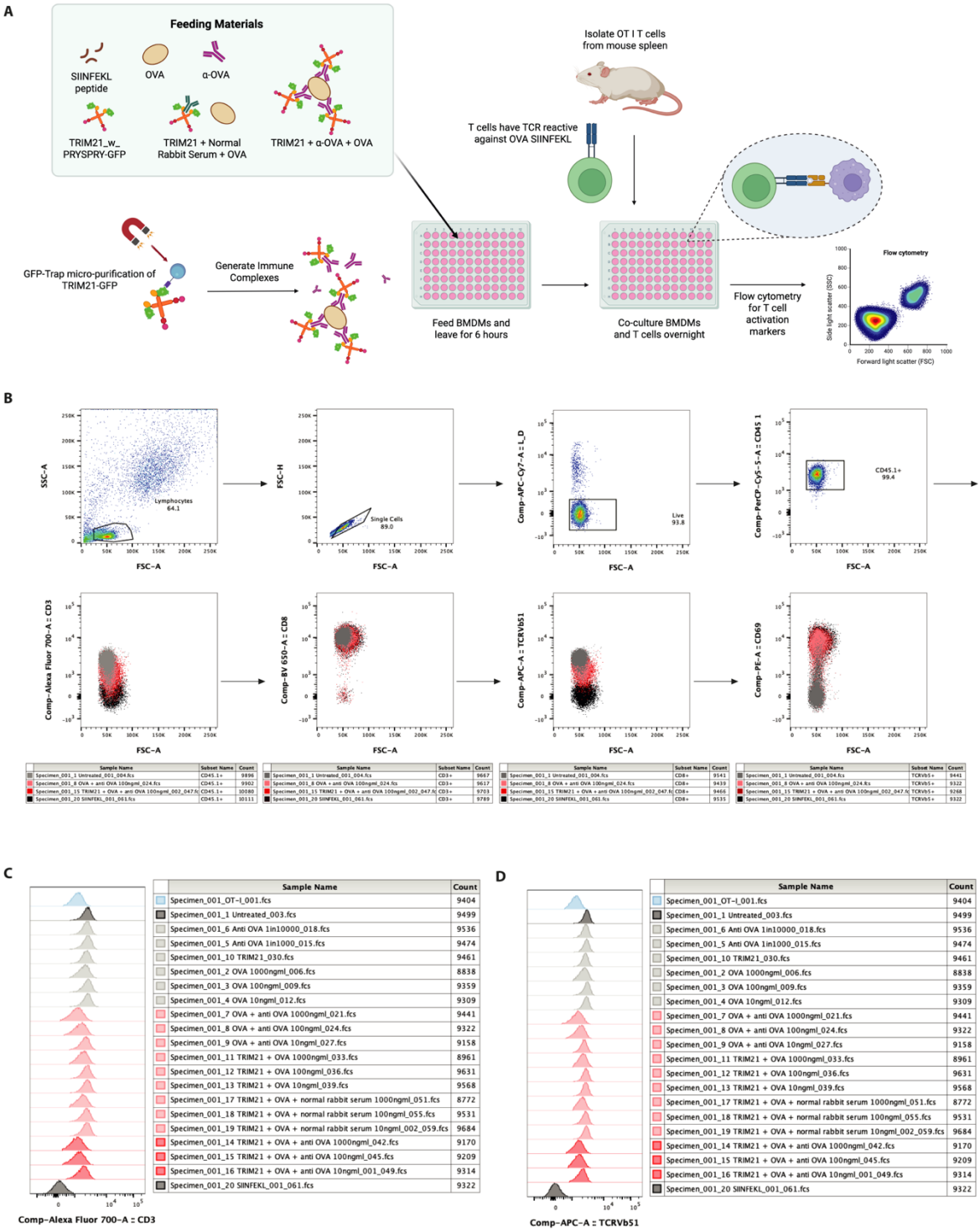

Sample Name	Count
Specimen_001_OT-I_001.fcs	9404
Specimen_001_1 Untreated_003.fcs	9499
Specimen_001_6 Anti OVA 1in10000_018.fcs	9536
Specimen_001_5 Anti OVA 1in1000_015.fcs	9474
Specimen_001_10 TRIM21_030.fcs	9461
Specimen_001_2 OVA 1000ngml_006.fcs	8838
Specimen_001_3 OVA 100ngml_009.fcs	9359
Specimen_001_4 OVA 10ngml_012.fcs	9309
Specimen_001_7 OVA + anti OVA 1000ngml_021.fcs	9441
Specimen_001_8 OVA + anti OVA 100ngml_024.fcs	9322
Specimen_001_9 OVA + anti OVA 10ngml_027.fcs	9158
Specimen_001_11 TRIM21 + OVA 1000ngml_033.fcs	8961
Specimen_001_12 TRIM21 + OVA 100ngml_036.fcs	9631
Specimen_001_13 TRIM21 + OVA 10ngml_039.fcs	9568
Specimen_001_17 TRIM21 + OVA + normal rabbit serum 1000ngml_051.fcs	8772
Specimen_001_18 TRIM21 + OVA + normal rabbit serum 100ngml_055.fcs	9531
Specimen_001_19 TRIM21 + OVA + normal rabbit serum 10ngml_002_059.fcs	9684
Specimen_001_14 TRIM21 + OVA + anti OVA 1000ngml_042.fcs	9170
Specimen_001_15 TRIM21 + OVA + anti OVA 100ngml_045.fcs	9209
Specimen_001_16 TRIM21 + OVA + anti OVA 10ngml_001_049.fcs	9314
Specimen_001_20 SIINFEKL_001_061.fcs	9322

Fig. S9. TRIM21-OVA antigen presentation in vitro experimental set up and analysis. BMDMs were stimulated with 100 ng/ml mIFN-γ for ~24 hours and fed with 10 µl of the following materials: OVA (± rabbit α-OVA), GFP-trap eluted TRIM21 (± OVA, OVA–anti-OVA or OVA–normal rabbit serum), 50 ng/ml of SIINFEKL peptide. (A) Schematic illustration of antigen presentation experimental setup (*87*). (B) Example gating strategy to select for $CD45.1^{+}CD8\alpha^{+}CD3^{+}$ OT-I cells and then for TCRVβ5.1 and CD69 expression. Gating shown for T cells cocultured with the following BMDM experimental conditions; UT, OVA–anti-OVA (100 ng/ml), TRIM21 + OVA–anti-OVA (100 ng/ml), and SIINFEKL (50 ng/ml). Representative histograms for (C) CD3 and (D) TcrbV5.1 expression. Results shown for one of two biologically independent experiments.

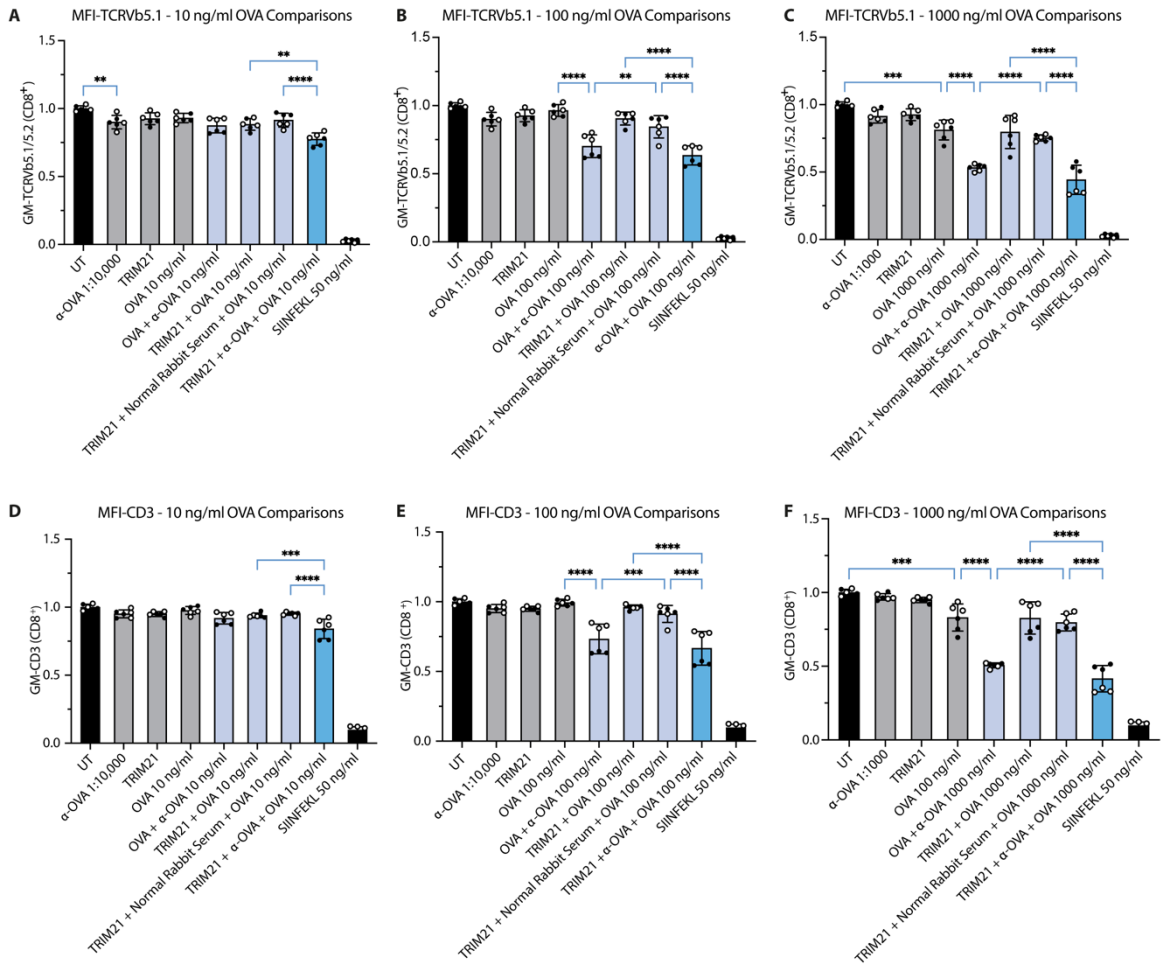

Fig. S10. TRIM21-OVA antigen presentation in vitro, summary of TCR changes. BMDMs were stimulated with 100 ng/ml of mIFN-γ for ~24 hours and fed as described in fig. S8. (A) CD3 mean fluorescence intensity (MFI) and (B) TCRVβ5.1 MFI were determined for a range of OVA concentrations; 10 ng/ml, 100 ng/ml and 1000 ng/ml. Results from two biologically independent experiments were pooled, normalized to UT, and analyzed by one-way ANOVA and Tukey's post-hoc test. Duplicate experiments are distinguished by filled or empty symbols. Data represented as mean + SD for each condition. $*P \leq 0.05$, $**P \leq 0.01$, and $***P \leq 0.001$.

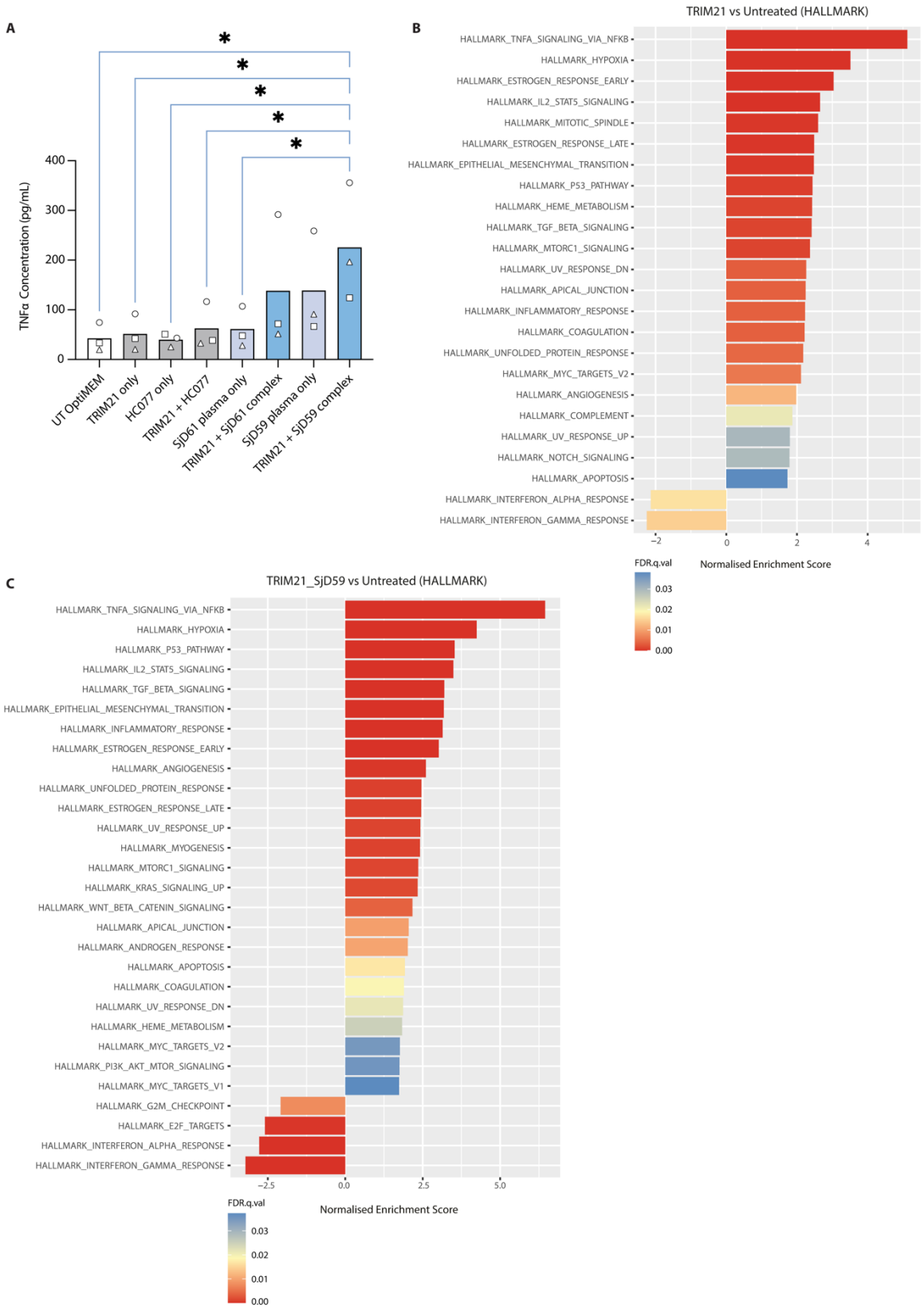

Fig. S11. Proinflammatory and transcriptional changes in HMDM following TRIM21 and TRIM21-IC feeding. (A) TNFα release from HMDMs primed with human IFN-γ and fed with TRIM21_w_PRYSPRY-GFP (± complexed with indicated plasma). SN were analyzed by ELISA for human TNF. Average results from three biologically independent experiments were pooled and analyzed by one-way ANOVA and Fisher's least significant difference post-hoc

test. Each HMDM donor is represented by different symbols. *$P \leq 0.05$. (B, C) HMDMs from three donors (D8, D10, D11) were fed with 20 μl of GFP-trap eluted TRIM21 (± complexed with patient plasma). After 6 hours, RNA was extracted, sequenced, aligned to reference genome and analyzed. Significance was calculated using the Wald test (two-tailed), followed by Bonferroni correction. Hallmark gene set enrichment analysis of bulk RNA sequencing results showing differentially expressed gene sets in HMDMs treated with (B) TRIM21-GFP alone or (C) TRIM21-GFP_SjD59 ICs.

Fig. S12. KEGG gene set enrichment analysis of RNA sequencing results. RNA sequencing results from three donors was analyzed for differential expression of KEGG gene sets. Results from (A) TRIM21_w_PRYSPRY-GFP versus UT and (B) TRIM21_w_PRYSPRY-GFP_SjD59 versus UT gene set enrichment analyses.

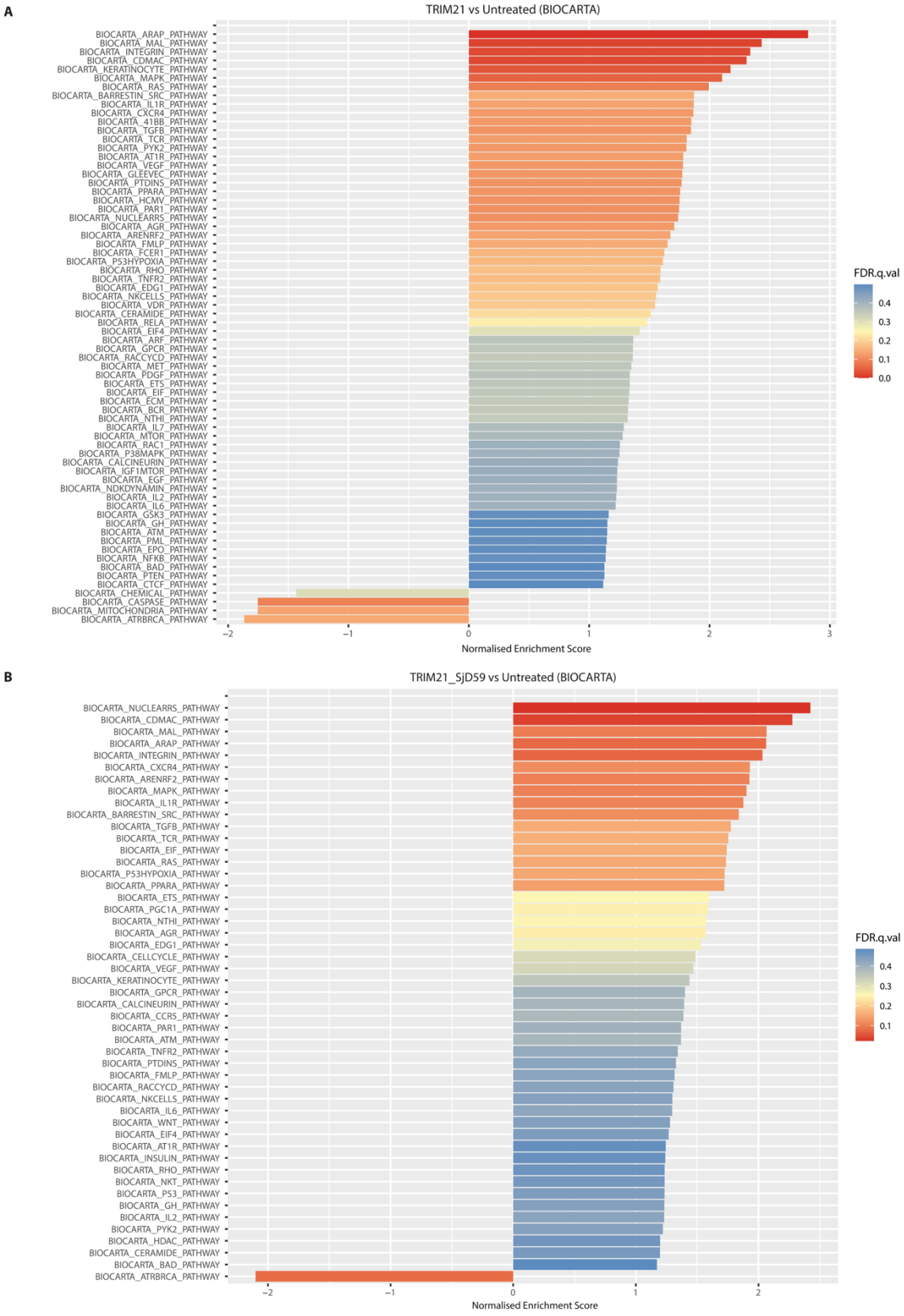

Fig. S13. Biocarta gene set enrichment analysis of RNA sequencing results. RNA sequencing results from three donors were analyzed for differential expression of KEGG gene sets. Results from (A) TRIM21_w_PRYSPRY-GFP versus UT and (B) TRIM21_w_PRYSPRY-GFP_SjD59 versus UT gene set enrichment analyses.

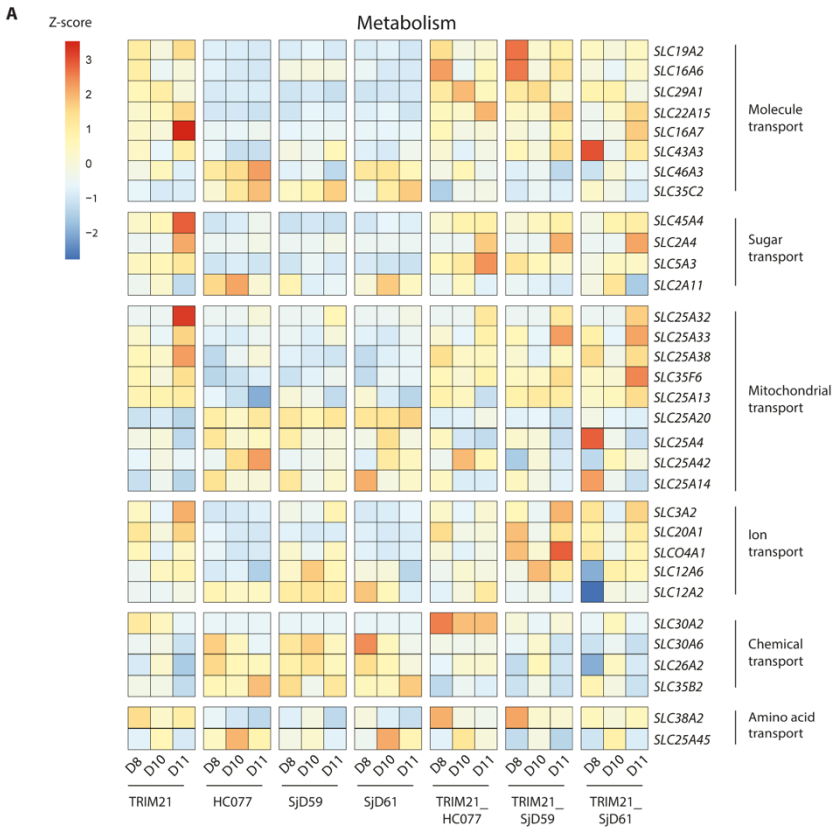

Fig. S14. Differential expression of metabolic genes. RNA sequencing results from three donors were analyzed. Heatmap showing expression changes in metabolic genes for HMDMs from three donors following treatment with TRIM21_w_PRYSPRY-GFP alone, plasma alone, or TRIM21_w_PRYSPRY-GFP complexed with different plasmas as indicated.

Slide	Ro	La	SjD	ACR 2016	Area (mm^2)	Foci	Focus Score (4 × Foci / mm^2)	Age	Sex
1	1	1	1	1	14.62	4	1.09	28	F
2	1	0	1	1	Atrophy, could not evaluate			71	F
8	1	1	1	1	8.87	4	1.80	35	F
12	1	0	1	1	4.71	2	1.70	75	F
14	1	1	1	1	15.60	7	1.79	74	F
4	0	0	0	0	16.76	2	0.48	66	F
5	0	0	0	0	15.51	0	0	47	F
18	0	0	0	0	10.63	0	0	60	F
20	0	0	0	0	11.65	2	0.69	41	F
21	0	0	0	0	6.06	0	0	67	F

Table S1. Sicca and SjD SG biopsy information. OASIS (Birmingham) FFPE biopsy slides were H&E-stained and analyzed for the following: area, foci, and focal score. Information about "Ro/La" antibody expression, SjD diagnosis, ACR2016 confirmation, and patient demographics is provided.

Sample	SjD or control	Ro	Age	Sex
SjD58	SjD	1	66	F
SjD59	SjD	1	73	F
SjD61	SjD	1	80	M
HC077	Healthy control	0	44	F
HC085	Healthy control	0	47	M
HC099	Healthy control	0	35	M

Table S2. Plasma samples used in this study.

Caption for movie S1

Movie S1. Live microscopy of HeLa cells overexpressing TRIM21-GFP undergoing apoptosis. HeLa overexpressing TRIM21_w_PRYSPRY-GFP were imaged for 4 hours by live confocal microscopy time-lapse recording of the same field of view. 30 mins prior to imaging, cells were treated with 1 μM of sirDNA dye to stain DNA (magenta). Apoptosis was induced by combined 1 μM ABT737 and 10 μM MCL1i drug treatments. Movie is representative of 3 independent experiments. Scale bar, 50 μm.

Captions for data files S1 to S4

Data file S1. List of all reagents, resources and commercial sources used in this manuscript. Antibody dilutions and applications are listed. Media and buffers, including their application are listed.

Data file S2. Sequences and maps of TRIM21-GFP expression constructs.

Data file S3. Raw tabulated data for all figures.

Data file S4. Full uncut images of all immunoblots.

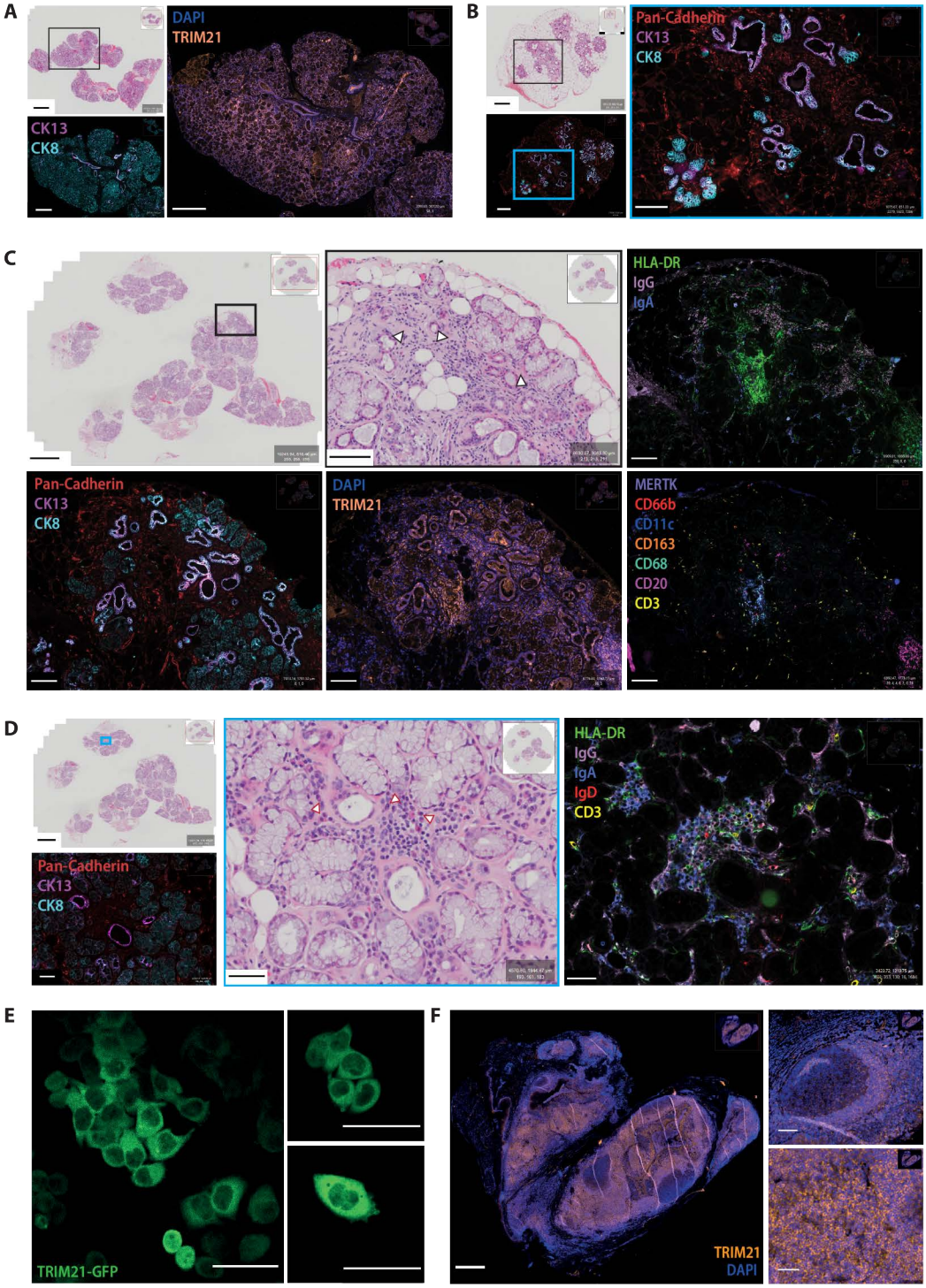
A
DAPI
TRIM21
CK13
CK8
B
Pan-Cadherin
CK13
CK8
C
HLA-DR
IgG
IgA
Pan-Cadherin
CK13
CK8
DAPI
TRIM21
MERTK
CD66b
CD11c
CD163
CD68
CD20
CD3
D
Pan-Cadherin
CK13
CK8
HLA-DR
IgG
IgA
IgD
CD3
E
TRIM21-GFP
F
TRIM21
DAPI

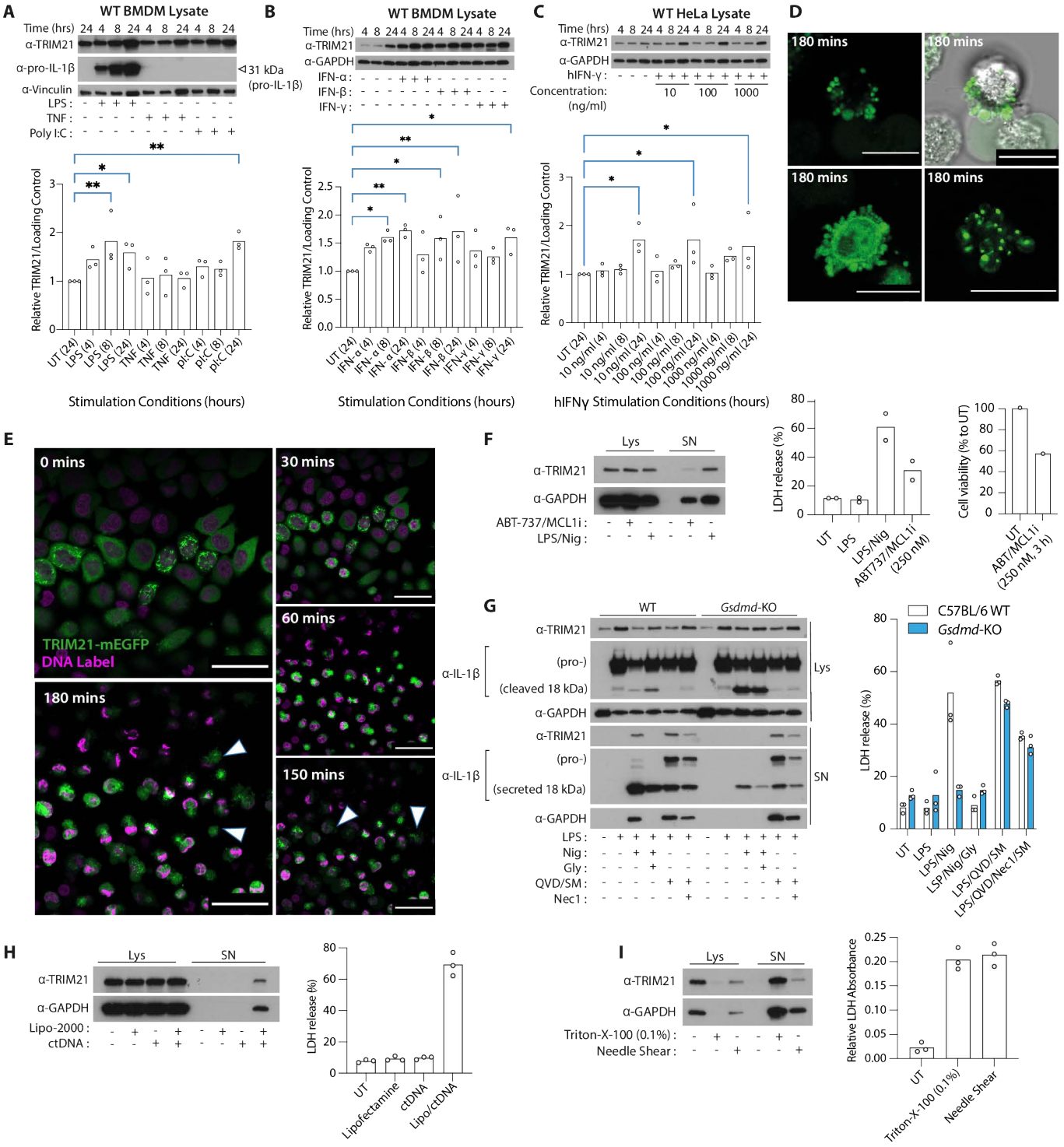
A
WT BMDM Lysate
Time (hrs) 24 4 8 24 4 8 24 4 8 24
α-TRIM21
α-pro-IL-1β
31 kDa (pro-IL-1β)
α-Vinculin
LPS :
TNF :
Poly I:C :
Relative TRIM21/Loading Control
UT (24)
LPS (4)
LPS (8)
LPS (24)
TNF (4)
TNF (8)
TNF (24)
pI:C (4)
pI:C (8)
pI:C (24)
Stimulation Conditions (hours)
B
WT BMDM Lysate
Time (hrs) 4 8 24 4 8 24 4 8 24 4 8 24
α-TRIM21
α-GAPDH
IFN-α :
IFN-β :
IFN-γ :
Relative TRIM21/Loading Control
UT (24)
IFN-α (4)
IFN-α (8)
IFN-α (24)
IFN-β (4)
IFN-β (8)
IFN-β (24)
IFN-γ (4)
IFN-γ (8)
IFN-γ (24)
Stimulation Conditions (hours)
C
WT HeLa Lysate
Time (hrs) 4 8 24 4 8 24 4 8 24 4 8 24
α-TRIM21
α-GAPDH
hIFN-γ :
Concentration: (ng/ml)
10
100
1000
Relative TRIM21/Loading Control
UT (24)
10 ng/ml (4)
10 ng/ml (8)
10 ng/ml (24)
100 ng/ml (4)
100 ng/ml (8)
100 ng/ml (24)
1000 ng/ml (4)
1000 ng/ml (8)
1000 ng/ml (24)
hIFNγ Stimulation Conditions (hours)
D
180 mins
180 mins
180 mins
180 mins
E
0 mins
30 mins
60 mins
150 mins
180 mins
TRIM21-mEGFP
DNA Label
F
Lys
SN
α-TRIM21
α-GAPDH
ABT-737/MCL1i :
LPS/Nig :
LDH release (%)
UT
LPS
LPS/Nig
ABT737/MCL1i (250 nM)
Cell viability (% to UT)
UT
ABT/MCL1i (250 nM, 3 h)
G
WT
Gsdmd-KO
α-TRIM21
α-IL-1β
(pro-)
(cleaved 18 kDa)
α-GAPDH
α-TRIM21
α-IL-1β
(pro-)
(secreted 18 kDa)
α-GAPDH
Lys
SN
LPS :
Nig :
Gly :
QVD/SM :
Nec1 :
C57BL/6 WT
Gsdmd-KO
LDH release (%)
UT
LPS
LPS/Nig
LSP/Nig/Gly
LPS/QVD/SM
LPS/QVD/Nec1/SM
H
Lys
SN
α-TRIM21
α-GAPDH
Lipo-2000 :
ctDNA :
LDH release (%)
UT
Lipofectamine
ctDNA
Lipo/ctDNA
I
Lys
SN
α-TRIM21
α-GAPDH
Triton-X-100 (0.1%) :
Needle Shear :
Relative LDH Absorbance
UT
Triton-X-100 (0.1%)
Needle Shear

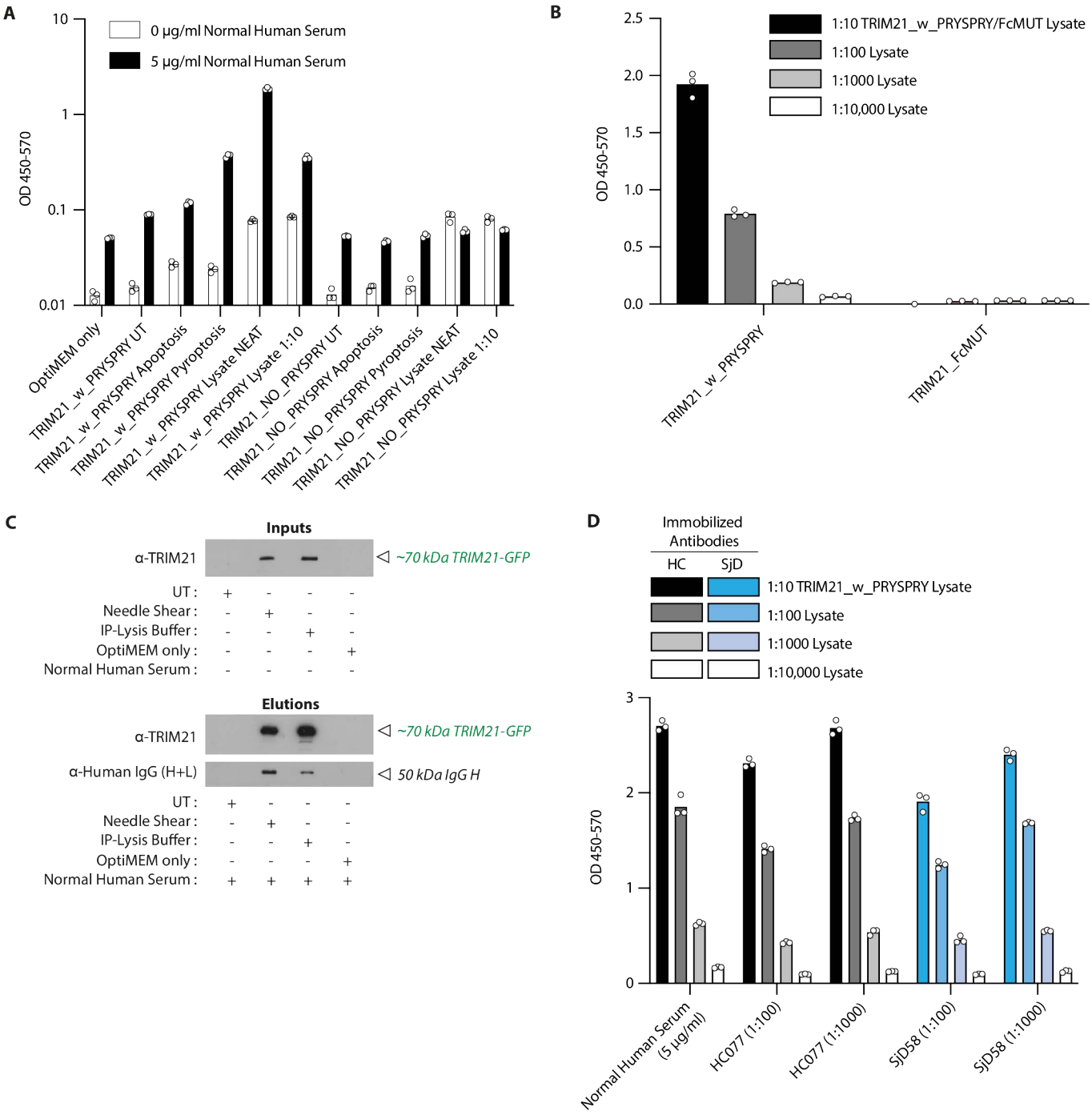
A
0 µg/ml Normal Human Serum
5 µg/ml Normal Human Serum
OD 450-570
10
1
0.1
0.01
OptiMEM only
TRIM21_w_PRYSPRY UT
TRIM21_w_PRYSPRY Apoptosis
TRIM21_w_PRYSPRY Pyroptosis
TRIM21_w_PRYSPRY Lysate NEAT
TRIM21_w_PRYSPRY Lysate 1:10
TRIM21_NO_PRYSPRY UT
TRIM21_NO_PRYSPRY Apoptosis
TRIM21_NO_PRYSPRY Pyroptosis
TRIM21_NO_PRYSPRY Lysate NEAT
TRIM21_NO_PRYSPRY Lysate 1:10
B
1:10 TRIM21_w_PRYSPRY/FcMUT Lysate
1:100 Lysate
1:1000 Lysate
1:10,000 Lysate
OD 450-570
2.5
2.0
1.5
1.0
0.5
0.0
TRIM21_w_PRYSPRY
TRIM21_FcMUT
C
Inputs
α-TRIM21
~70 kDa TRIM21-GFP
UT :
Needle Shear :
IP-Lysis Buffer :
OptiMEM only :
Normal Human Serum :
Elutions
α-TRIM21
~70 kDa TRIM21-GFP
α-Human IgG (H+L)
50 kDa IgG H
D
Immobilized Antibodies
HC
SjD
1:10 TRIM21_w_PRYSPRY Lysate
1:100 Lysate
1:1000 Lysate
1:10,000 Lysate
OD 450-570
3
2
1
0
Normal Human Serum (5 µg/ml)
HC077 (1:100)
HC077 (1:1000)
SjD58 (1:100)
SjD58 (1:1000)

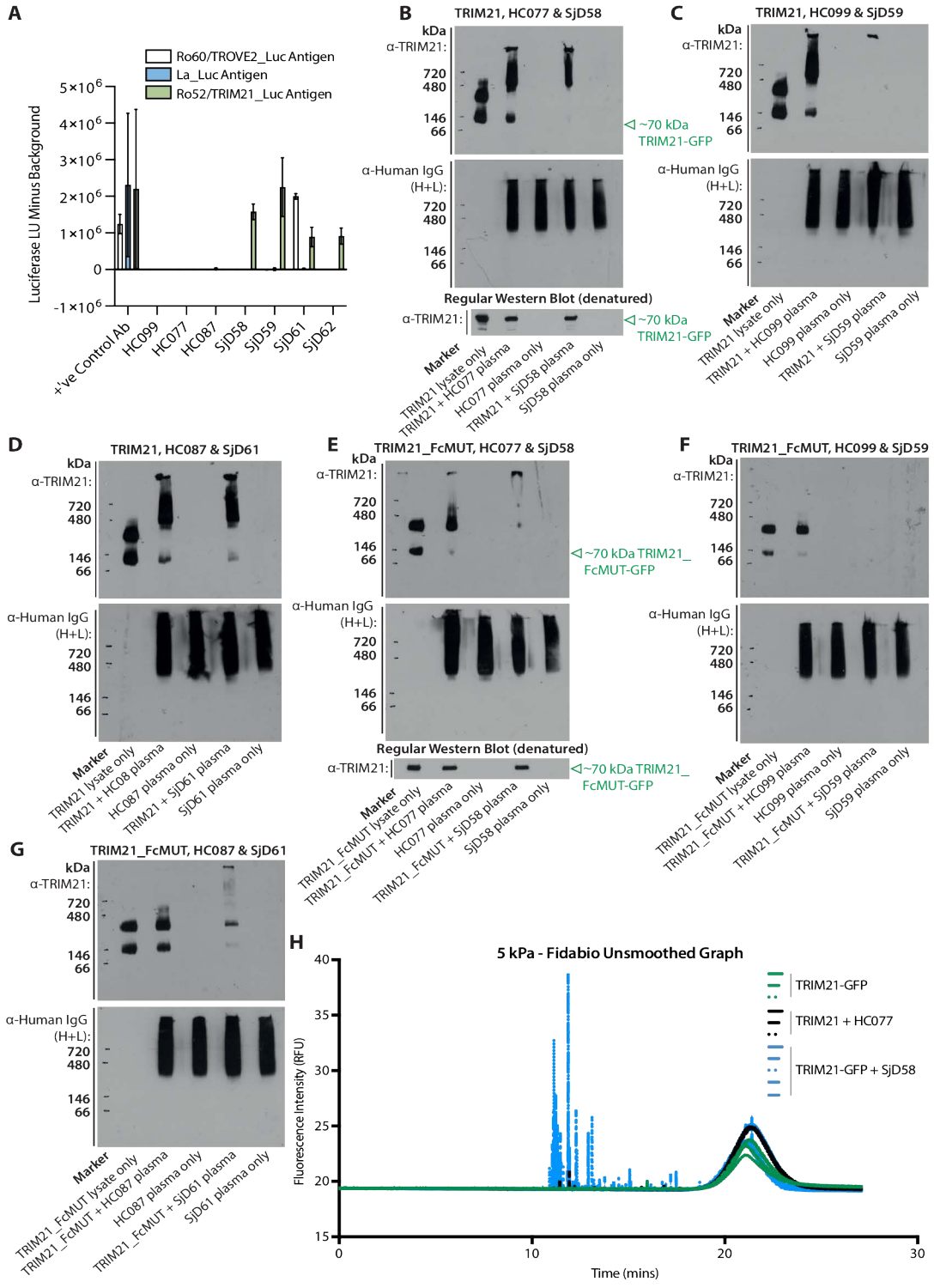
A
Ro60/TROVE2_Luc Antigen
La_Luc Antigen
Ro52/TRIM21_Luc Antigen
Luciferase LU Minus Background
5×10^6
4×10^6
3×10^6
2×10^6
1×10^6
0
-1×10^6
+'ve Control Ab
HC099
HC077
HC087
SjD58
SjD59
SjD61
SjD62
B
TRIM21, HC077 & SjD58
kDa
α-TRIM21:
720
480
146
66
◁ ~70 kDa TRIM21-GFP
α-Human IgG (H+L):
Regular Western Blot (denatured)
Marker
TRIM21 lysate only
TRIM21 + HC077 plasma
HC077 plasma only
TRIM21 + SjD58 plasma
SjD58 plasma only
C
TRIM21, HC099 & SjD59
TRIM21 lysate only
TRIM21 + HC099 plasma
HC099 plasma only
TRIM21 + SjD59 plasma
SjD59 plasma only
D
TRIM21, HC087 & SjD61
TRIM21 + HC08 plasma
HC087 plasma only
TRIM21 + SjD61 plasma
SjD61 plasma only
E
TRIM21_FcMUT, HC077 & SjD58
◁ ~70 kDa TRIM21_ FcMUT-GFP
TRIM21_FcMUT lysate only
TRIM21_FcMUT + HC077 plasma
TRIM21_FcMUT + SjD58 plasma
F
TRIM21_FcMUT, HC099 & SjD59
TRIM21_FcMUT + HC099 plasma
TRIM21_FcMUT + SjD59 plasma
G
TRIM21_FcMUT, HC087 & SjD61
TRIM21_FcMUT + HC087 plasma
TRIM21_FcMUT + SjD61 plasma
H
5 kPa - Fidabio Unsmoothed Graph
Fluorescence Intensity (RFU)
40
35
30
25
20
15
0
10
20
30
Time (mins)
TRIM21-GFP
TRIM21 + HC077
TRIM21-GFP + SjD58

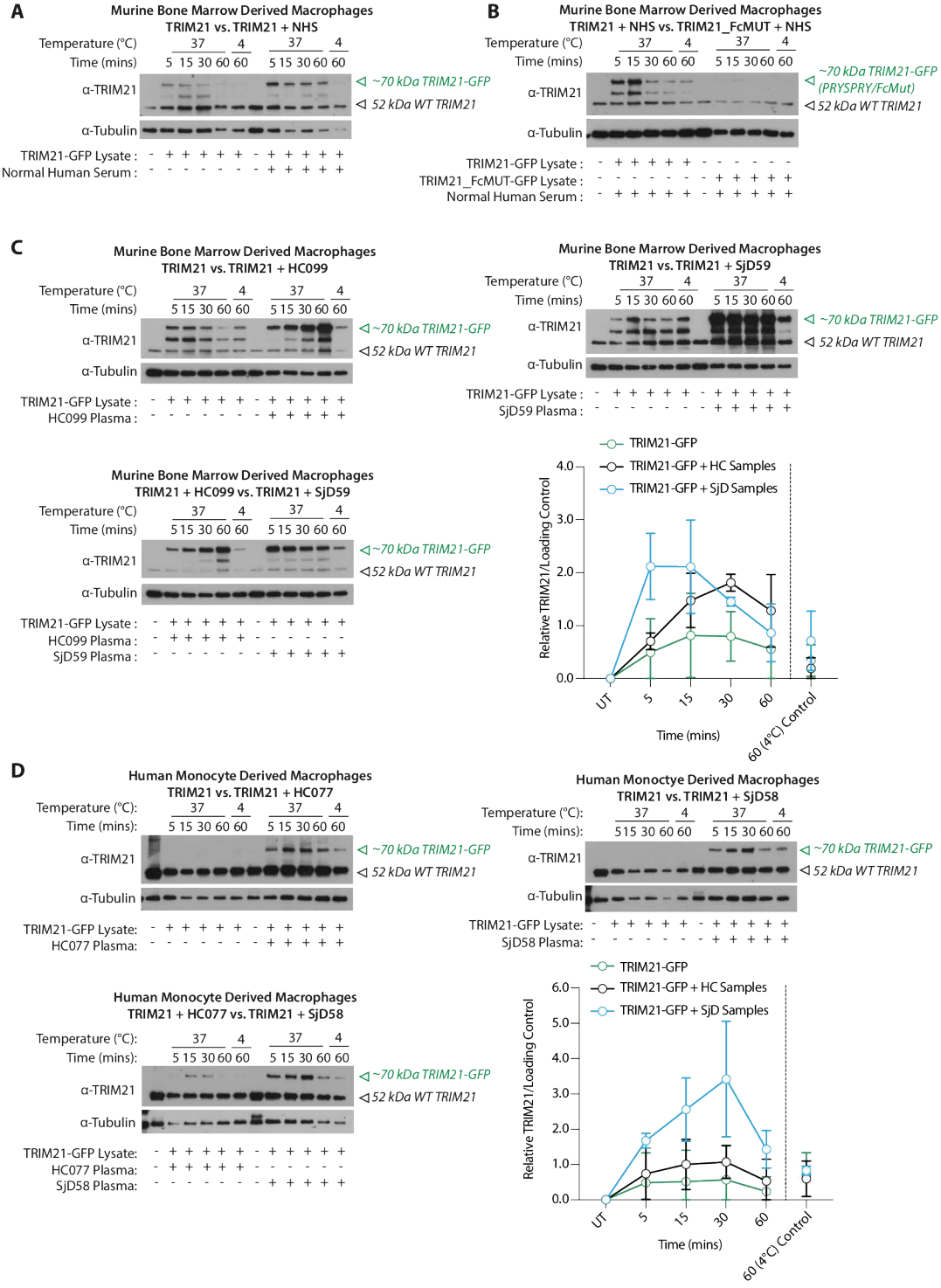
A
Murine Bone Marrow Derived Macrophages
TRIM21 vs. TRIM21 + NHS
Temperature (°C) 37 4 37 4
Time (mins) 5 15 30 60 60 5 15 30 60 60
α-TRIM21
~70 kDa TRIM21-GFP
52 kDa WT TRIM21
α-Tubulin
TRIM21-GFP Lysate : - + + + + + - + + + + +
Normal Human Serum : - - - - - - - + + + + +
B
Murine Bone Marrow Derived Macrophages
TRIM21 + NHS vs. TRIM21_FcMUT + NHS
Temperature (°C) 37 4 37 4
Time (mins) 5 15 30 60 60 5 15 30 60 60
α-TRIM21
~70 kDa TRIM21-GFP (PRYSPRY/FcMut)
52 kDa WT TRIM21
α-Tubulin
TRIM21-GFP Lysate : - + + + + + - - - - - -
TRIM21_FcMUT-GFP Lysate : - - - - - - - + + + + +
Normal Human Serum : - + + + + + - + + + + +
C
Murine Bone Marrow Derived Macrophages
TRIM21 vs. TRIM21 + HC099
Temperature (°C) 37 4 37 4
Time (mins) 5 15 30 60 60 5 15 30 60 60
α-TRIM21
~70 kDa TRIM21-GFP
52 kDa WT TRIM21
α-Tubulin
TRIM21-GFP Lysate : - + + + + + - + + + + +
HC099 Plasma : - - - - - - - + + + + +
Murine Bone Marrow Derived Macrophages
TRIM21 vs. TRIM21 + SjD59
Temperature (°C) 37 4 37 4
Time (mins) 5 15 30 60 60 5 15 30 60 60
α-TRIM21
~70 kDa TRIM21-GFP
52 kDa WT TRIM21
α-Tubulin
TRIM21-GFP Lysate : - + + + + + - + + + + +
SjD59 Plasma : - - - - - - - + + + + +
Murine Bone Marrow Derived Macrophages
TRIM21 + HC099 vs. TRIM21 + SjD59
Temperature (°C) 37 4 37 4
Time (mins) 5 15 30 60 60 5 15 30 60 60
α-TRIM21
~70 kDa TRIM21-GFP
52 kDa WT TRIM21
α-Tubulin
TRIM21-GFP Lysate : - + + + + + - + + + + +
HC099 Plasma : - + + + + + - - - - - -
SjD59 Plasma : - - - - - - - + + + + +
TRIM21-GFP
TRIM21-GFP + HC Samples
TRIM21-GFP + SjD Samples
Relative TRIM21/Loading Control
4.0
3.0
2.0
1.0
0.0
UT 5 15 30 60 60 (4°C) Control
Time (mins)
D
Human Monocyte Derived Macrophages
TRIM21 vs. TRIM21 + HC077
Temperature (°C): 37 4 37 4
Time (mins): 5 15 30 60 60 5 15 30 60 60
α-TRIM21
~70 kDa TRIM21-GFP
52 kDa WT TRIM21
α-Tubulin
TRIM21-GFP Lysate: - + + + + + - + + + + +
HC077 Plasma: - - - - - - - + + + + +
Human Monocyte Derived Macrophages
TRIM21 + HC077 vs. TRIM21 + SjD58
Temperature (°C): 37 4 37 4
Time (mins): 5 15 30 60 60 5 15 30 60 60
α-TRIM21
~70 kDa TRIM21-GFP
52 kDa WT TRIM21
α-Tubulin
TRIM21-GFP Lysate: - + + + + + - + + + + +
HC077 Plasma: - + + + + + - - - - - -
SjD58 Plasma: - - - - - - - + + + + +
Human Monocyte Derived Macrophages
TRIM21 vs. TRIM21 + SjD58
Temperature (°C): 37 4 37 4
Time (mins): 5 15 30 60 60 5 15 30 60 60
α-TRIM21
~70 kDa TRIM21-GFP
52 kDa WT TRIM21
α-Tubulin
TRIM21-GFP Lysate: - + + + + + - + + + + +
SjD58 Plasma: - - - - - - - + + + + +
TRIM21-GFP
TRIM21-GFP + HC Samples
TRIM21-GFP + SjD Samples
Relative TRIM21/Loading Control
6.0
5.0
4.0
3.0
2.0
1.0
0.0
UT 5 15 30 60 60 (4°C) Control
Time (mins)

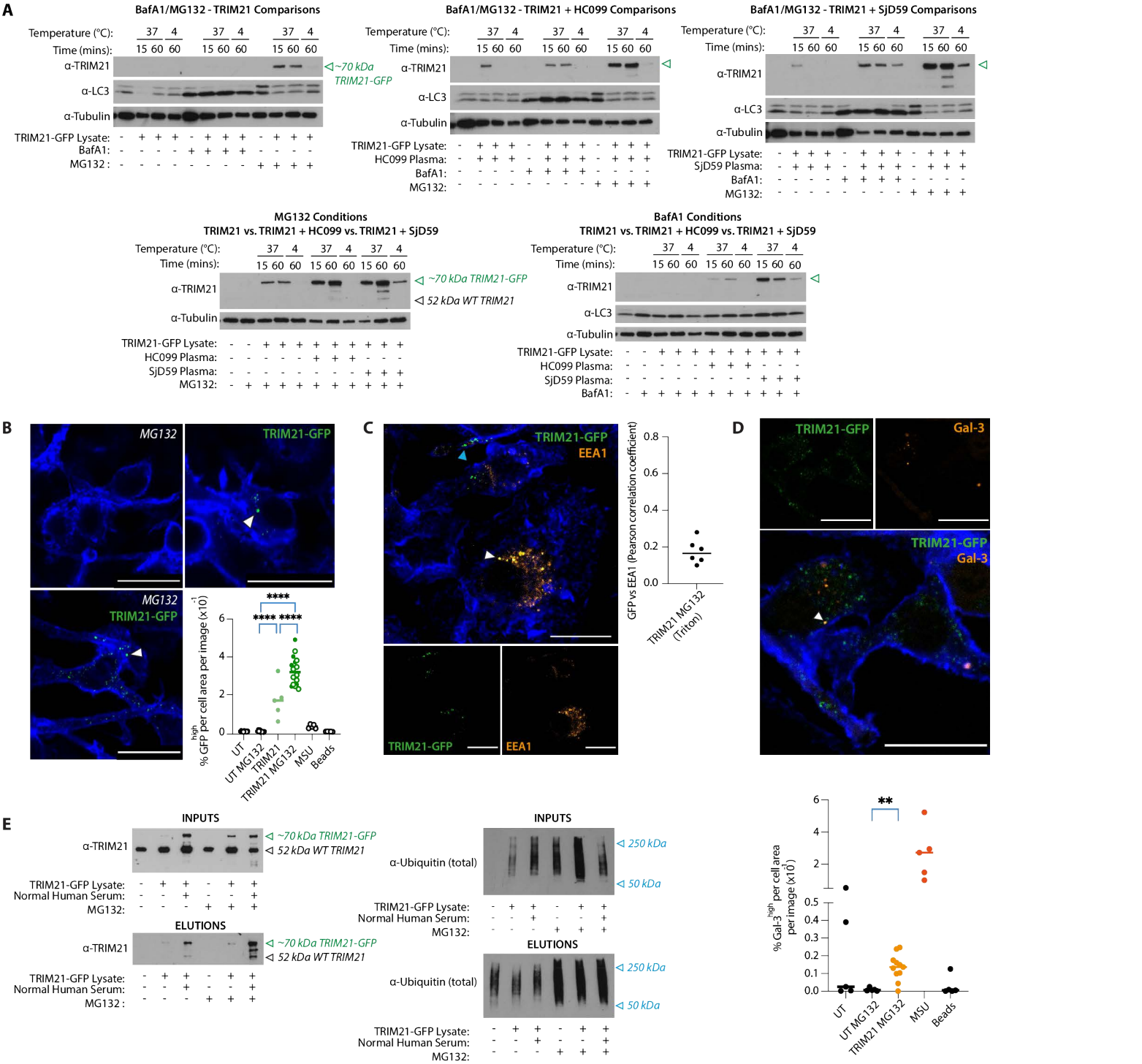
A
BafA1/MG132 - TRIM21 Comparisons
BafA1/MG132 - TRIM21 + HC099 Comparisons
BafA1/MG132 - TRIM21 + SjD59 Comparisons
Temperature (°C):
Time (mins):
α-TRIM21
α-LC3
α-Tubulin
~70 kDa TRIM21-GFP
TRIM21-GFP Lysate:
BafA1:
MG132 :
HC099 Plasma:
SjD59 Plasma:
MG132 Conditions
TRIM21 vs. TRIM21 + HC099 vs. TRIM21 + SjD59
BafA1 Conditions
TRIM21 vs. TRIM21 + HC099 vs. TRIM21 + SjD59
52 kDa WT TRIM21
B
MG132
TRIM21-GFP
% GFP per cell area per image (x10)
UT
UT MG132
TRIM21
TRIM21 MG132
MSU
Beads
C
EEA1
GFP vs EEA1 (Pearson correlation coefficient)
TRIM21 MG132 (Triton)
D
Gal-3
% Gal-3 per cell area per image (x10)
E
INPUTS
ELUTIONS
α-Ubiquitin (total)
250 kDa
50 kDa
Normal Human Serum:

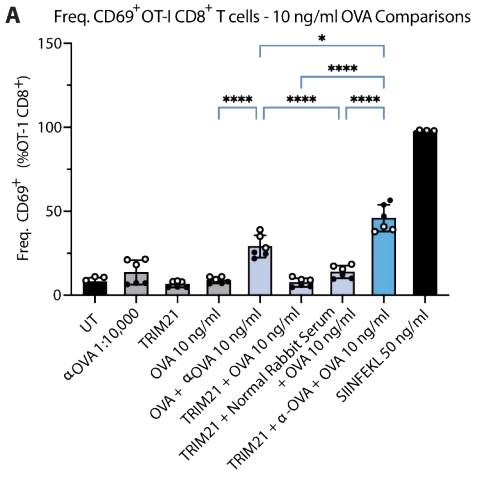
A
Freq. CD69+ OT-I CD8+ T cells - 10 ng/ml OVA Comparisons
Freq. CD69+ (%OT-1 CD8+)
150
100
50
0
*
****
****
****
****
UT
α-OVA 1:10,000
TRIM21
OVA 10 ng/ml
OVA + α-OVA 10 ng/ml
TRIM21 + OVA 10 ng/ml
TRIM21 + Normal Rabbit Serum + OVA 10 ng/ml
TRIM21 + α-OVA + OVA 10 ng/ml
SIINFEKL 50 ng/ml

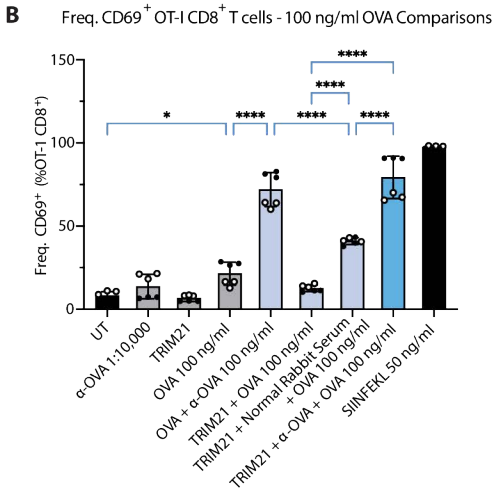
B
Freq. CD69+ OT-I CD8+ T cells - 100 ng/ml OVA Comparisons
Freq. CD69+ (%OT-1 CD8+)
150
100
50
0
*
****
****
****
****
UT
α-OVA 1:10,000
TRIM21
OVA 100 ng/ml
OVA + α-OVA 100 ng/ml
TRIM21 + OVA 100 ng/ml
TRIM21 + Normal Rabbit Serum + OVA 100 ng/ml
TRIM21 + α-OVA + OVA 100 ng/ml
SIINFEKL 50 ng/ml

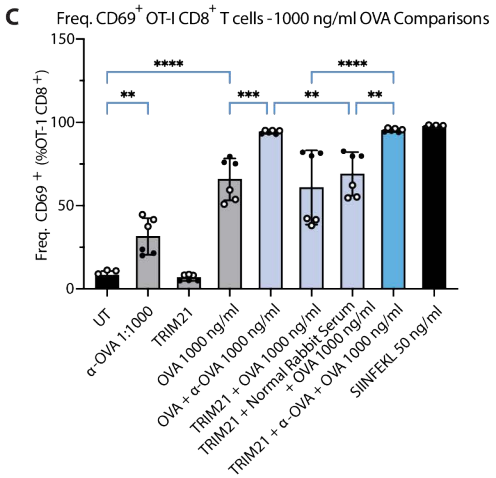
C
Freq. CD69+ OT-I CD8+ T cells - 1000 ng/ml OVA Comparisons
Freq. CD69+ (%OT-1 CD8+)
150
100
50
0
****
**
***
**
****
**
UT
α-OVA 1:1000
TRIM21
OVA 1000 ng/ml
OVA + α-OVA 1000 ng/ml
TRIM21 + OVA 1000 ng/ml
TRIM21 + Normal Rabbit Serum + OVA 1000 ng/ml
TRIM21 + α-OVA + OVA 1000 ng/ml
SIINFEKL 50 ng/ml

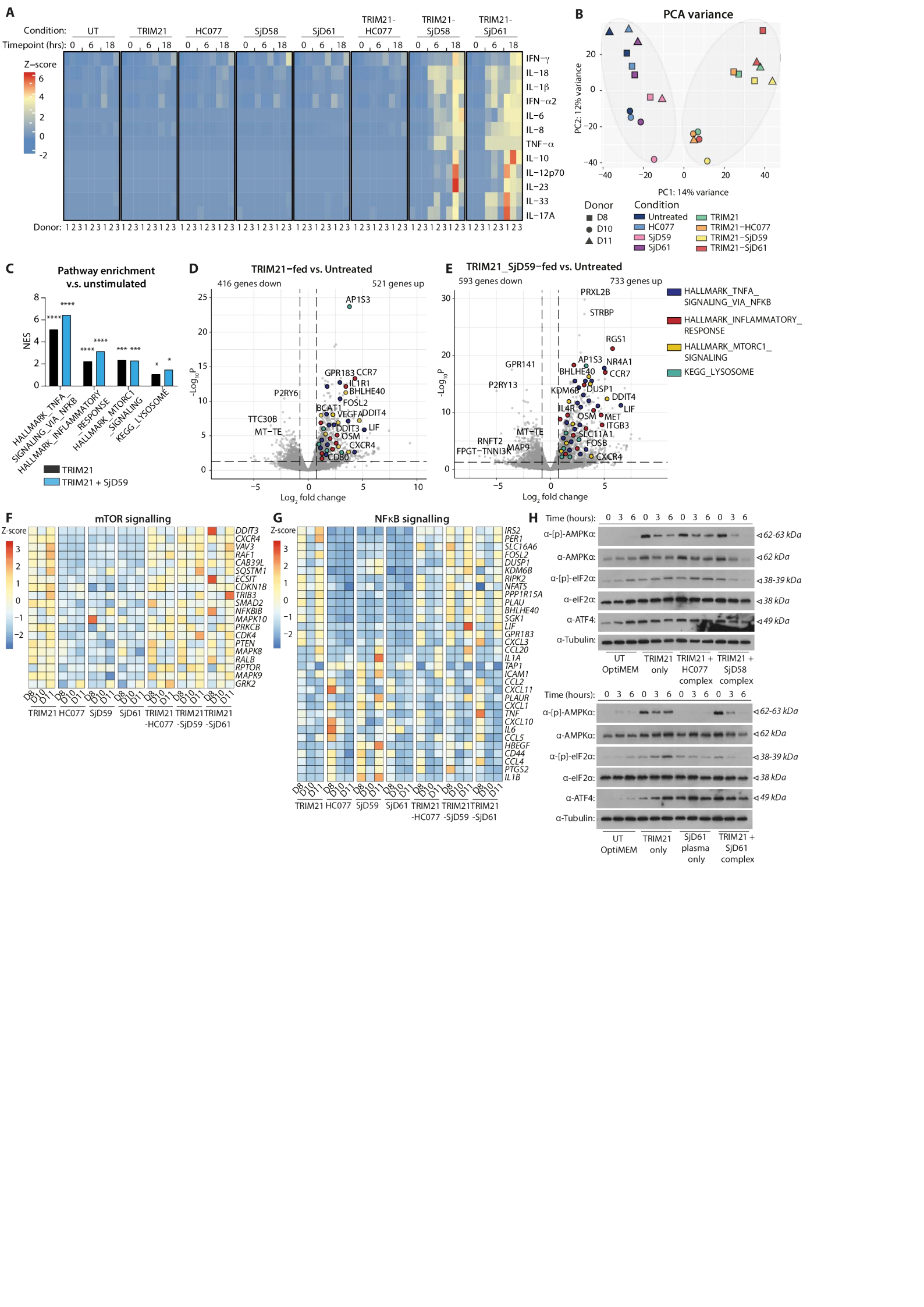
A
Condition: UT TRIM21 HC077 SjD58 SjD61 TRIM21-HC077 TRIM21-SjD58 TRIM21-SjD61
Timepoint (hrs): 0 6 18
Z–score
IFN–γ
IL–18
IL–1β
IFN–α2
IL–6
IL–8
TNF–α
IL–10
IL–12p70
IL–23
IL–33
IL–17A
Donor: 1 2 3
B
PCA variance
PC2: 12% variance
PC1: 14% variance
Donor
D8
D10
D11
Condition
Untreated
HC077
SjD59
SjD61
TRIM21
TRIM21–HC077
TRIM21–SjD59
TRIM21–SjD61
C
Pathway enrichment v.s. unstimulated
NES
HALLMARK_TNFA_SIGNALING_VIA_NFKB
HALLMARK_INFLAMMATORY_RESPONSE
HALLMARK_MTORC1_SIGNALING
KEGG_LYSOSOME
TRIM21
TRIM21 + SjD59
D
TRIM21–fed vs. Untreated
416 genes down
521 genes up
-Log10 P
Log2 fold change
AP1S3
GPR183
CCR7
IL1R1
P2RY6
BHLHE40
FOSL2
BCAT1
VEGFA
DDIT4
TTC30B
DDIT3
LIF
MT–TE
OSM
CXCR4
CD80
E
TRIM21_SjD59–fed vs. Untreated
593 genes down
733 genes up
PRXL2B
STRBP
RGS1
GPR141
AP1S3
NR4A1
BHLHE40
CCR7
P2RY13
KDM6B
DUSP1
DDIT4
IL4R
LIF
OSM
MET
ITGB3
MT–TE
SLC11A1
RNFT2
FOSB
FPGT–TNNI3K
MAP9
CXCR4
HALLMARK_TNFA_SIGNALING_VIA_NFKB
HALLMARK_INFLAMMATORY_RESPONSE
HALLMARK_MTORC1_SIGNALING
KEGG_LYSOSOME
F
mTOR signalling
Z-score
DDIT3
CXCR4
VAV3
RAF1
CAB39L
SQSTM1
ECSIT
CDKN1B
TRIB3
SMAD2
NFKBIB
MAPK10
PRKCB
CDK4
PTEN
MAPK8
RALB
RPTOR
MAPK9
GRK2
D8 D10 D11
TRIM21 HC077 SjD59 SjD61 TRIM21-HC077 TRIM21-SjD59 TRIM21-SjD61
G
NFκB signalling
Z-score
IRS2
PER1
SLC16A6
FOSL2
DUSP1
KDM6B
RIPK2
NFAT5
PPP1R15A
PLAU
BHLHE40
SGK1
LIF
GPR183
CXCL3
CCL20
IL1A
TAP1
ICAM1
CCL2
CXCL11
PLAUR
CXCL1
TNF
CXCL10
IL6
CCL5
HBEGF
CD44
CCL4
PTGS2
IL1B
D8 D10 D11
TRIM21 HC077 SjD59 SjD61 TRIM21-HC077 TRIM21-SjD59 TRIM21-SjD61
H
Time (hours): 0 3 6 0 3 6 0 3 6 0 3 6
α-[p]-AMPKα:
α-AMPKα:
α-[p]-eIF2α:
α-eIF2α:
α-ATF4:
α-Tubulin:
62-63 kDa
62 kDa
38-39 kDa
38 kDa
49 kDa
UT OptiMEM
TRIM21 only
TRIM21 + HC077 complex
TRIM21 + SjD58 complex
Time (hours): 0 3 6 0 3 6 0 3 6 0 3 6
α-[p]-AMPKα:
α-AMPKα:
α-[p]-eIF2α:
α-eIF2α:
α-ATF4:
α-Tubulin:
62-63 kDa
62 kDa
38-39 kDa
38 kDa
49 kDa
UT OptiMEM
TRIM21 only
SjD61 plasma only
TRIM21 + SjD61 complex